University of Calgary

PRISM Repository **https://prism.ucalgary.ca**

The Vault Open Theses and Dissertations

2013-12-04

Analytical Modeling of Cyclic Steam Stimulation Process for a Horizontal Well Configuration

Saripalli, Hari

Saripalli, H. (2013). Analytical Modeling of Cyclic Steam Stimulation Process for a Horizontal Well Configuration (Master's thesis, University of Calgary, Calgary, Canada). Retrieved from https://prism.ucalgary.ca. doi:10.11575/PRISM/24826

http://hdl.handle.net/11023/1173

Downloaded from PRISM Repository, University of Calgary

UNIVERSITY OF CALGARY

Analytical Modeling of Cyclic Steam Stimulation Process for a Horizontal Well Configuration

by

Hari Kaushik Saripalli

A THESIS

SUBMITTED TO THE FACULTY OF GRADUATE STUDIES

IN PARTIAL FULFILLMENT OF THE REQUIREMENTS FOR

THE DEGREE OF MASTER OF SCIENCE

DEPARTMENT OF CHEMICAL AND PETROLEUM ENGINEERING

CALGARY, ALBERTA

DECEMBER, 2013

© Hari Kaushik Saripalli 2013

Abstract

Cyclic steam stimulation is one of the most widely used heavy oil recovery methods. Steam is injected into a formation at high rates for several weeks through a vertical well. The well is then shut-in for a certain period of time, which is called “soak” period. Steam condenses in the formation, thus heating the reservoir rock and fluids around the wellbore. During this period the oil viscosity is reduced by many times. The heated sand contains mobile oil, steam and water. The oil and other fluids are expelled out as the sand face pressure is lowered when the well is put on production. Oil is produced until the oil rate reaches an economic limit and the cycle is repeated again.

There are many analytical models that predict the performance of a conventional Cyclic Steam Stimulation process for vertical wells. However, there are only very few models that are applicable to a horizontal well configuration. The objective of this study is to model heavy oil production using cyclic steam stimulation with a horizontal well configuration. Reasonable assumptions were made to simplify the problems to an extent that they can be solved using analytical or semi-analytical methods. Such analytical or semi-analytical solutions are required for more advanced understanding of the physical problem under investigation and validation of more sophisticated numerical models. The practical value of these solutions lies in the fact that they aid to improve interpretations and conduct fast sensitivity analysis and fast computations.

In order to predict oil production the governing equations of heat and fluid flow in cylindrical coordinate need to be solved. Average temperatures in the formation during the steam injection process are calculated by solving the transient heat transfer equations. The heat transfer model is then coupled to a fluid in flow model to predict the fluid rates. The fluid inflow model is a two phase model that takes into account the relative permeability of oil and water. The developed model is validated with the fine grid numerical simulation of the problem using STARS® numerical simulator from CMG. Since, a lot of simplifying assumptions are involved modifications, such as a correction for the pressure drawn-down and water relative permeability, were made during the

history matching with STARS, in order to get a good match for the fluid rates. These modifications include altering the relative permeability of water and making an initial guess of the pressure draw down based on the results from the simulator. The robustness of the model was tested by comparing the model results with the results from the numerical simulator by changing various parameters such as: steam injection rates, reservoir permeability, relative permeability, oil viscosity and reservoir diffusivity.

With some reasonable assumptions, it is seen that the results from the developed model are very close to the results obtained using STARS numerical simulator from CMG and it can be concluded that the proposed model captures the essential mechanism of the process. The model is relatively simple and all the calculations can be performed using a user friendly spreadsheet in just a few minutes. Currently, the proposed model can be used to optimize production from a single well. The model can be coupled with an economic model to optimize steam injection rates and production rates based on the reservoir properties.

Acknowledgements

First of all, I would like to express my sincere appreciation to my supervisor, Dr. Hassan Hassanzadeh, for his outstanding support, constant guidance, and encouragement, throughout the course of this research and my master's program at the University of Calgary. It has truly been a great privilege for me to work with him. Without his support and help, this work would not be accomplished.

I am also grateful to the members of my thesis committee, Dr. Sudarshan A Mehta, Dr. Brij Maini, and Dr. Abdulmajeed Mohamad, for taking time out of their busy schedule to read my thesis and for their valuable comments. My gratitude also goes to the Department of Chemical and Petroleum Engineering at the University of Calgary and PennWest Exploration for their financial support. I would like to acknowledge Majid Saeedi, without whom the project would not have been successful.

I am thankful to my friends and fellow graduate students for their support and help during my research.

Last but most importantly, I thank my parents for the encouragement and continuous support they have given me all the way.

Table of Contents

Abstract i
Acknowledgements iii
Table of Contents iv
List of Tables vii
List of Figures viii
Nomenclature xiii

1 INTRODUCTION 1

1.1 Typical Reservoir Properties 1
1.2 Thermal Recovery Methods 2
1.2.1 In situ combustion 2
1.2.2 Cyclic steam stimulation 3
1.2.3 Wellbore heating 5
1.2.4 Steam flooding 5
1.2.5 Hot water flooding 5
1.2.6 Steam assisted gravity drainage 5
1.3 Motivations and Objectives 5
1.4 Organization of Thesis 6

2 LITERATURE REVIEW 8

2.1 Existing CSS and Horizontal Well Models 8
2.1.1 Cyclic steam injection using vertical wells 8
2.1.2 Models for pressure depleted gravity drainage reservoirs 15
2.1.3 In-flow equations for horizontal wells: 17
2.1.4 Cyclic steam stimulation using horizontal wells 20
2.2 Concluding Remarks 23

3 ANALYTICAL MODELING 24

3.1 Cyclic Steam Stimulation for Horizontal wells 24
3.1.1 Model assumptions 25
3.1.2 Volume of steam zone 25
3.1.3 Heat remaining in the reservoir 26
3.1.4 Average steam zone temperature: 27
3.1.5 Oil and water viscosities 34
3.1.6 Fluid saturations and relative permeabilities 34
3.1.7 Fluid- inflow equation 35
3.1.8 Flow chart showing important steps in calculations 37
3.2 Summary 39

4 VALIDATION OF THE MODEL AND SENSITIVITY ANALYSES 40

4.1 Base Case 40
4.1.1 Input data 40
4.1.2 Relative permeability model 42
4.1.3 Relative permeability adjustment 43
4.1.4 Pressure drop model and inflow equation 45
4.2 Sensitivity Analyses 49
4.2.1 Grid sensitivity 50
4.2.2 Steam injection rates 53
4.2.3 Length of horizontal well 57
4.2.4 Absolute permeability 60
4.2.5 Relative permeability of oil and water 65
4.2.6 Thermal diffusivity 68
4.2.7 Types of oil viscosity 71
4.2.8 Number of cycles 73
4.3 Summary 78

5 CONCLUSIONS AND RECOMMENDATIONS 79

5.1 Results 79
5.2 Future Work 80
5.2.1 Economic studies 80
5.2.2 Pressure drop model and water relative permeability adjustment 80

APPENDIX 81
REFERENCES 85

List of Tables

Table 1.1: Definitions of heavy oil based on properties 1

Table 3.1 Reservoir parameters and PVT data 32

Table 3.2 Operational parameters 33

Table 4.1 Operational parameters 40

Table 4.2 Reservoir parameters and PVT data 41

Table 4.3 Viscosity data 41

Table 4.4 Model dimensions and grid data 41

List of Figures

Figure 1.1: A typical cyclic steam injection process 4

Figure 2.1: Plot of F_1 versus dimensionless time (after Marx- Langenheim)..... 10

Figure 2.2: A Schematic diagram representing heat transfer and fluid flow 12

Figure 2.3: $\overline{V}_r$ and $\overline{V}_Z$ versus dimensionless time (after Boberg and Lantz). 13

Figure 2.4 a) Schematic diagram of heated area geometry; b) differential element of the heated area. 21

Figure 2.5: Schematic diagram of area of cross section of heated area. 22

Figure 3.1: Schematic diagram of model 28

Figure 3.2: A plot of dimensionless temperature of Zone 1 and Zone 2 versus dimensionless time..... 31

Figure 3.3: A plot of the average temperature of Zone 1 and Zone 2 versus time 32

Figure 3.4: Volume and radius of steam zone for three cycles..... 33

Figure 3.5: Plot of the average steam zone temperature versus time for three cycles 34

Figure 4.1: Oil and water relative permeabilities..... 42

Figure 4.2: Water saturations in the heated zone obtained from developed model and STARS 43

Figure 4.3: Oil relative permeability obtained from developed model and STARS 44

Figure 4.4: Water relative permeability obtained from developed model and STARS 44

Figure 4.5: Comparison of oil production rate, q_o, obtained from the model versus STARS simulator. 47

Figure 4.6: Comparison of cumulative oil production, Q_o, from the model versus STARS. 47

Figure 4.7: Comparison of water rate, q_w, obtained from model versus STARS simulator 48

Figure 4.8: Comparison of cumulative water production, Q_w, from the model versus STARS. 49

Figure 4.9: Plot of oil production rate, q_o, versus time for different grid sizes. 51

Figure 4.10: Plot of cumulative oil production, Q_o, versus time for different grid sizes.. 51

Figure 4.11: Plot of water production rates, q_w, versus time for different grid sizes..... 52

Figure 4.12: Plot of cumulative water production, Q_w, versus time for different grid sizes. 52

Figure 4.13: Comparison of oil production rates from STARS and model for a steam injection rate of 1800 bpd. 54

Figure 4.14: Comparison of oil production rates from STARS and model for a steam injection rate of 2500 bpd. 54

Figure 4.15: Comparison of oil rate from STARS and model for steam injection rate of 3000 bpd..... 55

Figure 4.16: Cumulative oil production versus time for different steam injection rates. . 55

Figure 4.17: Comparison of water production rate from STARS and model for different steam injection rates..... 56

Figure 4.18: Comparison of cumulative water production obtained from STARS and analytical model for different steam injection rates..... 56

Figure 4.19: Comparison of oil rates from STARS and model for a well length of 1000ft. 57

Figure 4.20: Comparison of oil production rates from STARS and model for a well length of 1250ft. 58

Figure 4.21: Cumulative oil production versus time for different lengths of the horizontal well. 58

Figure 4.22: Comparison of water production rate from STARS and model for different horizontal well lengths. 59

Figure 4.23: Comparison of cumulative water production from STARS and model for different lengths of horizontal well. 59

Figure 4.24: Comparison of oil rate from STARS and model for absolute permeability of 150 mD. 60

Figure 4.25: Comparison of oil rate from STARS and model for absolute permeability of 200 mD. 61

Figure 4.26: Comparison of cumulative oil production versus time from, STARS and developed model, for different absolute permeability values. 61

Figure 4.27: Comparison of water production rate versus time, form STARS and developed model, for different absolute permeability values. 62

Figure 4.28: Comparison of cumulative water production versus time, from STARS and developed model, for different absolute permeability values. 62

Figure 4.29: Plot of oil production rate, q_o, obtained from STARS and analytical model for a permeability of 1000 mD. 63

Figure 4.30: Plot of cumulative oil production, Q_o, obtained from STARS and analytical model for a permeability of 1000 mD. 64

Figure 4.31: Plot of water production rate, Q_w, obtained from STARS and analytical model for a permeability of 1000 mD. 64

Figure 4.32: Plot of cumulative water production, Q_w, obtained from STARS and analytical model for a permeability of 1000 mD. 65

Figure 4.33: Different types of relative permeability curves versus water saturation. 66

Figure 4.34: Comparison of oil production rate versus time, from STARS and developed model, for a different relative permeability model. 66

Figure 4.35: Comparison of cumulative oil production versus time, from STARS and developed model, for different relative permeability curves. 67

Figure 4.36: Comparison of water production rate versus time, from STARS and developed model, for a different relative permeability model. 67

Figure 4.37: Comparison of cumulative water production versus time, from STARS and developed model, for a different relative permeability model. 68

Figure 4.38: Comparison of oil rate versus time, from STARS and developed model, for a new diffusivity value. 69

Figure 4.39: Comparison of cumulative oil production versus time, form STARS and developed model, for a different thermal diffusivity value. 69

Figure 4.40: Comparison of water production rates versus time, form STARS and developed model, for a different thermal diffusivity value. 70

Figure 4.41: Comparison of cumulative water production versus time, from STARS and developed model, for different thermal diffusivities. 70

Figure 4.42: Comparison of oil rate versus time, from STARS and developed model, for PennWest oil viscosity. 71

Figure 4.43: Comparison of cumulative oil production versus time, from STARS and developed model, for different types of oil- viscosity. 72

Figure 4.44: Comparison of water production rate versus time, from STARS and model, for PennWest oil viscosity. 72

Figure 4.45: Comparison of cumulative water production versus time, from STARS and developed model, for PennWest oil viscosity. 73

Figure 4.46: Comparison of oil production rate versus time, from STARS and developed model, for ten cycles. 74

Figure 4.47: Comparison of cumulative oil production versus time, from STARS and developed model, for ten cycles. 74

Figure 4.48: Comparison of water production rate versus time, from STARS and developed model, for ten cycles. 75

Figure 4.49: Comparison of cumulative water production versus time, obtained from STARS and developed model, for ten cycles. 75

Figure 4.50: Plot of cumulative steam oil ratio versus time 77

Figure 4.51: Plot of average steam oil ratio versus the number of cycles 77

Nomenclature

Symbols

$A(t)$	Heated zone area at any time t, ft^2
C_r	Dry rock specific heat, Btu/ lb- ^oF
C_w	Specific heat of water, Btu/ ft-hr- ^oF
C_o	Oil specific heat, Btu/ ft-hr- ^oF
D	Over-burden thermal diffusivity, ft^3/hr
f_{sdh}	Down-hole steam quality
h	Pay thickness, ft
h_w	Enthalpy of water, Btu/lb
H_o	Heat injection rate, Btu/ hr
H_{last}	Heat remaining in the reservoir from the previous cycle, Btu
k	Absolute permeability of the reservoir rock
k_x	Reservoir permeability in x-direction
k_y	Reservoir permeability if y-direciton
k_{ro}	Relative permeability to oil
k_{rw}	Relative permeability to water
K	Over-burden thermal conductivity, Btu/ ft-hr- ^oF
L	Length of horizontal well, ft
L_{vdh}	Latent heat of vaporization, Btu/lb

M	Heat capacity, Btu/ ft^3-^oF
P_w	Producing bottom-hole pressure, psia
P_{wv}	Saturated vapor pressure of water at T_{avg}, psia
q_o	Oil production rate, Bpd
q_w	Water production rate, Bpd
Q_i	Heat injected per unit mass of steam, Btu/lb
Q_o	Cumulative oil produced, Bbl
Q_s	Steam injection rate, Bpd
Q_w	Cumulative water produced, Bbl
r	Radius, ft
r_h	Radius of steam zone, ft
r_e	Reservoir radius, ft
R_g	Gas oil ratio, scf/ bbl
R_{wv}	Water produced in the vapor state per stock tank bbl oil produced
s_o	Oil saturation
s_w	$_W$ater saturation
s_w	water saturation
s_{wir}	irreducible water saturation
s_{orw}	residual oil saturation to water
t	Time, days
t_{inj}	Injection time, days

T	Temperature, ^{o}F
T_S	Steam temperature, ^{o}F
T_R	Reservoir temperature, ^{o}F
T_{Avg}	Average steam zone temperature, ^{o}F
$\overline{V}_r$	Dimensionless heat loss in radial direction
$\overline{V}_z$	Dimensionless heat loss in vertical direction
V_s	Volume of steam zone, ft^3
W_p	Cumulative water produced, Bbl
WIP	Water-in-place, Bbl
α	Reservoir thermal diffusivity, ft^2/hr
μ_o	Viscosity of oil, cp
μ_{oh}	Viscosity of oil in the heated zone, cp
μ_{oc}	Viscosity of oil in the cold zone, cp
μ_w	Viscosity of water, cp
μ_{wh}	Visocisty of water in the heated zone, cp
μ_{wc}	Viscosity of water in the cold zone, cp
Δp	Pressure drawdown, psi
ϕ	Formation porosity
ρ_r	Rock grain density, lb/ft^3
ρ_w	Water density, lb/ft^3

ρ_o	Oil density, lb/ft^3
ρ_w	Density of water, lb/ft^3
ρc_t	Volumetric heat capacity of the reservoir rock, Btu/ft^3-^{o}F
δ	Dimensionless heat loss due to the produced hot fluids

Subscripts

1	Zone 1
2	Zone 2
Avg.	Average
h	heated zone boundary
o	Oil
w	Water
R	Reservoir
S	Steam

CHAPTER ONE:

1 Introduction

Heavy oil and oil sands are important hydrocarbon resources that play an important role in the oil supply of the world, and North America particularly. Oil sands account for one fourth of the oil production of Canada[1]. The resource base of heavy oil and oil sands is much larger than the in-place conventional oil. Conventional oils have an API gravity of 25^{o} or higher. Heavy oil and oil (tar) sands are petroleum or petroleum-like liquids or semi-solids occurring in porous formations, mainly sands and also carbonates. The definitions, according to 1982 UNITAR conference is summarized below:

Table 1.1: Definitions of heavy oil based on properties

Classification	Viscosity (cp at Res. Temp.)	Density at $15^{o}C$ (kg/m^3)	API Gravity
Heavy Crude	100-10000	943-1000	20-10
Oil Sand Crude (Bitumen)	>10000	1000	<10

1.1 Typical Reservoir Properties

Most of the heavy oil and bitumen occur in shallow (around 1000 m), high permeability (One to several Darcies), highly porous (30%), and poorly consolidated formations. The

oil saturation is generally high (typically greater than 50% pore volume) and the formation thickness may range from 10 to hundreds of meters[1]. However, there are some exceptions as well. For example, in Saskatchewan, 85% of the oil occurs in formations of less than 3 m thickness. Most heavy oils in California and Venezuela have viscosities in the range of 1000-2000 m.Pa.s whereas; those in Cold Lake, Alberta is around 100,000 m.Pa.s. The temperatures in the heavy oil reservoirs of Canada are very low, for example, around 15-20^{o}C at the depths of around 500 m[1].

1.2 Thermal Recovery Methods

Thermal methods aim to reduce the viscosity of oil by application of heat. This can be achieved by either hot fluid injection or by in- situ combustion. The thermal processes currently used are briefly reviewed in the following.

1.2.1 In situ combustion

The process is applicable for a wide range of oil gravities. In-situ combustion can be classified into: i) Forward Dry combustion, ii) Forward Wet Combustion and iii) Reverse Combustion. Forward dry combustion involves injection of oxygen rich air, ignition within the oil sand, and propagation of a combustion front through the reservoir. Oil is displaced by hot gas (nitrogen and carbon dioxide) passing ahead of the combustion front and by steam obtained from the combustion process and vaporization of the connate water. Forward wet combustion involves simultaneous injection of air and water. Theoretically, it should be the most efficient of all thermal drive processes as it has mechanisms of both a steam drive and dry- combustion drive process. However, in practice, gravitational forces cause separation of air and water, and the process is very difficult to control. The challenges of predicting the field performance of air injection projects using laboratory and numerical modeling has been addressed by Gutierrez et al.[2]. They proposed that an optimum design cycle can be obtained by performing laboratory testing that would help in the design and monitoring of a pilot scale field operation. The data from pilot operation, as well as laboratory data can be used to history match and fine tune the analytical models for prediction of the full field operation.

In reverse combustion, air flow is counter to the direction of the combustion front. Air is injected until there is a communication with the procuring wells and then using a downhole heater to ignite the oil sand around the producing well. The combustion front burns back towards the injection well. However, this process has been unsuccessful in the field.

1.2.2 Cyclic steam stimulation

This technique is by far the most popular[3] thermal stimulation process and will be discussed in great detail in this thesis. Steam is injected into a formation at high rates for several weeks through a vertical well. The well is then shut-in for a certain period of time, which is called "soak" period. Steam condenses in the formation, thus heating the reservoir rock and fluids around the wellbore. During this period the oil viscosity is reduced by many times. The amount of oil produced in a cyclic steam injection process depends largely on the how much the viscosity of oil is reduced, which is controlled by the amount of heat that is transferred from the injected steam to the reservoir. The heated sand contains mobilized oil, steam and water. The oil and other fluids are expelled out as the sand face pressure is lowered when the well is put on production. Oil is produced until the well reaches an economic limit and the cycle is repeated again. A typical CSS process is shown in Figure 1.1

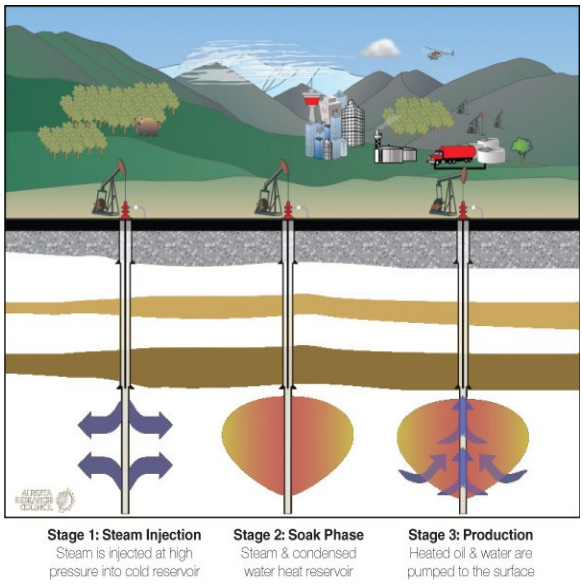

Figure 1.1: A typical cyclic steam injection process[4]

There are several mechanics of oil production during this process. In high pressure reservoirs, oil is produced at higher rates due to the availability of the driving force, increase in oil mobility as a result of decreased viscosity. Gravity drainage is also a significant mechanism in thick formations, pressure depleted reservoirs. The low density phase i.e., steam, in this case, displaces the oil as it drains. Another mechanism is the compaction drive, which is seen in Bolivar Coast in Western Venezuela. As the pore pressure falls, there is a consolidation in the reservoir rock, which results in decrease in average porosity, and hence, oil is squeezed out from the porous rock. Another significant mechanism which is the key to success in Cold Lake is formation fracturing. Steam is injected at fracture pressure creating fractures in the formation and resulting in increase in the productivity of the reservoir. A part of the injected energy is stored in the form of potential energy by lifting the ground at the surface. When the well is put on production, the fluids are squeezed out of the formation[5].

1.2.3 Wellbore heating

Down-hole electrical, gas, and steam heaters have been used to improve the mobility of oil in the near vicinity of the well bore.[6] Though steam stimulation offers much deeper heat penetration and much greater stimulation effect, wellbore heating is sometimes used for low production rate wells where depth, excessive injection pressure or swelling clays prevent the application of steam. Well-bore heating techniques have a potential to be used in the recovery of oil shale, where steam injection is not possible because of extremely low permeability of the reservoir.

1.2.4 Steam flooding

The main advantage of this multi well pattern type method is its large areal coverage and high recovery factor (around 50%). However, this method has drawbacks such as high heat losses and long payout times and high expenditure.[1]

1.2.5 Hot water flooding

In this method, heat losses in the wellbore and formation cause a large drop in temperature and is less effective in reducing the oil viscosity. However, this process can be applied in deep heavy oil reservoirs where steam may not be very successful. Hot water flooding is used in Kaparuk filed in Alaska.[1]

1.2.6 Steam assisted gravity drainage

In this process, a pair of horizontal wells is drilled at a certain vertical distance near the base of the formation. Steam is injected into the upper well. Steam rises up in the formation and forms a steam chamber that heats the oil at the interface. The steam chamber grows upwards and laterally, as oil is mobilized and produced, along with condensed water, is produced from the lower well. This process is sensitive to geology and extremely effective in highly viscous oil formations[1].

1.3 Motivations and Objectives

Traditionally, vertical wells have been utilized in the majority of the cyclic steam stimulation projects. However, since CSS with vertical well configuration may not be efficient in thin formations, application of horizontal wells becomes inevitable as the

industry is moving toward production from such formations. Horizontal well technology provides a more efficient access to oil resources that are not recoverable using vertical wells. In general, horizontal wells have better injectivity, and their productivity is higher than vertical wells draining the same volume of reservoir. For a given reservoir, a horizontal well has a higher contact area than a vertical well and hence, the heated zone around a horizontal well will be larger than that of a vertical well. Hence, cyclic steam stimulation using horizontal wells can be very useful in thin-heavy oil reservoirs.

Empirical correlations are very helpful to correlate data within a field for predicting the performance of new wells in that field. Compositional or black-oil thermal reservoir simulators can be used to predict the performance of cyclic steam stimulation. These thermal models are based on mass and heat balance equations. Fluid flow is related to pressure gradient through the concept of relative permeability. In addition, a thermal model is sensitive to input data such as rock properties, fluid properties and geological features that are often not known or available. Also, because of the complex nature of the cyclic steam stimulation process, it could be very difficult and expensive to use thermal reservoir simulators. Hence, an analytical model of cyclic steam injection might be useful to describe basic features of reservoir heating and oil production.

Analytical or semi-analytical models with reasonable assumptions need to be developed to better understand the shape of steam zone during steam injection, to calculate the oil production rate, and also optimize the process based on process variables studies. The objective of this study is to develop analytical models that can predict the performance of a cyclic steam stimulation process for a horizontal well configuration.

1.4 Organization of Thesis

The outline for the remainder of this thesis is as follows:

Chapter 2 reviews the relevant literature on the existing models for a cyclic steam stimulation process. Heat transfer models as well as fluid in flow models for horizontal wells are reviewed.

Chapter 3 describes the analytical model developed in this study that is able to simulate heat transfer and fluid flow and outlines the steps to perform the calculations for predicting oil and water flow rates for a CSS process with a horizontal well configuration.

Chapter 4 presents the simulation studies of CSS process using the thermal simulator STARS by CMG. Sensitivity analysis has been performed and the model is validated for an expected range of parameters. A comparison of the results obtained from the developed analytical model and results from simulation are presented in this chapter.

Finally, Chapter 5 presents conclusions of this thesis and makes recommendations for future works.

CHAPTER TWO:

2 Literature Review

2.1 Existing CSS and Horizontal Well Models

Existing models can be divided into four categories: i) cyclic steam injection using vertical wells, ii) models for pressure depleted gravity drainage reservoirs, iii) in-flow equations for productivity of horizontal wells and iv) cyclic steam injection using horizontal wells.

2.1.1 Cyclic steam injection using vertical wells

Steam is injected at a fixed rate and a known well-head quality. As the steam enters the reservoir, there is some heat loss in the wellbore. The amount of heat reaching the reservoir during the steam injection is essentially a function of the steam injection temperature and well-bore heat losses. The bottom hole steam quality and pressure can be predicted from a wellbore model as described by Fontilla and Aziz[7]. Marx and Langenheim[8] described a method for estimating thermal invasion rates, cumulative heated area, and theoretical economic limits for sustained hot fluid injection at a constant rate into an idealized reservoir. Full allowance is made for non-productive reservoir heat losses. The method is very simplistic and does not require extensive mathematical calculations.

The heated zone area $A(t)$, at any time t, can be calculated using the method described by Marx-Langenheim[8] (Equation. 2.1).

$$A(t) = \frac{H_o MhD}{4K^2(T_S - T_R)} F \tag{2.1}$$

$$F_1 = e^{t_d} ercf\sqrt{t_d} + 2\sqrt{\frac{t_d}{\pi} - 1} \tag{2.2}$$

t_d is dimensionless time, which is defined as

$$t_d = \frac{4K^2}{M^2 h^2 D} t \tag{2.3}$$

where,

$A(t)$	=	heated zone area at any time t, ft^2
H_o	=	heat injection rate, Btu/ hr
M	=	heat capacity, $[(1-\phi)\rho_r C_r + S_w\phi\rho_w C_w + S_o\phi\rho_o C_o]$, Btu/ ft^3-^oF
h	=	pay thickness, ft
D	=	over-burden thermal diffusivity, ft^3/hr
K	=	over-burden thermal conductivity, Btu/ ft-hr-^oF
T_s	=	steam temperature, ^oF
T_r	=	reservoir temperature, ^oF
ϕ	=	formation porosity
ρ_r	=	rock grain density, lb/ft^3
ρ_w	=	water density, lb/ft^3
ρ_0	=	oil density, lb/ft^3
C_r	=	dry rock specific heat, Btu/ lb-^oF
C_w	=	water specific heat, Btu/ ft-hr-^oF

C_o = oil specific heat, Btu/ ft-hr- ^oF

S_o, S_w = initial oil and water saturations, respectively

t = time since the start of injection, hours

Figure 2.1 shows a plot of F_1 vs. t_d and it can be used to calculate the values of F_1.

$$F_1 = e^{t_d} erfc\sqrt{t_d} + 2\sqrt{\frac{t_d}{\pi}} - 1$$

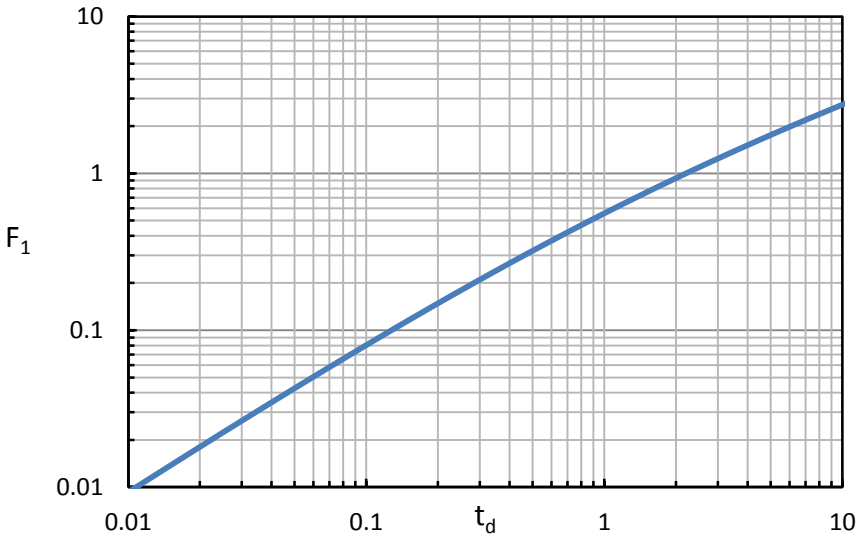

Figure 2.1: Plot of F_1 versus dimensionless time (after Marx- Langenheim[4])

During the injection period the temperature gradient of the hot zone can be estimated using Marx and Langenheim's equation[4]

$$\frac{dT}{dr} = \frac{H_o\left(e^{t_d^2} erfc(t_d)\right)}{2\pi rhk} \qquad (2.4)$$

The solution for the heated area is based on the fluid flow analogy by Carter[9], does not depend upon the direction of development of the heated area and hence, can be applied for heat injection in any type of well pattern with any specified swept area. For a vertical well, assuming a cylindrical heated area, the radius of the heated zone can easily be calculated using the above equations.

Boberg and Lantz[10] developed the first analytical model of cyclic steam stimulation for a vertical well. They considered the reservoir pressure as the main driving mechanism for oil production, ignoring the gravity drainage. The steam zone is assumed to propagate radially outward from the wellbore during the steam injection. Radius of the steam zone is based on the model developed by Marx and Langenheim[8]. During the soak and production period, an average temperature is calculated taking into account the heat losses in vertical direction (both overburden and under-burden), heat losses in radial direction (i.e., outlying cold sand) and heat losses of production of hot fluids. A schematic diagram representing the heat transfer and the fluid flow considered in the model is shown in Fig. 2.2

It is assumed that oil sands are invaded by steam radially and uniformly. After steam injection is stopped, the oil sands start to cool down because of conduction, and the unheated shale and oil sand beyond $r>r_h$ begin to warm. To calculate the oil production rate, an idealized step function temperature distribution in the reservoir is assumed where the original temperature exists for $r> r_h$ and an average elevated temperature exists for $r< r_h$. The average temperate in the heated sand region is computed as a function of time, and from the average temperature the oil viscosity is determined, from which oil production rate can be calculated using a steady state radial flow equations.

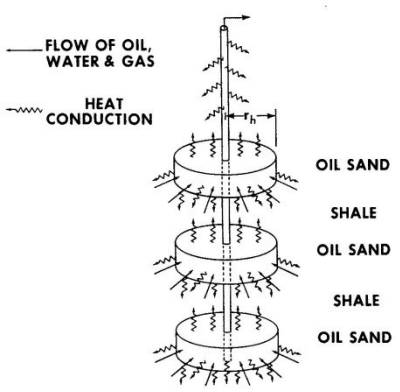

Figure 2.2: A Schematic diagram representing heat transfer and fluid flow[10]

2.1.1.1 Calculation of average temperature in the steam chamber:

Temperature of the heated region $r_w < r < r_h$:

The average temperature of the heated region T_{avg}, after the injection period, is given by

$$T_{avg} = T_R + (T_S - T_R)\left[\overline{V}_r \overline{V}_z (1-\delta) - \delta\right], \text{ °F} \tag{2.5}$$

where,

δ accounts for the heat loss due to the produced hot fluids. $\overline{V}_r$ and $\overline{V}_Z$ represent heat losses in radial and vertical direction, respectively and are represented graphically as functions of dimensionless time and can be read from Figure 2.3.

The energy removed from the produced hot fluids, δ is given by

$$\delta = \frac{1}{2}\int_{t_i}^{t} \frac{H_f dt}{Z\pi r_h^2 (\rho c)_1 (T_S - T_R)} \tag{2.6}$$

where,

$$Z = \sum_{i=1}^{N_S} \overline{h}_i \tag{2.7}$$

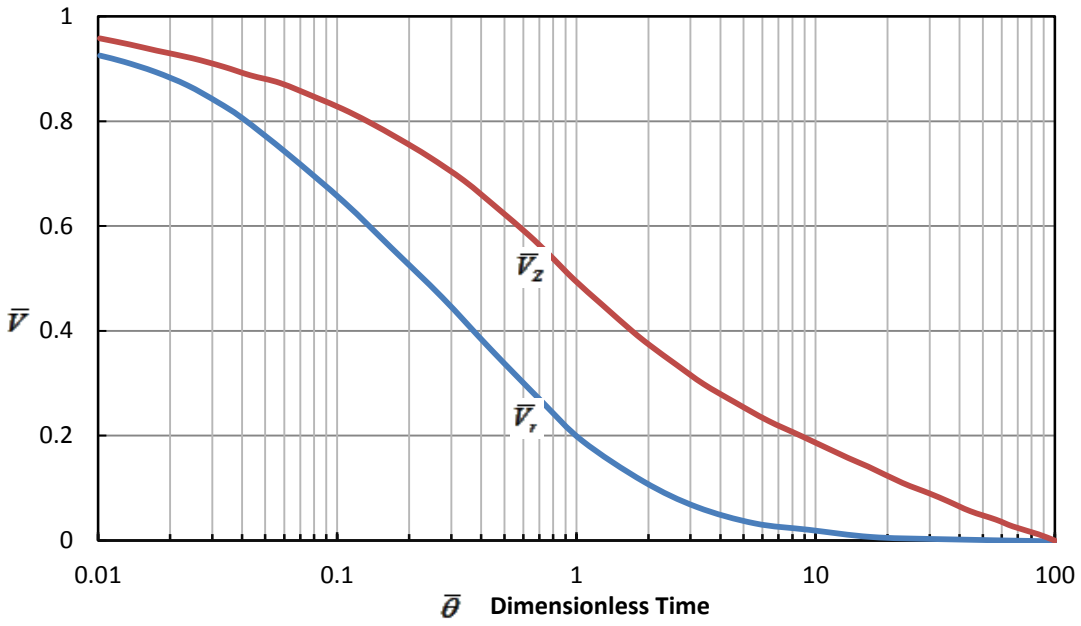

Figure 2.3: $\bar{V}_r$ and $\bar{V}_Z$ versus dimensionless time (after Boberg and Lantz [6]).

H_f = Rate at which energy is removed from the formation with the produced fluids at time t, in Btu/D

$H_f = q_{oh}(H_{og} + H_w)$, Btu/D (2.8)

where,

$$H_{og} = \left[5.615\rho_o c_o + R_g \rho_g c_g\right]\left(T_{Avg.} - T_R\right), \text{ Btu/ STB oil}$$

$$H_w = 5.625\rho_w\left[WOR\left(h_f - h_r\right) + R_{wv}h_{fg}\right], \text{ Btu/STB oil}$$

H_{og} = Heat removed from the formation by the produced oil and gas

H_w = Heat removed from the formation by produced water

R_g = GOR, scf/ bbl

R_{wv} = water produced in the vapor state per stock tank bbl oil produced

$$R_{wv} = 0.0001356\left(\frac{P_{wv}}{P_w - P_{wv}}\right) Rg, \quad \frac{\text{bbl liquid water at } 60\,^0\text{F}}{\text{bbl} - \text{stock tank oil}}$$

P_w = Producing bottom-hole pressure, psia

P_{wv} = Saturated vapor pressure of water at T_{avg}, psia

when $P_w > P_{wv}$ and $R_{wv} < R_w$, $R_{wv} = R_w$

when $P_{wv} > P_w$, and if R_{wv} calculated is greater than R_w, then $R_{wv} = R_w$

The main drawback of this method is that they made an assumption that steady state flow exists from the start of the production. However, in reality, transient flow prevails at an early stage, and thus this method predicts the oil production rate, which is less than the actual production rate. Also, this method is limited to use in reservoirs with relatively light oil and high primary productivity.

Later, Bensten and Donohue[11] developed a model where they used the transient flow model to calculate oil rate. They assumed that transient flow occurs until the rate predicted by the steady state model is greater than that predicted by transient model.

Bidner and Kostiria[12] proposed a modification to the Bensten and Donohue's[10] model that consists of numerically solving the diffusivity equation for transient radial flow for different outer boundary conditions. The reservoir is divided into two concentric cylinders. The zone extending from the well bore to the heated radius is called the hot zone. The outer zone, from the heated radius to the drainage radius is called the cold zone. Temperature during the injection period is calculated using the Marx- Langenheim[8] model. Temperature during the soak period and production period is estimated using the method, as described by Boberg and Lantz[10].

The advantages of this model over the Bensten and Donohue[10] model are that: 1) arbitrary definitions dividing transient and steady state flow are unnecessary; 2) van Everdingen and Hurst's[13] tables can be avoided; 3) pressure distribution as a function of radius and time can be found. The main application of this method is to calculate the oil production for different flowing well conditions (inner boundary conditions) in terms of the Flowing Bottom Hole Pressure (FBHP); or flow rate as a function of time for

different outer boundary conditions (i.e. no flow, constant pressure, and infinite medium). The pressure variation at the cold/hot interface is calculated at each time step. However, steady state radial flow solutions are used to calculate the oil production, at each time-step.

2.1.2 Models for pressure depleted gravity drainage reservoirs

Towson and Boberg[14] predicted gravity drainage production rates using a semi-steady state model developed by Mathews and Leftkovits[15]. They used the following equation in conjugation with the equation used in the Boberg and Lantz[6] i.e., radial model to calculate the q_{oh} and choose the larger of the two values.

$$q_{oh} = \frac{\pi k \rho_o g (h_h^2 - h_w^2)}{\mu_o \left(\ln\left(\frac{r_h}{r_w}\right) - \frac{1}{2} \right)} \tag{2.9}$$

where,

h_h = height of oil column

h_w = fluid level in the well

They presented an equation to calculate h_h at each time step. They assumed that the average temperature in the steam zone varied with time and the temperature outside the steam zone is maintained at the original reservoir temperature.

Seba and Perry[16] developed a model addressing gravity drainage phenomenon. They made some limiting assumptions, such as, constant hot zone radius and temperature and harmonic decline in oil production, which limits the application of the model to only a specific set of parameters. The model developed by Kuo et al.[17] predicts the production performance of steam soak process in which oil is produced by gravity drainage. They found out that the largest improvement in the cumulative oil production is achieved when the hot zone radius is less than one-quarter of the outer drainage radius. However, this model does not consider the performance of individual steam-soak cycles.

The amount of heat reaching the reservoir depends upon the injection temperature, injection pressure, surface steam quality and well-bore heat losses. These injection parameters were not calculated in the previous models[7,8,14]. Jones[18] presented a simple cyclic steam model for gravity drainage in pressure depleted heavy–oil reservoirs. Boberg and Lantz[6] procedure was used as the basis for the reservoir shape and temperature calculations versus time. Here, the only driving force assumed is gravity, and hence, the model tends to calculate lower initial oil rates than observed in the field. They used some empirical factors to match the measured values.

Butler et al.[19] developed an analytical model for gravity-drainage of heavy-oils during in situ steam heating, the Steam Assisted Gravity Drainage (SAGD) method. In SAGD pattern, two horizontal wells are used i.e., a horizontal injector above a horizontal producer. The method described consists of an expanding steam zone as a result of steam injection into the upper injector and production of oil through the producer below via the mechanism of gravity-drainage along the steam/oil interface of the expanding steam chamber. As the oil is removed from the steam chamber, more space is left in the reservoir for the steam to flow in. The steam chamber thus grows upwards and sideways such that the steam zone has a shape of an inverted triangle in the vertical cross sectional view.

Oil flow rate is derived starting from Darcy's law. Heat transfer takes into account the thermal diffusivity of the reservoir and it is proportional to the square root of the driving force. In the case of an infinite reservoir, an analytical dimensionless expression is derived that describes the position of the interface. When the outer boundary of the reservoir is considered, the position of the interface and the oil rate are calculated numerically. Oil production rate scales with the square root of the height of the steam chamber. An equation describing the growth of the steam chamber is also presented. The method is limited to gravity-drainage and linear flow of heavy oil from horizontal wells.

Gontigo and Aziz[20] used a similar approach for radial flow to vertical wells. The following assumptions were made: 1) steam occupies a conical volume; 2) oil is mobilized in a thin layer below the steam-oil interface; 3) pseudo-steady state flow inside the heated zone; 4) the flow potential is a combination of pressure drop and gravity

forces; 5) pressure drawdown is based on the steam pressure and the average temperature in the heated zone. They solved a combined Darcy flow and a heat conduction problem. Heat remaining in the formation from the previous cycles was included.

The average temperature of the steam zone (T_{avg}) is calculated using Boberg and Lantz[10] model; however, a simple method to calculate the heat losses, using some reasonable approximations, applicable to conical steam zone shape, was presented. Details on the calculation of the heat loss parameters can be found in the paper[15]. Further details on calculating the oil and water viscosities, fluid saturations and relative permeabilities are also presented in the paper.

The model by Gonzito and Aziz[20] is easy to use and seems to be an ideal choice for calculating the well performance under cyclic steam stimulation process. However, a scaling factor had to be introduced to obtain a good match. The above mentioned gravity drainage models cannot be used for a horizontal well CSS process because of the significant difference in the physical mechanism of the process. Though the approach is essentially the same, a different model will apply for calculating the fluid flow rate. Hence, we need to review some models to calculate the fluid flow rate in horizontal wells.

2.1.3 In-flow equations for horizontal wells:

Several models are available in the literature to calculate the steady- state flow rate in horizontal wells. The steady state analytical solutions assume that pressure at any point in the reservoir does not change with time. In practice, this may not be true for most reservoirs but steady state solutions are used widely as they are easy to derive analytically and the steady state results can be easily verified in a laboratory using physical models. Borisov[21] developed an equation to calculate the steady state oil production for a horizontal well however. Later, using Borisov's equation Giger[22] and Giger et al.[23] presented reservoir engineering aspects of horizontal wells. Renard and Dupuy[24] have also reported a similar solution. These solutions in generalized units are given below:

Borisov[21]

$$q_h = \frac{2\pi k_h h \Delta p / (\mu_o B_o)}{\ln\left[(4r_{eh}/L)\right] + (h/L)\ln\left[h/(2\pi r_w)\right]} \tag{2.10}$$

Giger[22]

$$q_h = \frac{2\pi k_h L \Delta p / (\mu_o B_o)}{(L/h)\ln\left(\dfrac{1+\sqrt{1-\left[L/(2r_{eh})\right]^2}}{L/(2r_{eh})}\right) + \ln\left[h/(2\pi r_w)\right]} \tag{2.11}$$

Giger, Reiss & Jourdan[23]

$$J_h / J_v = \frac{\ln(r_{ev}/r_w)}{\ln\left[\left(\dfrac{1+\sqrt{1-\left[L/(2r_{eh})\right]^2}}{L/(2r_{eh})}\right)\right] + (h/L)\ln\left[h/(2\pi r_w)\right]} \tag{2.12}$$

Renard and Dupuy[24]

$$q_h = \frac{2\pi k_h \Delta p}{\mu_0 B_0}\left[\frac{1}{\cosh^{-1}(X) + (h/L)\ln\left[h/(2\pi r w)\right]}\right] \tag{2.13}$$

X = 2a/L for ellipsoidal drainage area

a = half of the major axis of drainage ellipse

Joshi[25] developed an equation to calculate the productivity of horizontal wells. To simplify the solution, he reduced the three dimensional problem to two 2-D problems and the solutions were added to calculate the oil production. An equation to include the horizontal well eccentricity was also presented. However, a basic assumption on the Joshi's inflow equation is that the well bore pressure is constant in the horizontal well. This assumption neglects the pressure drop in the horizontal well length, which could be very important[26].

Joshi's in-flow model[25]:

$$q_h = \frac{2\pi k_h \Delta p/(\mu_o B_o)}{\ln\left[\frac{a+\sqrt{a^2-(L/2)^2}}{L/2}\right]+(h/L)\ln[h/(2r_w)]} \tag{2.14}$$

$$a = L/2\left[0.5+\sqrt{0.25+(2r_{eh}/L)^4}\right]^{0.5} \tag{2.15}$$

In all the above equations, L represents the horizontal well length, h represents reservoir height, r_w represents wellbore radius, r_{ev} and r_{eh} represent drainage radius of vertical and horizontal wells, respectively. μ_o represents the oil viscosity and B_o is the oil formation volume factor, Δp is the pressure drop from the drainage boundary to the wellbore and q_h is flow rate of a horizontal well.

The prediction made by the model neglecting the frictional pressure drop can lead to very optimistic results, particularly in wells where there is a significant pressure drop along the well length. The pressure at the heel of the horizontal well could be less than the pressure at the toe of the well. The pressure drop in the wellbore is affected mainly by factors such as wellbore roughness, well length, fluid viscosity and the wellbore diameter.

Unlike Joshi's model, Dikken's[26] model includes the frictional pressure loss in the wellbore. Several other models were developed to compute the pressure loss in the wellbore[27,28,29,30]. The correlation developed by Archer and Agbongiator[31] is simple and can be used in combination with Joshi's model to correct the error in horizontal well productivity calculations made by neglecting the frictional pressure drop in the well bore.

In 2001, Lu[32] developed a model by solving a 3D Laplace equation instead of the 2D solution as used by Joshi. Inflow equations were derived for calculating productivity of horizontal wells located at the center as well as for off-centered wells. He compared this model with previous models using the data from Liu-Hua Reservoir in South China. For this particular reservoir, the newly developed formula was found to be more accurate than previous models. It was concluded that a 3D model should be used to get a reliable productivity formulae.

2.1.4 Cyclic steam stimulation using horizontal wells

Gravity drainage is a significant mechanism for displacing the heated oil into the wellbore for a horizontal well CSS process and critically, this mechanism has not been included in any of the models discussed above.

Gunadi[33] developed an analytical model for predicting oil production rates for cyclic steam stimulation process using horizontal wells, and verified it with experimental results. The model was divided into two sub-models. The first sub-model is used to calculate the length and radius of steam zone during injection. The injection period is divided into a number of equal time steps. The growth in radius of steam zone around each segment and the length of steam zone is calculated using material balance equations, Darcy's law and heat balance equations. The second sub-model calculates the average temperature and production rates during the soak and injection period. The heat losses to the formation during the soak period and the heat losses through liquid production are based on Boberg and Lantz[10] method. The liquid production is calculated based on a slightly modified form of Boberg and Lantz[10] method. Liquid production from hot zone (occupied by steam) and warm zone (not occupied by steam) are calculated separately, based on relative permeability to oil and water, water saturation, average temperature and reservoir pressure at each time step.

As verified with the experimental results, this model is more accurate for the horizontal well at the base of the formation than horizontal well at the center of the reservoir, This model may underestimate the production rate in the early stages, as it is based on Boberg and Latz[10] method, that considers steady state flow right from the start of production, whereas, in reality, transient flow conditions prevail in the beginning. Also, this model does not include gravity drainage effect, which would be very significant mechanism in the later cycles. Although this model is fairly consistent with the experimental results, further research should be conducted using a larger physical model to improve the accuracy of the model.

Diwan and Kovseck[34] developed an analytical model assuming that the steam zone adopts a triangular shape in cross section when it is injected near the bottom of the

formation through a horizontal well. Steam heats the colder oil sand near the condensation front. During production oil drains along the condensation surface by a combination of gravity and pressure difference into the production well as does steam condensate. In addition, oil drains through the steam chamber into the production well.

Reduction of oil viscosity as a result of an increase in the temperature greatly improves the production response. Heat losses were included to the overburden as well as to the adjacent unheated oil-bearing formation but they neglected the heat losses to the under-burden. The approach used is similar to Butler et al[35] gravity drainage of heavy-oil reservoirs subjected to steam injection in which the theory was directed to linear flow from horizontal wells. However, the steam zone shape was assumed to be a prism with triangular cross section and the horizontal well lies at the bottom edge, as shown in Figure 2.4 and Figure 2.5.

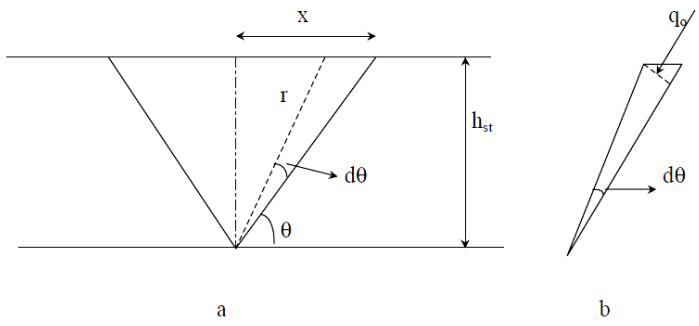

Figure 2.4 a) Schematic diagram of heated area geometry; b) differential element of the heated area.[27]

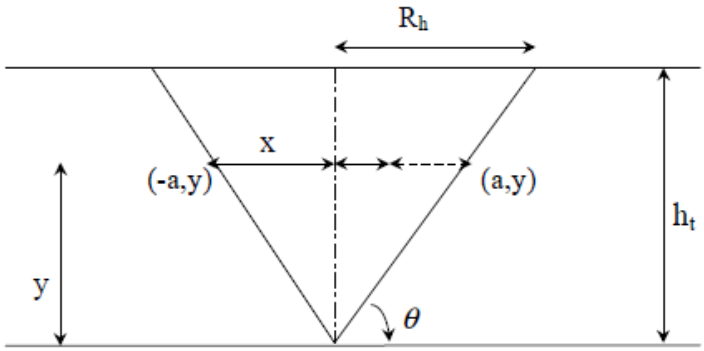

Figure 2.5: Schematic diagram of area of cross section of heated area. [27]

Wu et al.[36] presented a model to calculate the in-flow performance of a cyclic steam stimulated horizontal well under the influence of gravity drainage. The mechanisms of gravity drainage, pressure drawdown and two phase flow were included. The model couples the reservoir multi-phase flow and the frictional pressure loss in the wellbore. The basic assumptions that were made are that the reservoir is homogenous and isotropic with constant permeability and porosity. The horizontal well is approximated as a series of vertical wells and fluid flow from the reservoir into the wellbore is along the radial axis. It is further assumed that during the injection period steam forms a chamber in the shape of a cylinder. The assumption may not be valid if the reservoir is significantly anisotropic.

Further research should be carried out to determine the shape of the steam chamber to obtain accurate and reliable results. Also, this model presents an equation for horizontal well placed at the center of the reservoir. It would be necessary that the well be placed at the bottom of the reservoir so as to get the maximum advantage of the gravity drainage. However, it is possible that the placing a well at the bottom of the formation may increase the heat losses to the under-burden. Hence, it is advisable to place the well in such a location so as to optimize the heat losses as well as to get the maximum benefit from the gravity drainage mechanism.

2.2 Concluding Remarks

The available models use the Boberg and Lantz model for calculating the average temperatures in the steam zone. After reviewing the literature it was concluded that a new analytical model should to be developed that addresses the heat transfer phenomenon for a horizontal well during thermal recovery processes. The developed model can be verified by comparing it with direct numerical simulations or field test results, if available. To test the robustness of the model, sensitivity analysis to various operating and reservoir parameters should be conducted by testing the model with the parameters such as steam injection rates, thermal diffusivity, different types of oil (viscosity), relative permeability of oil and water, the length of the horizontal wellbore etc.

CHAPTER THREE:

3 Analytical Modeling

This chapter describes the development of a heat transfer model that is applicable for a cyclic steam stimulation process for horizontal wells. A radial heat transfer model was developed to predict the average temperature in the steam zone. To predict the fluid rates, a modified form of Joshi's inflow equation is used. The heat transfer model is coupled to the inflow model. Finally, detailed steps are shown and a flow chart is presented at the end of this chapter, which outlines the important steps involved in the performance prediction for a CSS process for horizontal wells.

3.1 Cyclic Steam Stimulation for Horizontal wells

Cyclic steam stimulation involves injection of steam into the formation at high pressure for several weeks, followed by soak period, and finally production period. The purpose of this study is to develop a new heat transfer model to predict the average temperatures in the steam zone during soak and production periods. The heat transfer model takes into account the heat lost by the steam zone to the adjacent reservoir. Steam zone is defined as the region that is at the steam temperature. Fluid viscosities are calculated based on the average steam zone temperatures. The heat transfer model is then coupled with a fluid flow model to predict the oil and water production rates.

3.1.1 Model assumptions

Steam is injected through a horizontal well placed at the centre of the formation. Steam displaces oil and forms a steam zone. Steam zone is defined as the region that is at the saturated steam temperature. Steam heats the adjacent colder formation by conduction. During the production period oil in the steam chamber is driven into the well bore due to pressure drawdown. Reduction of oil viscosity as a result of increase in temperature improves the production response significantly.

The main assumptions of the heat transfer model are:

i. The reservoir is initially saturated with oil and water
ii. Steam forms a cylindrical geometry
iii. During the injection period, the steam is considered as a heat source at a constant temperature, T_S.
iv. Heat is transferred from the steam zone to the cold oil zone through conduction

3.1.2 Volume of steam zone

The steam zone is defined as the region that is at the steam temperature, T_S. The volume of steam zone is based on a simple heat balance equation and was proposed by Gonzito and Aziz (1984)[37]:

$$V_S = \frac{Q_s t_{inj} \rho_w Q_i + H_{last}}{(\rho c_t)(T_S - T_R)} \tag{3.1}$$

where,

$$Q_i = C_w(T_S - T_R) + L_{vdh} f_{sdh} \tag{3.2}$$

Q_s = steam injection rate

t_{inj} = injection time

Q_i = heat injected per unit mass of steam

ρ_w = density of water

ρc_t = volumetric heat capacity of the reservoir rock

L_{vdh} = latent heat of vaporization

f_{sdh} = down- hole steam quality

H_{last} = heat remaining in the reservoir from the previous cycle

Specific heat of water is given by[38]

$$C_w = \frac{h_w(T_S) - h_w(T_R)}{(T_S - T_R)} \tag{3.3}$$

Enthalpy of water was calculated using the correlation given by Jones[18] and for steam latent heat correlation of Farouq Ali[39] was used:

$$h_w(T) = 68\left(\frac{T}{100}\right)^{1.24}, \text{ T is in } ^oF \tag{3.4}$$

$$L_{vdh} = 94(705 - TS)^{0.38}, \text{ T is in } ^oF \tag{3.5}$$

Assuming a cylindrical geometry, the radius of the steam zone is calculated by the equation:

$$r_h = \sqrt{\frac{V_S}{\pi L}} \tag{3.6}$$

3.1.3 Heat remaining in the reservoir

Initially, the amount of heat in the reservoir is set to zero. For later cycles, the heat remaining is calculated on the basis of the steam zone volume and the average temperature at the end of the previous cycle:

$$H_{last} = V_S(\rho c_t)(T_{avg} - T_R) \tag{3.7}$$

3.1.4 Average steam zone temperature:

When steam is injected it invades the formation and a steam zone is formed. During the production cycle, as time progresses, the temperature of the steam zone gradually decreases. Hence, the average temperature of the steam zone with respect to time has to be determined to find the oil and water viscosities, and thus predict the oil rates accurately.

It is assumed that initially temperature has a step function like profile i.e., the temperature is T_S in the steam zone, radius 'r_h', and beyond 'r_h' is at reservoir temperature T_R. This maybe a valid assumption since the heated steam zone is very small for the first cycle. It is further assumed that the heat loss to the zone beyond r_h is due to conduction in the radial direction. Heat conduction in radial direction was solved to predict the average steam zone temperature during the soak and production periods. Under the assumption of local themral equlibrium between the reservoir rock and fluids, the heat conduction in radial direction is given as:

$$\frac{1}{r}\frac{\partial}{\partial r}\left(r\frac{\partial T}{\partial r}\right)=\frac{1}{\alpha}\frac{\partial T}{\partial t} \tag{3.8}$$

Two zones were defined: Zone 1, which is at the temperature, T_S, initially, and Zone 2, region beyond r_h, that is initially at the reservoir temperature, T_R. Figure 3.1 shows a pictorial representation of the model.

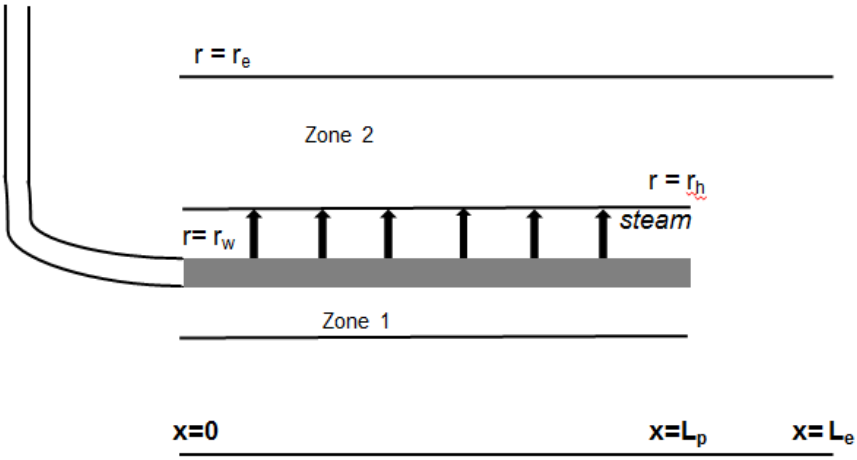

Figure 3.1: Schematic diagram of model

Let T_1 and T_2 be the temperatures of the Zone1 and Zone 2 at any time, t, respectively. The initial and boundary conditions are defined as below:

Initial Condition:

$T_1=T_s$ at t=0 (3.9)

Here, time t=0 represents the start of soak period when the heated zone is at a temperature Ts. During the soak period and production period, the steam zone loses heat due to conduction to the surround formation. The processed is modeled from the start of the soak period.

The net heat flux at r=0 is zero because of the radial symmetry. The total heat from the boundary of Zone 1 is equal to the amount of heat absorbed by the Zone 2. It is denoted by B.C. 2. These are represented mathematically as:

Boundary Conditions:

$$\frac{\partial T_1}{\partial r} = 0 \qquad \text{at} \qquad r=0 \tag{3.10}$$

$$kA\frac{\partial T_1}{\partial r}\bigg|_{r=a} = -V.\rho c_p \frac{\partial T_2}{\partial t} \qquad \text{at} \qquad r= r_h \tag{3.11}$$

For solving the PDE, the following dimensional parameters were defined and the equation is converted into a dimensionless form.

$$T_{D1} = \frac{T_S - T_1}{T_S - T_R} \tag{3.12}$$

$$T_{D2} = \frac{T_S - T_2}{T_S - T_R} \tag{3.13}$$

$$r_D = \frac{r}{r_w} \tag{3.14}$$

$$t_D = \frac{\alpha t}{r_w^{\,2}} \tag{3.15}$$

$$T_{D2(0)} = \frac{T_S - T_R}{T_S - T_R} \tag{3.16}$$

The governing equations in dimensionless form are given by:

$$\frac{\partial^2 T_{D1}}{\partial r_D^{\,2}} + \frac{1}{r_D}\frac{\partial T_{D1}}{\partial r_D} = \frac{\partial T_{D1}}{\partial t_D} \tag{3.17}$$

The initial condition (t_D=0) in dimensionless form is given by:

$$T_{D1} = 0 \qquad \text{at} \qquad t=0 \tag{3.18}$$

The boundary condition at the wellbore, in dimensionless form is given as:

$$\frac{\partial T_{D1}}{\partial r_D} = 0 \qquad \text{at} \qquad r_D = 0 \tag{3.19}$$

The boundary condition at the interface, r=r_h, is given by:

$$kA\frac{\partial T_{D1}}{\partial r_D} = -\frac{\alpha}{r_w}(\rho c_p . V)\frac{\partial T_{D2}}{\partial t_D} \quad \text{at} \qquad r_d = r_{dh} \tag{3.20}$$

The PDE is solved by using Laplace transform. The equation in Laplace domain is given below. Detailed derivation is given in Appendix A.

$$\frac{\partial^2 \widetilde{T}_{D1}}{\partial {r_D}^2} + \frac{1}{r_D}\frac{\partial \widetilde{T}_{D1}}{\partial r_D} = s\widetilde{T}_{D1} \tag{3.21}$$

The solutions for temperature in Zone 1 and Zone 2, in Laplace domain, are given as:

$$\widetilde{T}_{D1\cdot Avg} = \left(\frac{2}{{r_{Dh}}^2 - 1}\right)\left(\frac{1}{\sqrt{s}}\right)\left[\frac{Q.\left(r_{Dh} I_1(r_{Dh}\sqrt{S}) - I_1(\sqrt{s})\right)}{\sqrt{S} I_1(r_{Dh}\sqrt{S}) + QsI_0(r_{Dh}\sqrt{S})}\right] T_{D2(0)} \tag{3.22}$$

$$\widetilde{T}_{D2} = \frac{Q.I_0(r_{Dh}\sqrt{s}).T_{D2(0)}}{\sqrt{s} I_1(r_{Dh}\sqrt{s}) + QsI_0(r_{Dh}\sqrt{s})} \tag{3.23}$$

where,

$$Q = \frac{\alpha(\rho c_p).V}{r_w.kA} \tag{3.24}$$

The equations in Laplace domain are inverted to time domain using Gaver-Stehfest[40,41] algorithm in MATLAB. The average temperature at any time during the cycle is calculated by the following equations:

$$T_{1.Avg} = T_S - T_{D1\cdot Avg}(T_S - T_R) \tag{3.25}$$

and,

$$T_2 = T_S - T_{D2}(T_S - T_R) \tag{3.26}$$

Figure 3.2 shows a plot of the dimensionless average temperature of Zone 1 and Zone 2 versus the dimensionless time.

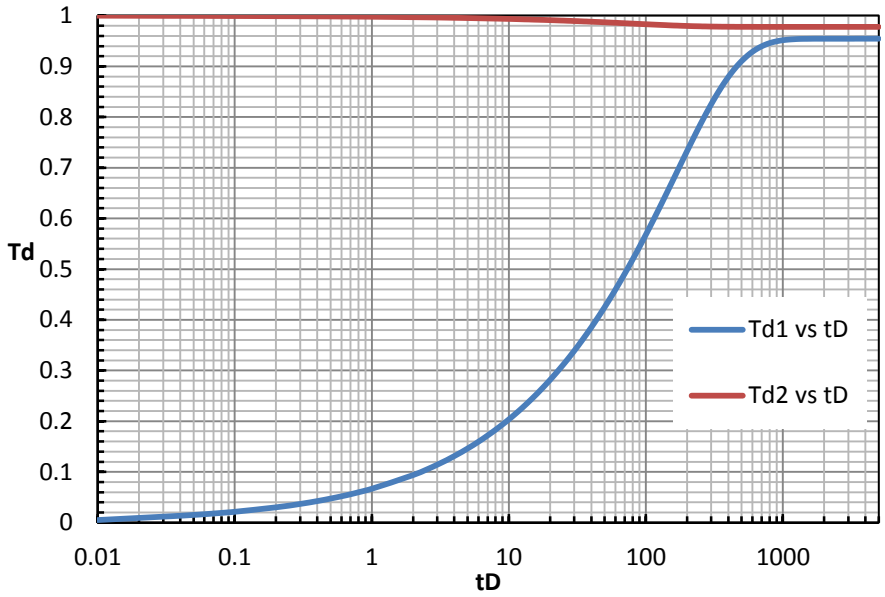

Figure 3.2: A plot of dimensionless temperature of Zone 1 and Zone 2 versus dimensionless time

Sample calculations were made for the radius of the steam zone and the average temperature of the steam zone. The reservoir and operational parameters used for these calculations are shown in Table 3.1 and Table 3.2. Figure 3.3 shows a plot of the average temperature in ^{o}F) of Zone 1 and Zone 2 versus time (days). The radius of steam zone and the temperature profile were plotted for three cycles using the operation parameters described in Table 3.2. Figure 3.4 shows a plot of the volume of steam zone and the radius of steam zone versus time and the average temperature for three cycles is shown in Figure 3.5. It can be seen from the plots that initially, at the start of the production period, the temperature is at steam temperature, T_S, and it gradually declines during the production period.

Table 3.1 Reservoir parameters and PVT data

Variable	**Value**
Reservoir porosity	0.2
Well radius (ft)	0.3
Initial reservoir temperature (^{o}F)	115
Saturated steam temperature (^{o}F)	415
Reservoir thermal conductivity (Btu/ft hr. ^{o}F)	1
Reservoir thermal diffusivity (ft^2/hr)	0.04
Injected steam quality	0.7
Steam injection rate (B/D)	600
API gravity of oil (^{o}API)	14
Injection pressure (psi)	300
Pay thickness, ft	80
Specific heat of water, Btu/lb^{o}F	1

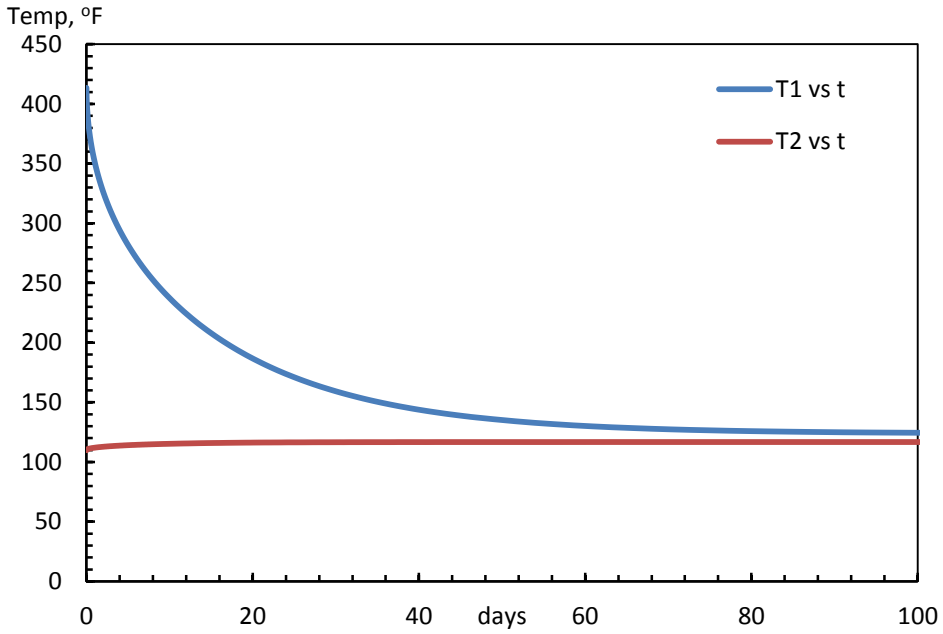

Figure 3.3: A plot of the average temperature of Zone 1 and Zone 2 versus time

Table 3.2 Operational parameters

	Cycle 1	**Cycle 2**	**Cycle 3**
Steam injection rate, BPD	600	600	600
Injection time, days	30	30	30
Soak time, days	10	10	10
Down- hole steam quality	0.7	0.7	0.7
Production time, days	100	100	100

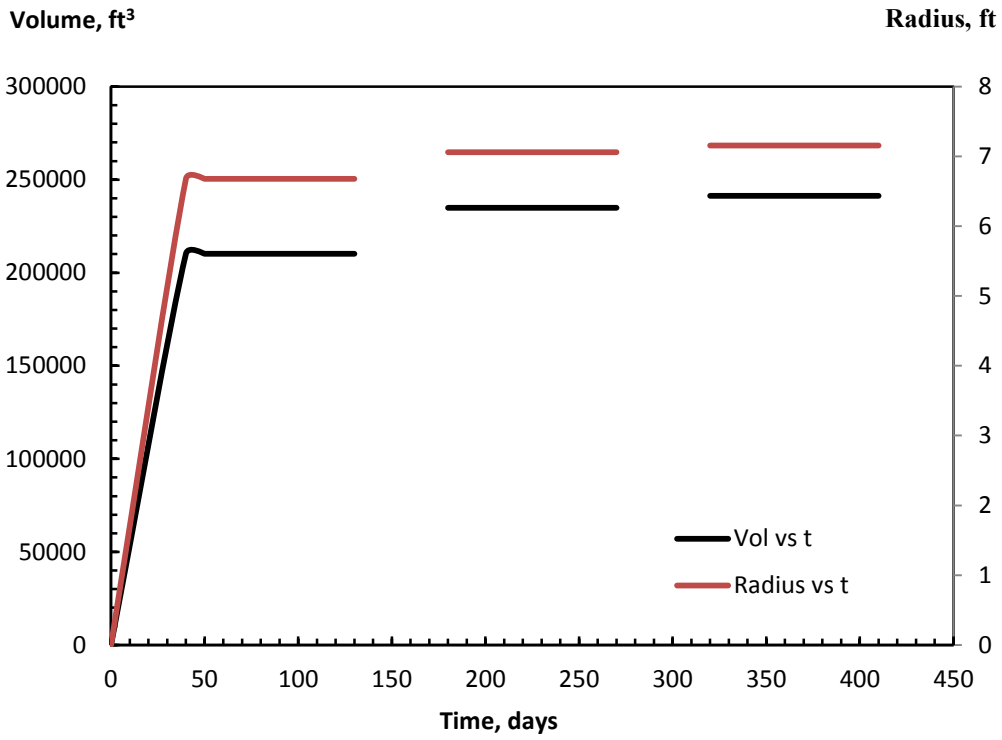

Figure 3.4: Volume and radius of steam zone for three cycles

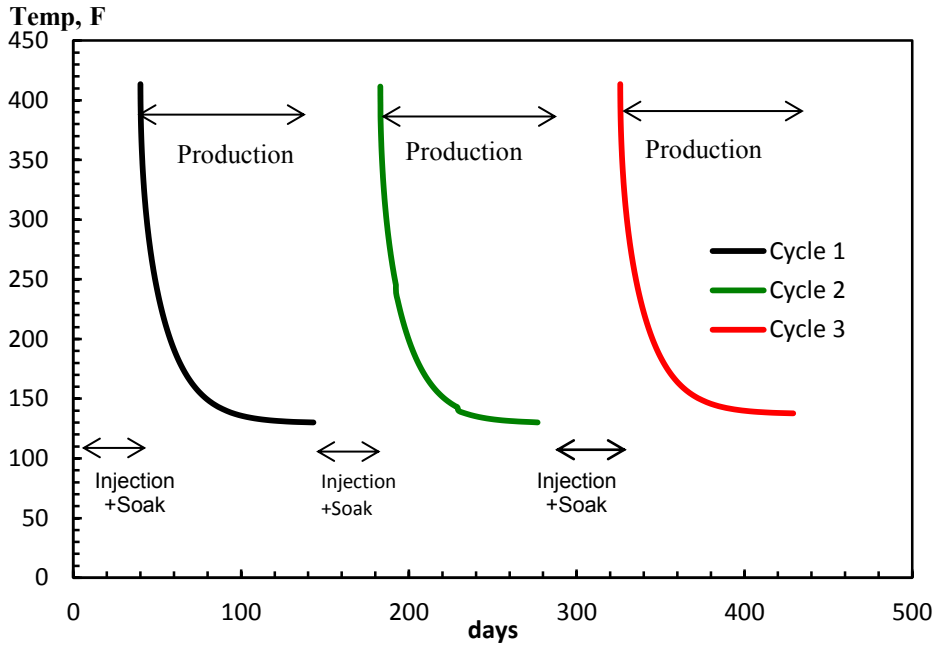

Figure 3.5: Plot of the average steam zone temperature versus time for three cycles

3.1.5 Oil and water viscosities

The oil and water viscosities are calculated using the available correlations given below[18]:

$$\mu_o = ae^{b/(T+460)} \tag{3.27}$$

$$\mu_w = 1.66\left[\frac{T}{100}\right]^{-1.14} \tag{3.28}$$

3.1.6 Fluid saturations and relative permeabilities

The oil and water relative permeabilities can be calculated using the generalized equations available for California reservoirs[18], as given by Gomaa:

$$k_{rw} = -0.002167S_w^* + 0.021467S_w^{*2} \tag{3.29}$$

$$k_{ro} = -0.9416 + 1.0808/S_w^* - 0.13856S_w^{*2} \tag{3.30}$$

with,

$$k_{ro} = 1 \text{ if } \quad S_w^* \le 0.2 \tag{3.31}$$

where,

$$S_w^* = (S_w - S_{wir})/(1 - S_{wir} - S_{orw}) \tag{3.32}$$

S_w = water saturation

S_{wir} = irreducible water saturation

S_{orw} = residual oil saturation to water

Water saturation, S_w, is given by:

$$S_w = \bar{S}_w - (\bar{S}_w - S_{wi})\frac{W_P}{WIP} \tag{3.33}$$

After the soak period, it is assumed that the only mobile phase around the well is water.

$$\bar{S}_w = 1 - S_{orw} \tag{3.34}$$

3.1.7 Fluid- inflow equation

We assume that pressure drawdown is the main driving force for fluid production and flow is through the steam chamber. Joshi's model was used to calculate the productivity index. The assumed steam zone is cylindrical in nature and hence, the model was modified for a cylindrical geometry. Joshi's (1988) solution for horizontal well in an anisotropic reservoir is given by:

$$q_H = \frac{0.007078h\sqrt{k_y k_x}\,\Delta p}{\mu_o B_o \left\{ \ln\left[\frac{a + \sqrt{a^2 - (L/2)^2}}{L/2}\right] + (\beta h/L)\ln\left[\frac{(\beta h/2)^2 + \beta^2\omega^2}{(\beta h r_w/2)}\right] + s_f \right\}} \tag{3.35}$$

where,

k_x and k_y are the permeability in horizontal and vertical direction respectively

$$\beta = \sqrt{\frac{k_y}{k_x}} \tag{3.36}$$

$$a = (L/2)\left[\frac{1}{2} + \sqrt{\frac{1}{4} + \frac{1}{(0.5L/r_{eh})^4}}\right]^{0.5} \tag{3.37}$$

and, ω is the distance of the well from mid- height of the formation

For an isotropic reservoir, if we assume that $k_x = k_y$ and 2a=L ('2a' is the major axis of the ellipse) and the well is located at the center of the formation, then the above equation reduces to a simple radial flow model:

$$q = \frac{0.007078kL\Delta p}{\mu_h \ln\left(\frac{r_h}{r_w}\right) + \mu_c \ln\left(\frac{r_e}{r_h}\right)} \quad \text{, Rb/day} \tag{3.38}$$

For two phase oil and water flow, the production rates can be calculated as:

$$q_o = \frac{0.007078kk_{ro}L\Delta p}{\mu_{oh} \ln\left(\frac{r_h}{r_w}\right) + \mu_{oc} \ln\left(\frac{r_e}{r_h}\right)} \tag{3.39}$$

$$q_w = \frac{0.007078kk_{rw}L\Delta p}{\mu_{wh} \ln\left(\frac{r_h}{r_w}\right) + \mu_{wc} \ln\left(\frac{r_e}{r_h}\right)} \tag{3.40}$$

3.1.8 Flow chart showing important steps in calculations

An outline is presented in Figure 3.6 that shows important steps in the calculating the average temperature of the steam zone and predicting the performance of a CSS process. The main inputs for the model are: reservoir temperature, reservoir properties, fluid saturations and the cyclic operational parameters. First, the volume (and radius) of the heated zone geometry are calculated based on the input properties. Second, the average temperature of the steam zone is calculated using the model developed in the *Section 3.1.4*. The oil and water viscosities are calculated based in the average temperature of the steam zone. Oil and water relative permeabilities are calculated from water saturation based on the correlations discussed in *Section 3.1.6*. After the end of the soak period, it is assumed the only mobile phase around the well bore is water. For the first time step, the water production, W_P, is zero. Based on this, the water saturation is calculated and the oil and water relative permeabilities are calculated using the water saturation, S_w, values. The oil and water flow rates, for small time steps, are calculated using the modified Joshi's equation described in *Section 3.1.7*. The cumulative oil and water production are calculated and fluid saturations are updated. The process is repeated until the end of the cycle and the amount of fluids and heat remaining in the reservoir is calculated at the end of the cycle. Finally, the same steps are repeated for a new cycle. Details of the calculations are presented in the following chapter.

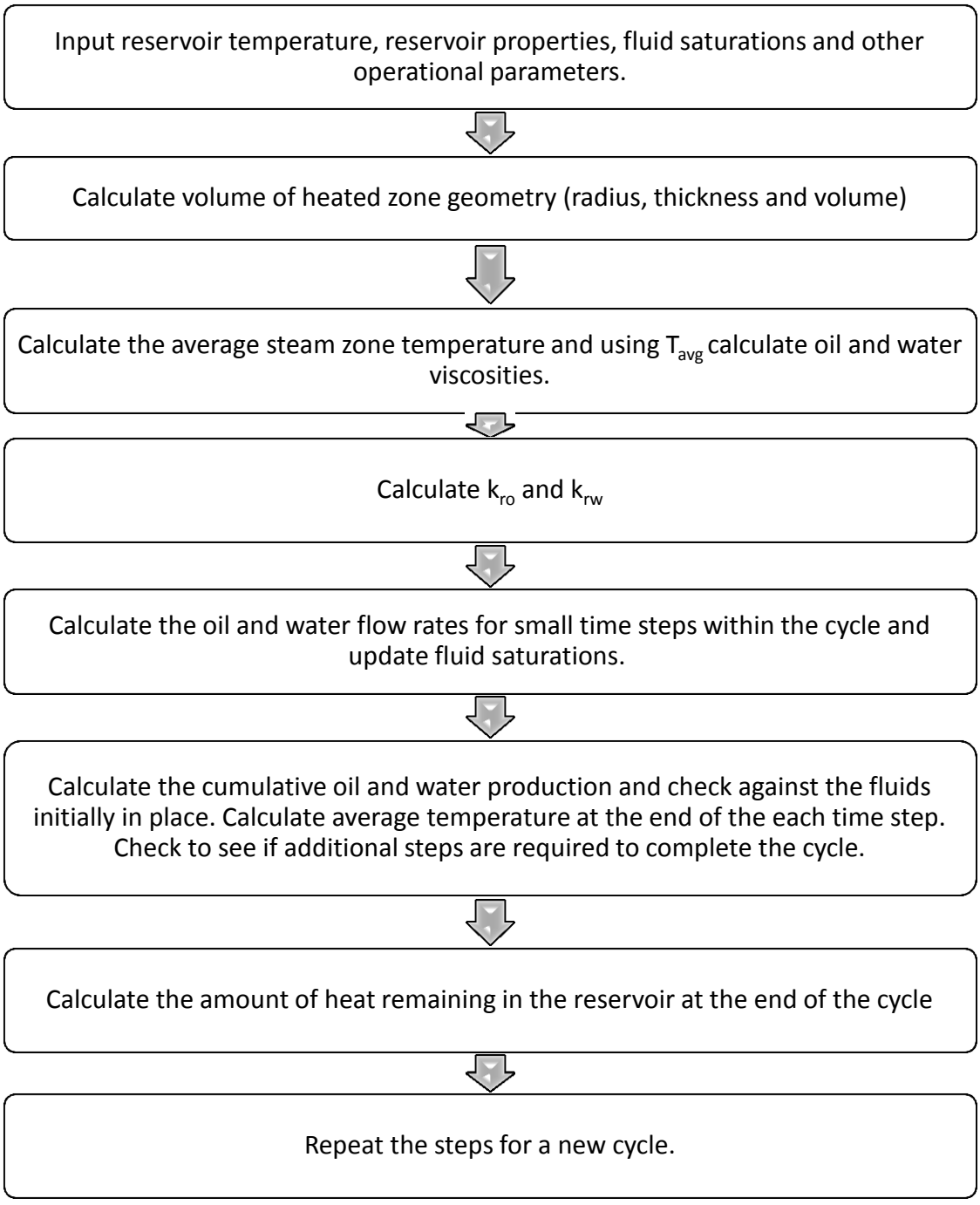

Figure 3.6: A flow chart outlining important steps in the calculation.

3.2 Summary

In this chapter, an analytical model that is applicable for a cyclic steam stimulation process for horizontal wells has been developed. A radial heat transfer model was developed to predict the average temperature in the steam zone. The oil and water viscosities are calculated based on the average steam zone temperature. Correlations for fluids saturation and relative permeabilities of oil and water are described. To predict the fluid rates, a modified form of Joshi's inflow equation is used. Finally, detailed steps are shown and a flow chart is presented at the end of this chapter which outlines the important steps involved in the performance prediction for a CSS process for horizontal wells.

The developed model will be validated using numerical simulation in CMG STARS in the next chapter. First, a base case will be run and checked if the results from the simulator match with that of the developed analytical model. Next, sensitivity analyses will be conducted to test the robustness of the model for a range of operating parameters.

CHAPTER FOUR:

4 Validation of the Model and Sensitivity Analyses

The robustness of the developed analytical model is tested for an expected range of parameters. All the calculations for the analytical model were done using an excel spreadsheet. The results obtained from the analytical model are compared with the results obtained from the numerical simulator. The findings are presented in this section.

4.1 Base Case

4.1.1 Input data

The proposed model is validated using numerical simulator from CMG. The operational parameters and reservoir properties are shown in Table 4.1 and Table 4.2, respectively.

Table 4.1 Operational parameters

	Cycle 1	**Cycle 2**	**Cycle 3**
Steam injection rate, BPD	3000	3000	3000
Injection time, days	10	10	10
Soak time, days	5	5	5
Down- hole steam quality	0.7	0.7	0.7
Production time, days	200	200	200

Table 4.2 Reservoir parameters and PVT data

Variable	**Value**
Reservoir Permeability	100 mD
Reservoir porosity	0.3
Well radius (ft)	0.5
Pay thickness, ft	80
Initial reservoir temperature (^{o}F)	85
Saturated steam temperature (^{o}F)	567
Initial water saturation	0.3
Residual oil saturation to steam	0.4
Reservoir thermal conductivity (Btu/ft hr. ^{o}F)	1
Reservoir thermal diffusivity (ft^2/hr)	0.04
Injected steam quality	0.7
Steam injection rate (B/D)	3000
API gravity of oil (^{o}API)	14
Injection pressure (psi)	1200
Specific heat of water, Btu/lb^{o}F	1

Table 4.3 Viscosity data

Temperature, ^{o}C	Viscosity, mPa.S
30	2710
180	4

Table 4.4 Model dimensions and grid data

Model Dimension	2000ft × 200ft × 80ft (i, j and k direction respectively)
Number of grids	100 × 50 × 20 (i, j and k direction respectively)

Aberfeldy field viscosity data, as shown in Table 4.3, was used to calculate oil viscosities at different temperatures[1]. Table 4.4 shows the model dimensions and grid data used for the numerical simulator. Using Andrade's equation to model the oil viscosity, the viscosity at any temperature can be obtained by $\mu = 7.596 \times 10^{-6} e^{596978/(T+273.15)}$

4.1.2 Relative permeability model

In order to compare and validate the model, it is important that the same relative permeability model is used for both the model and the numerical simulator. First, the relative permeability curves are generated in STARS and using simple curve fitting, the analytical expressions for relative permeabilities is obtained as:

$$k_{ro} = -10.593 S_w^{\ 3} + 25.075 S_w^{\ 2} - 19.314 S_w + 4.8314 \qquad (4.1)$$

$$k_{rw} = 2.0408 S_w^{\ 2} - 1.2245 S_w + 0.1837 \qquad (4.2)$$

Figure 4.1 shows a plot of the relative permeabilities of oil and water versus water saturation.

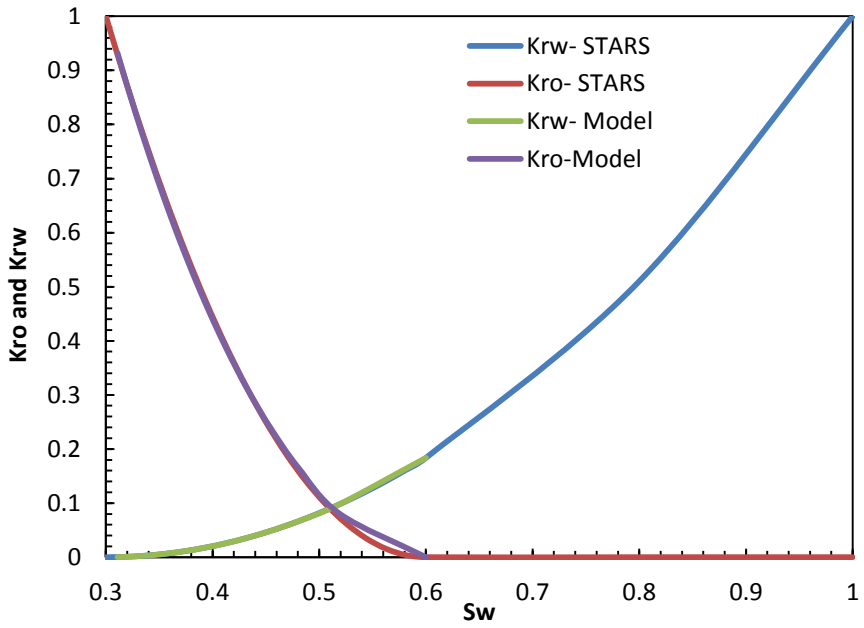

Figure 4.1: Oil and water relative permeabilities

4.1.3 Relative permeability adjustment

A comparision of water saturation in the heated zone, oil and water relative permeabilites obtained from the model and the numerical simulator are shown in Figure 4.2, 4.3 and 4.4, respectively. It can be seen from the plots that there is a slight different in the results from simulator and the developed model. The difference in the relative permeability of water is rather significant during the initial stages of the cycle. This resulted in a mismatch in the water production. Hence, a corrected relative permeability has to be used to get a good match for the water production between numerical simulator and the model.

The developed fluid flow model is a two phase-oil and water, model. The oil and water relative permeabilities are calculated using the water saturation obtained by mass balance in the heated zone. Relative permeabilities of oil and water play a significant role in determining the actual oil and water production. Hence, it is important to obtain a good match for the water saturation in the heated zone and, oil and water relative permeabilities.

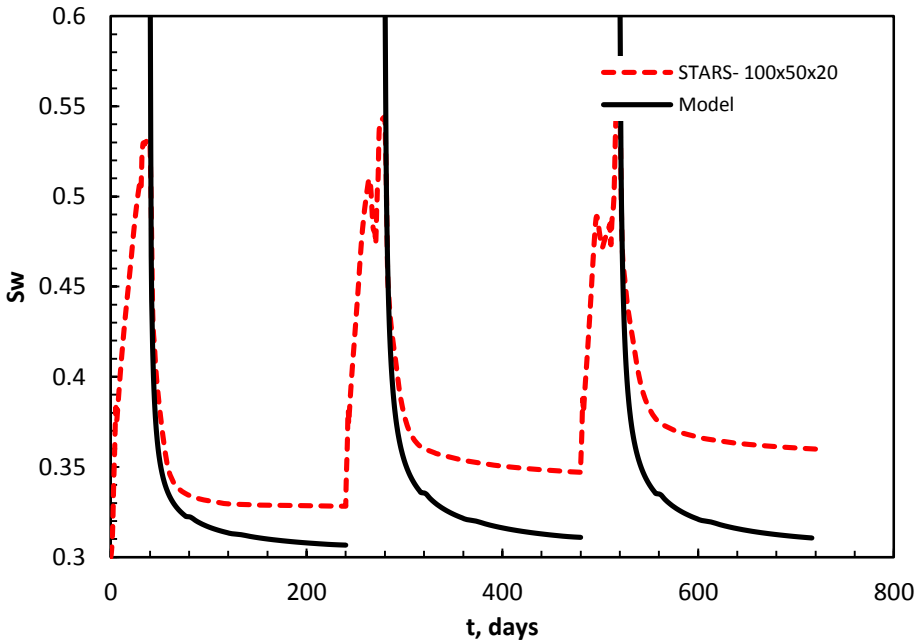

Figure 4.2: Water saturations in the heated zone obtained from developed model and numerical simulator

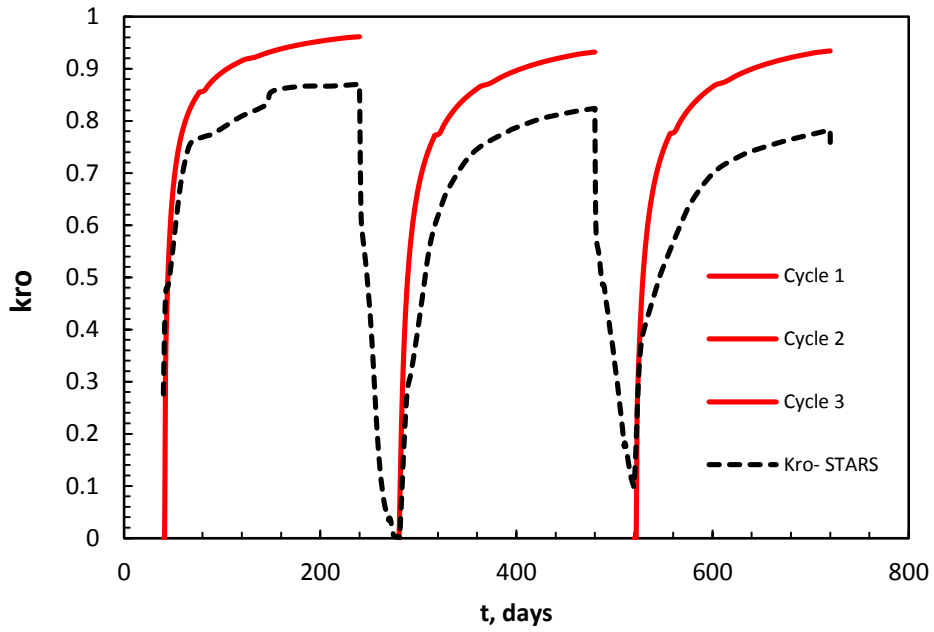

Figure 4.3: Oil relative permeability obtained from developed model and the numerical simulator

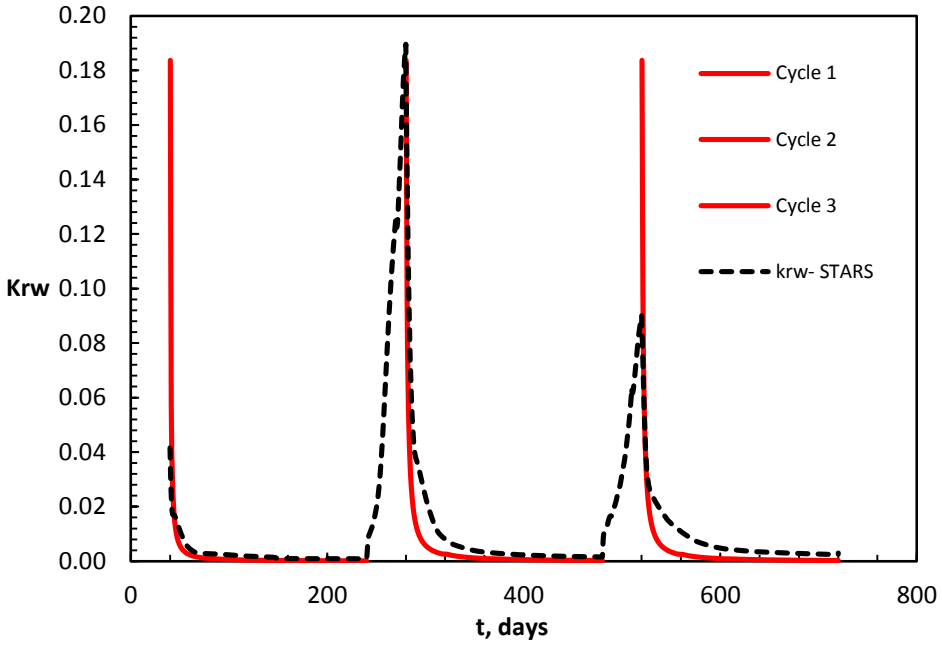

Figure 4.4: Water relative permeability obtained from developed model and the numerical simulator.

4.1.4 Pressure drop model and inflow equation

The following assumtions are made to obtain a good match with the results from the numerical simulator:

i. Oil production comes only from the heated zone. Oil rate is calculated using Equation 4.6 given below. This equation is a modified form of Equation 3.39.
ii. The mass balance is done only in the heated zone. The water saturation obtained from the mass balance equations is used to calculate the oil relative permeability.
iii. The same relative permeability model as the numerical simulator is used to calculate the oil relative permeability.
iv. Water production comes from the entire reservoir and is calcualted using Equation 4.7
v. A modified relative permeability model for water is used in the inflow equation to obtain a good match with the results from the simulator.

A comparision of oil production rate and cumulative oil production are shown in Figure 4.5 and 4.6, respectively. The three regions correspond to three cycles and the flat zones in between are the injection and soak intervals. There is no production during injection and soak interval. Oil production is very high at the early times during the production cycle as the temperature is high and the viscosity is low. It is assumed that the oil production comes only from the heated zone and the pressure does not propagate through the cold, highly viscous oil outside the heated zone.

It should be noted that in calculation of oil produciton rate, the pressure drawdown refers to pressure difference between the heated zone boundary and the botom-hole pressure of the well. The pressure at the heated boundary is calculated using the following equations:

$$p(r_w, t) = p_h - \left(\frac{141.2 q_o B_o \mu_o}{k k r_o L} \right) p_D \tag{4.3}$$

where

$$p_D = \frac{1}{2}\left[\ln(t_D) + 0.80907\right] \tag{4.4}$$

$$t_D = \frac{0.002637 k k_{rw} t}{\varphi \mu c_t r_h^2} \tag{4.5}$$

$$q_o = \frac{0.007078 k k_{ro} L (p_h - p_w)}{B_o \mu_o \ln\left(\frac{r_h}{r_w}\right)} \tag{4.6}$$

The actual inflow equation that accounts for the production from both the hot zone and the cold zone is given by Equation 3.39. However, in order to get a match with STARS, the equation is modified to consider the oil production only from the heated zone and is given by the above Equation 4.6.

Computational procedure for calculating the pressure at the heated zone boundary, p_h, involves trial and error and is summarized in the following steps:

i) Assume an average value for p_h
ii) Calculate the oil and water production rates using the radial flow model discussed above.
iii) Calculate t_D and p_D using the equations described above.
iv) Calculate p_h using the q_o and p_D values and check to see if the value for the first few time steps matches with the assumed value.
v) Repeat the process till a good match is obtained.

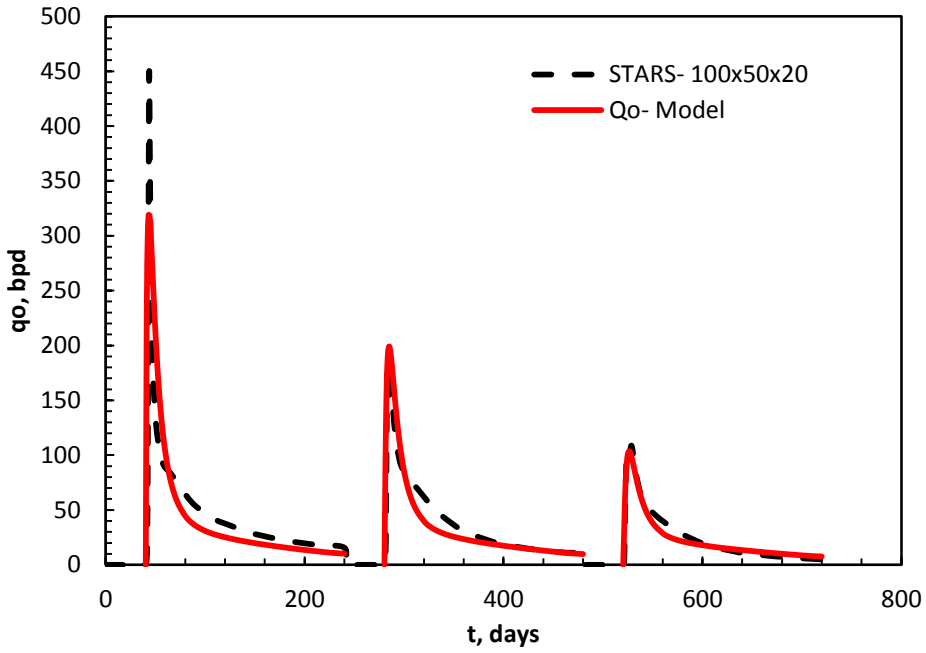

Figure 4.5: Comparison of oil production rate, q_o, obtained from the model versus the numerical simulator.

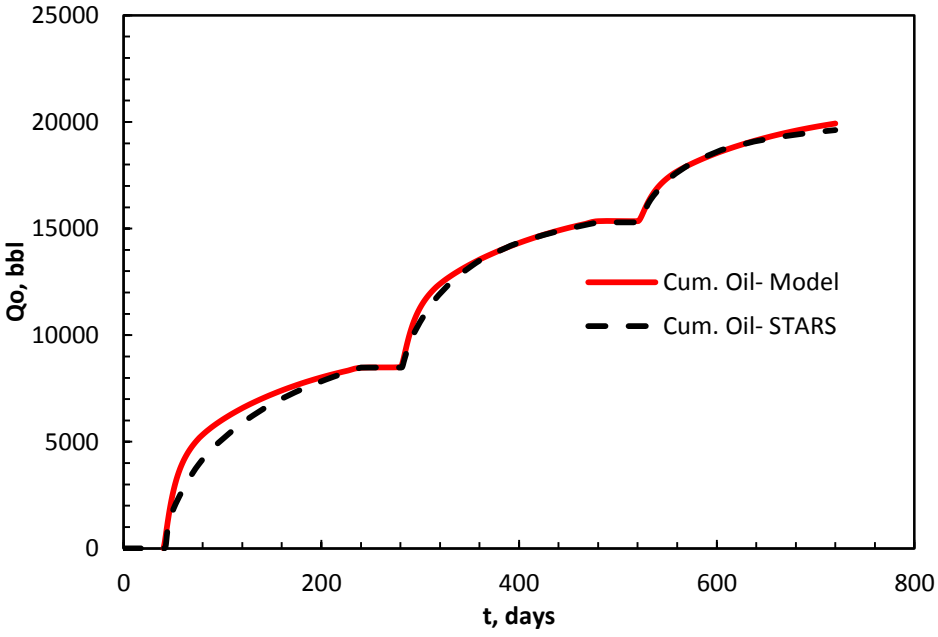

Figure 4.6: Comparison of cumulative oil production, Q_o, from the model versus the numerical simulator.

It is assumed that water production comes from both the heated zone and the outside cold zone. The following equation is used to calculate the water production rates:

$$Q_w = \frac{0.007078 k k_{rw}^* L (p_i - p_w)}{B_w \left(\mu_{wh} \ln\left(\frac{r_h}{r_w}\right) + \mu_{wc} \ln\left(\frac{r_e}{r_h}\right) \right)} \tag{4.7}$$

The water mass balance calculations are all performed using the actual water relative permeability curve (Equation 4.2). To obtain a good match with the results from the simulator, a modified relative permeability model is used for water in the inflow equation. The modified water relative permeability is obtained in history mathing of the water production rate from the numerical simulator and the developed model. The modified water relative permeability is only used for calculation of the water production rate using the inflow Equation 4.7 and is given by:

$$k_{rw}^* = (0.0637 S_w - 0.01827) \tag{4.8}$$

A comparision of water production rate and cumulative water production are shown in Fig. 4.7 and 4.8, respectively. The instantaneous water rate is also very high because of the condensed steam around the well-bore and it delines rapidly at later times.

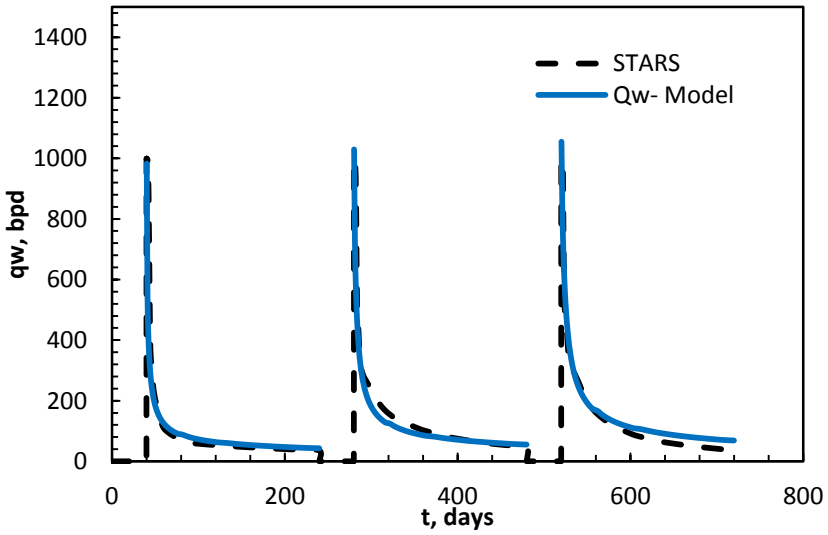

Figure 4.7: Comparison of water rate, q_w, obtained from model versus STARS simulator

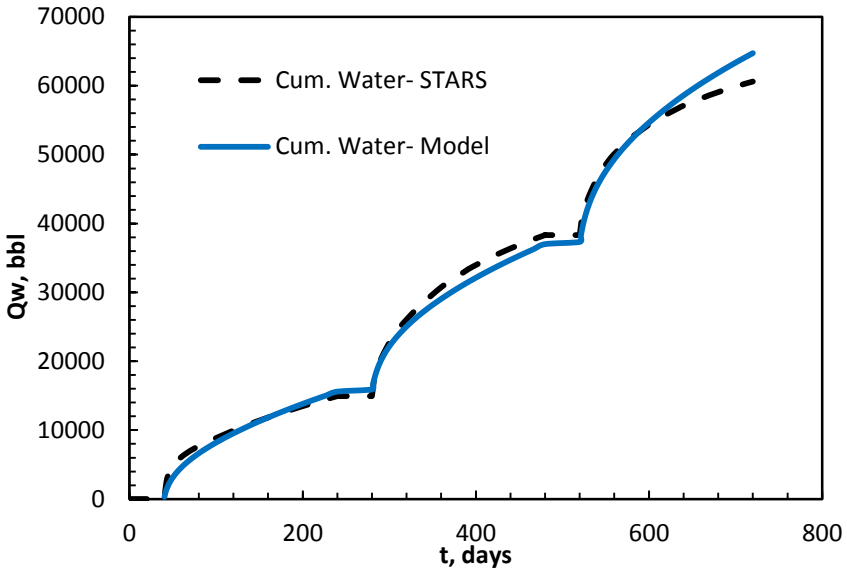

Figure 4.8: Comparison of cumulative water production, Q_w, from the model versus STARS.

4.2 Sensitivity Analyses

The robustness of the analytical model is tested by comparing the results obtained from the developed model with the results from the numerical simulator, for an expected range of parameters. In all sensitivity analyses, the same data as base case is used, except noted otherwise. The following parameters were considered:

i. Grid Sensitivity
ii. Steam Injection rates
iii. Length of horizontal well
iv. Absolute Permeability
v. Relative permeability of oil and water
vi. Thermal Diffusivity
vii. Types of oil: viscosity
viii. Number of Cycles

4.2.1 Grid sensitivity

For simulation, a reservoir of dimensions 2000ft × 200ft × 80ft (i, j, k direction respectively) is considered. The following four different grid size configurations were considered and a comparison of results obtained from these configurations is shown in Figure 4.5, Figure 4.6, Figure 4.7 and Figure 4.8. The horizontal well of length 1500ft is placed at the center of the reservoir and is produced at a constant bottom-hole pressure of 100 psi.

i. 100×50×10 (number of grid blocks in i, j, and k direction, respectively)
ii. 100×50×20
iii. 100×50×40
iv. 200×50×20

The three time intervals in the plot of oil production rate versus time shown in Figure 4.5 started with a peak that correspond to three cycles. The flat zones in the cumulative oil production plot in Figure 4.10 represent the injection and soak intervals. There is no production during the soak period. The soak interval in a given cycle is followed by the production interval. At early times in the production interval, the instantaneous oil rate increases rapidly as shown by the steep gradients in the Figure 4.9, because the oil is hot and viscosity is very low. At later times, the production of oil decreases as the formation begins to lose heat, temperature declines and the oil viscosity increases. Similarly, the water production rate is very high at early times, as shown in Figure 4.11, in the production interval due to the condensed steam around the wellbore. At later times water production declines. The flat zones in the cumulative water production plot in Figure 4.12 represent the injection and soak intervals. It can be seen from these plots that the results for different grid sizes are fairly close to each other and the results are independent of the grid size configurations. The results for the grid configuration of 100×50×10 produces erroneous results and slightly under- estimates the fluid production as there is not enough resolution in the k direction. Based on these results, the simulation model with a grid size of 100×50×20 was used for all the validation and sensitivity studies in the next sections.

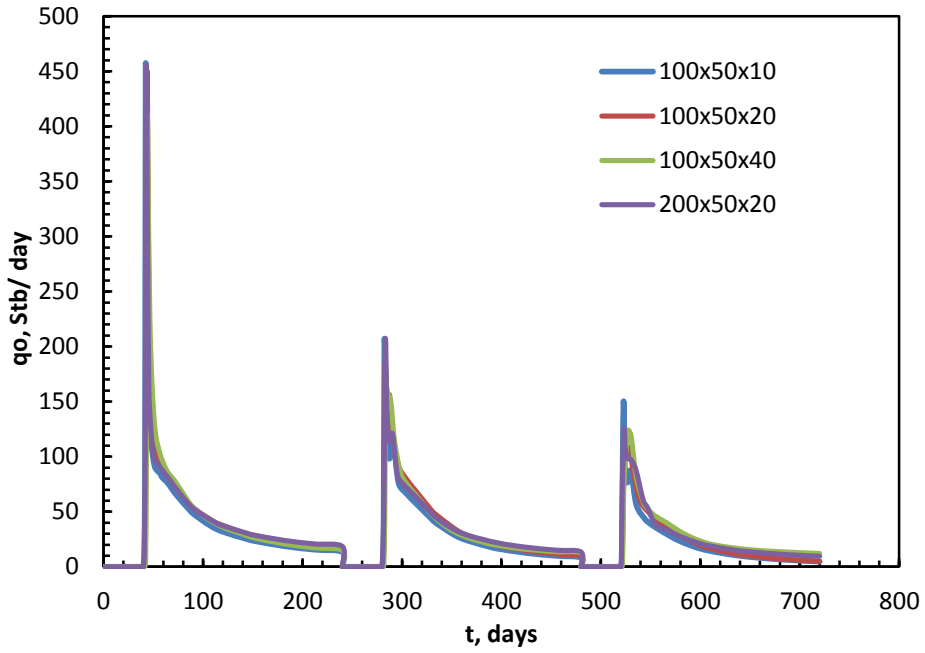

Figure 4.9: Plot of oil production rate, q_o, versus time for different grid sizes.

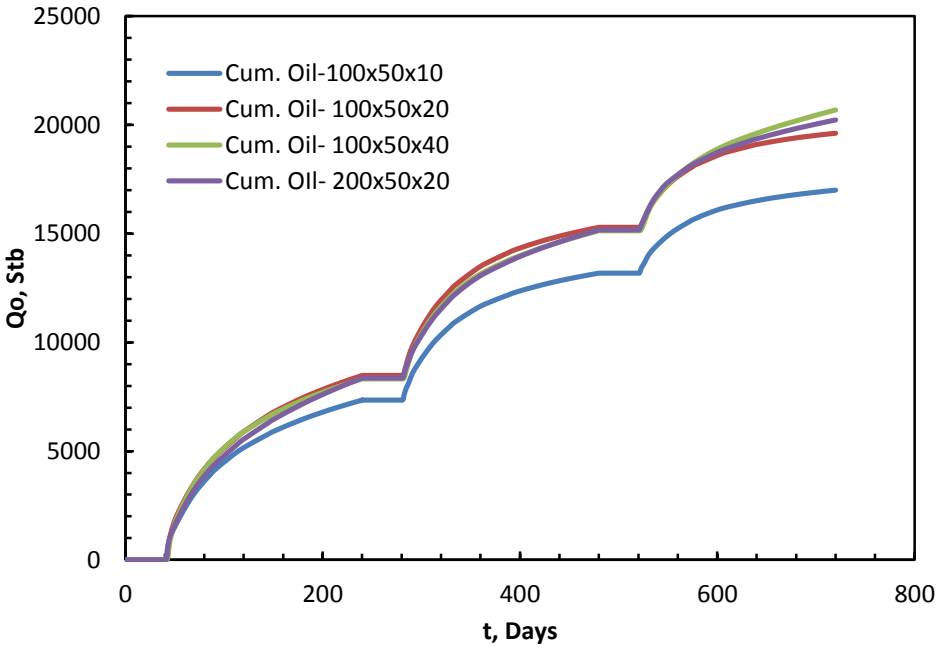

Figure 4.10: Plot of cumulative oil production, Q_o, versus time for different grid sizes.

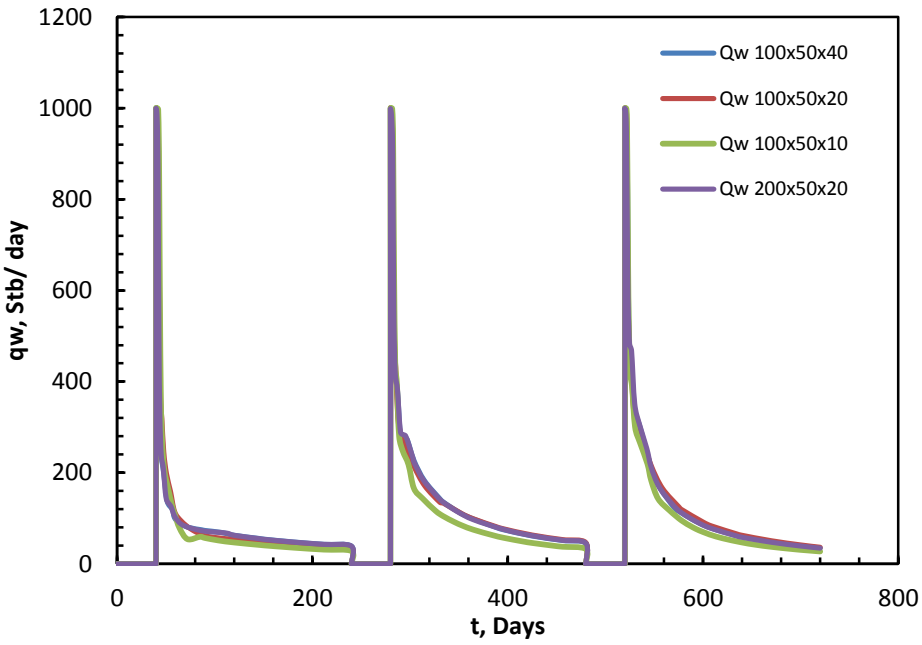

Figure 4.11: Plot of water production rates, q_w, versus time for different grid sizes.

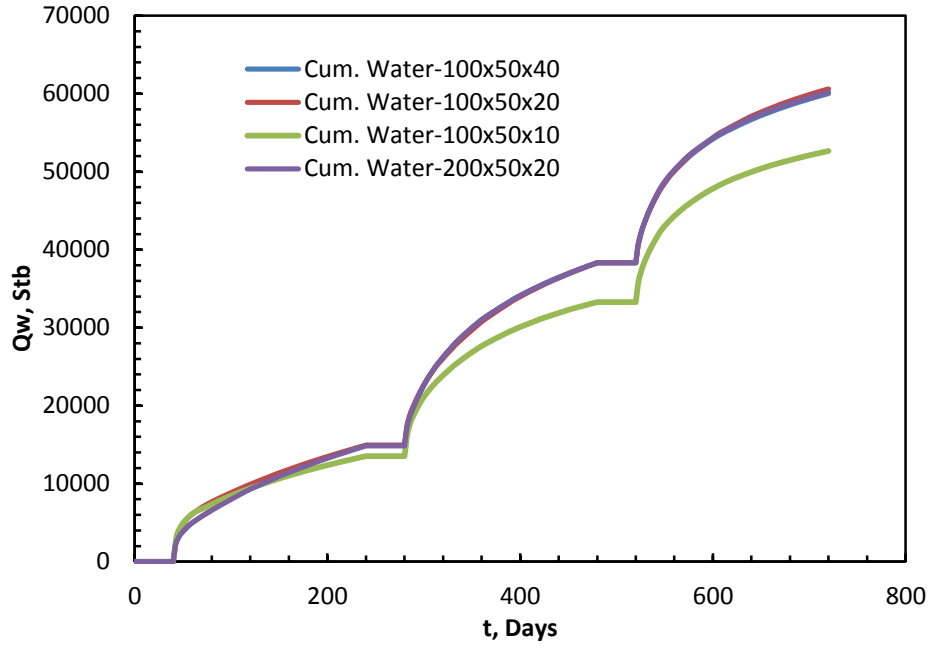

Figure 4.12: Plot of cumulative water production, Q_w, versus time for different grid sizes.

4.2.2 Steam injection rates

This case was run for three different values of steam injection rates: 1800 bpd, 2500 bpd, and 3000 bpd using the same data used for the base case except for the steam injection rate. Figures 4.13, 4.14 and 4.15 show the comparison plots of oil production rate versus time for the results obtained from the developed model and the simulator for different steam injection rates. It can be seen from the plots that the results from the model and the numerical simulator are fairly close to each other. Figure 4.16 depicts the cumulative oil production versus time. As the steam injection rate increases the cumulative oil production increases as greater amount of heat is injected and a greater amount of reservoir is heated. However, it can be seen that the increase in oil production is not proportional to the increase in the steam injection rates. Figure 4.17 shows a plot of the water production rates obtained from the numerical simulator and the developed analytical model and it can be seen from the plot that the results are fairly close to each other. Figure 4.18 shows a plot of cumulative water production obtained from the simulator and the developed analytical model. The results are fairly close and it can be seen that as the steam injection rate is increased, water production increases significantly, as greater amount of heat and water is injected and a greater volume of the reservoir is contacted.

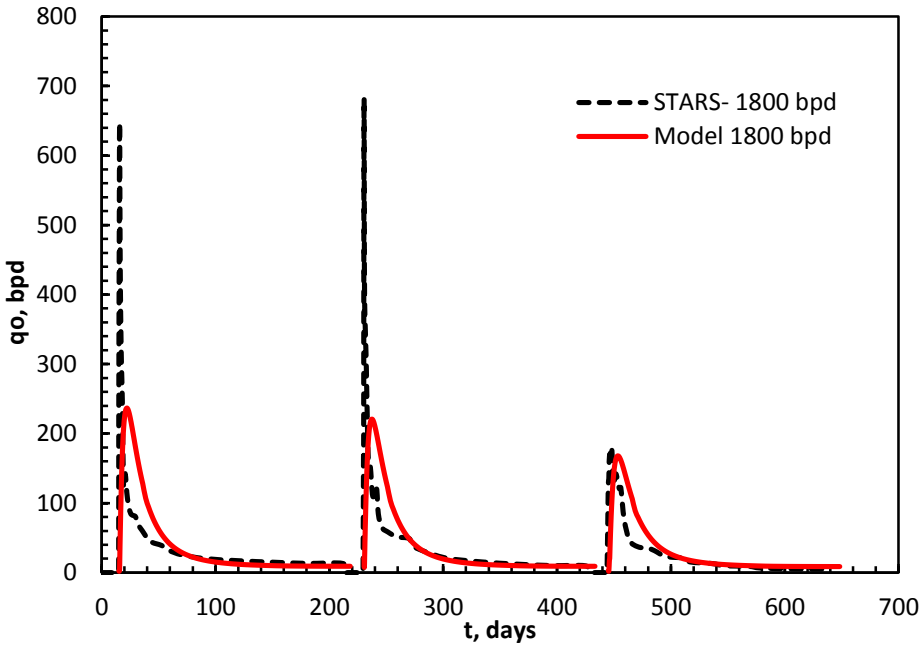

Figure 4.13: Comparison of oil production rates from STARS and model for a steam injection rate of 1800 bpd.

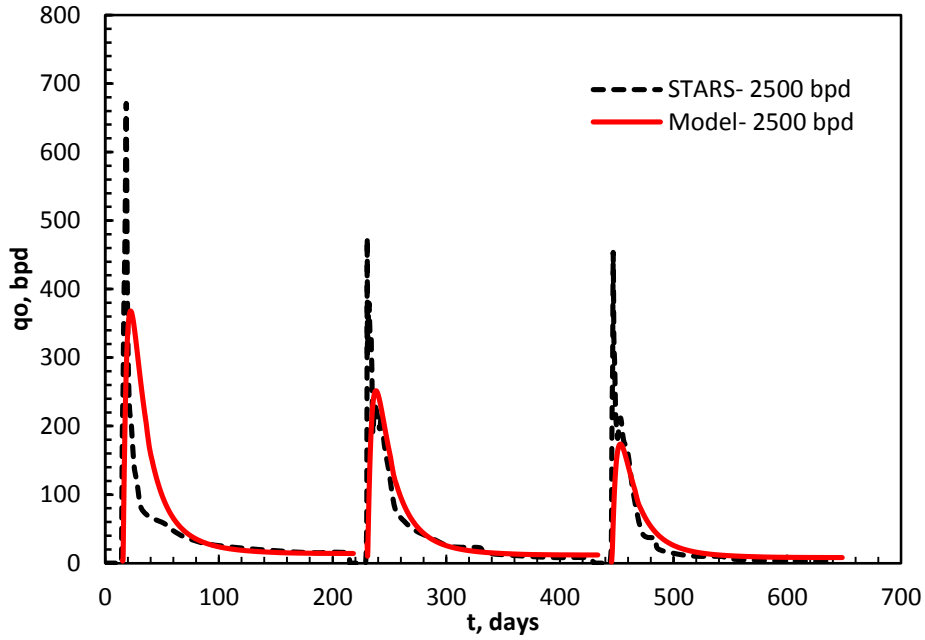

Figure 4.14: Comparison of oil production rates from STARS and model for a steam injection rate of 2500 bpd.

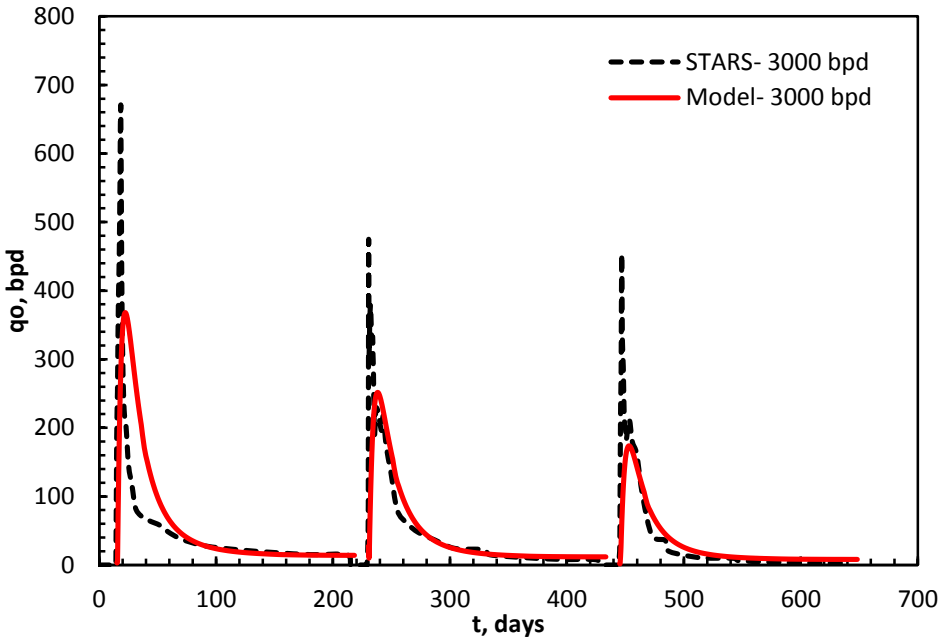

Figure 4.15: Comparison of oil rate from STARS and model for steam injection rate of 3000 bpd.

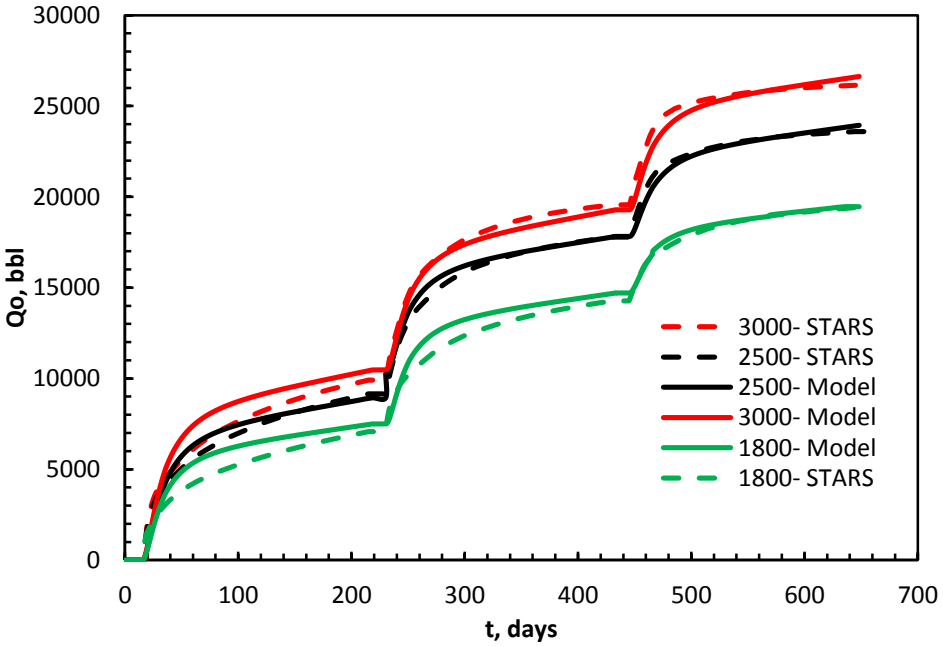

Figure 4.16: Cumulative oil production versus time for different steam injection rates.

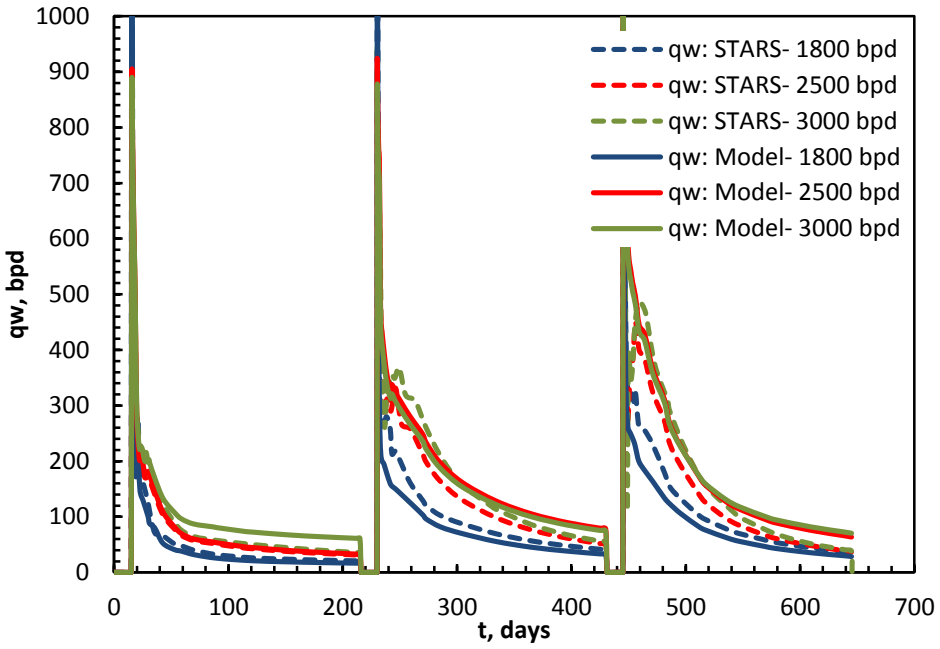

Figure 4.17: Comparison of water production rate from STARS and model for different steam injection rates.

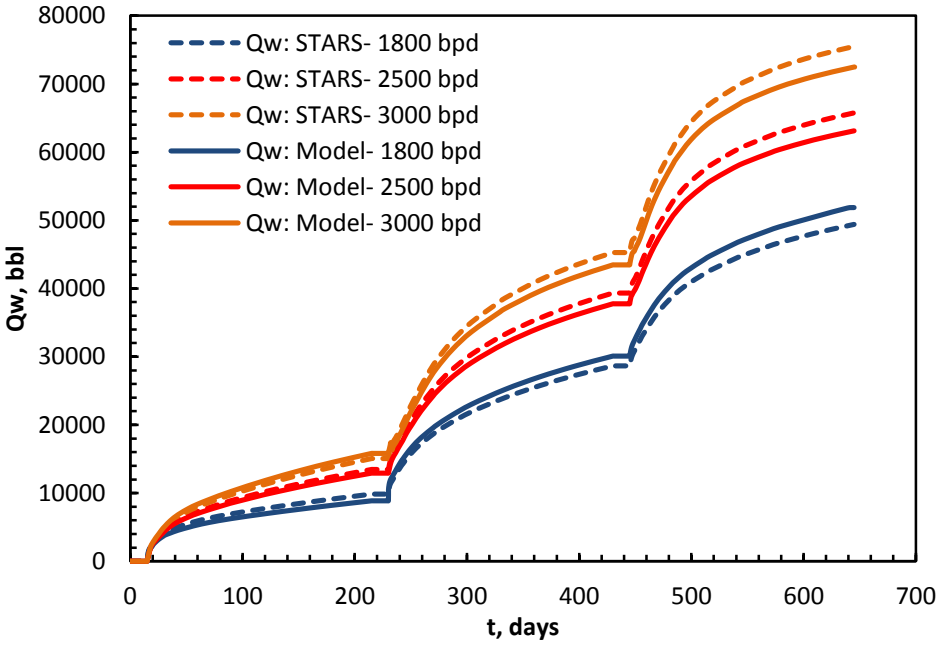

Figure 4.18: Comparison of cumulative water production obtained from STARS and analytical model for different steam injection rates.

4.2.3 Length of horizontal well

This case was run for three different lengths of the horizontal well: 1000 ft, 1250 ft and 1500 ft using the same data as base case except for the length of the horizontal well. Figure 4.19 and Figure 4.20 show the comparison of oil production rate obtained from STARS simulator and the developed model for a horizontal well length of 1000 ft and 1250 ft, respectively. Figure 4.21 shows a comparison of the cumulative oil production time for different horizontal well lengths. It can be seen that increase in the length of well-bore will result in the increase in cumulative oil production. Figure 4.22 shows a plot of the water production rate for different cases and it can be seen that the results obtained from the developed model and the simulator are fairly close to each other. Figure 4.23 depicts a plot of the cumulative water production versus time. Again, as expected, increase in the length of the wellbore results in the increase in the cumulative water production.

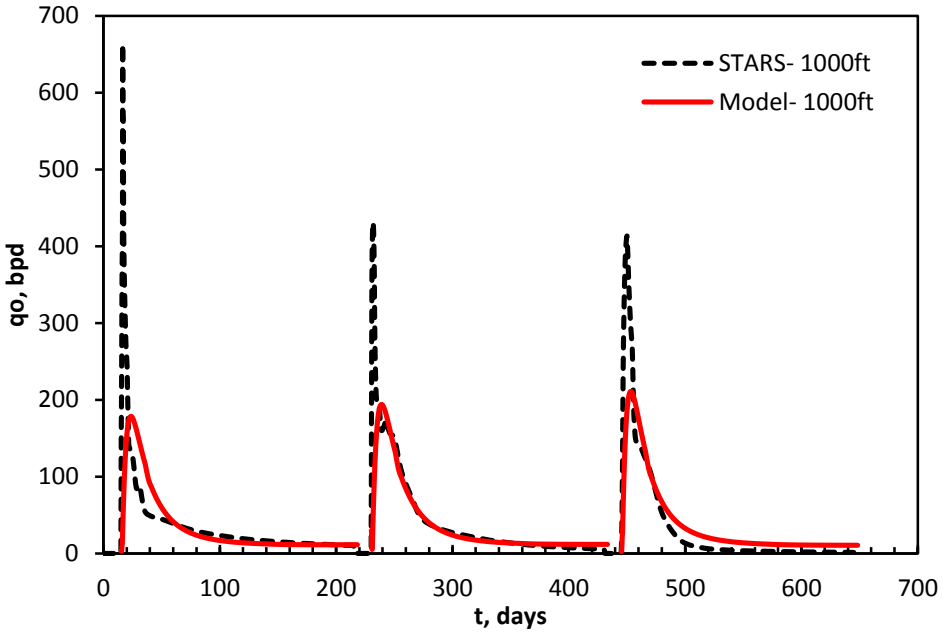

Figure 4.19: Comparison of oil rates from STARS and model for a well length of 1000ft.

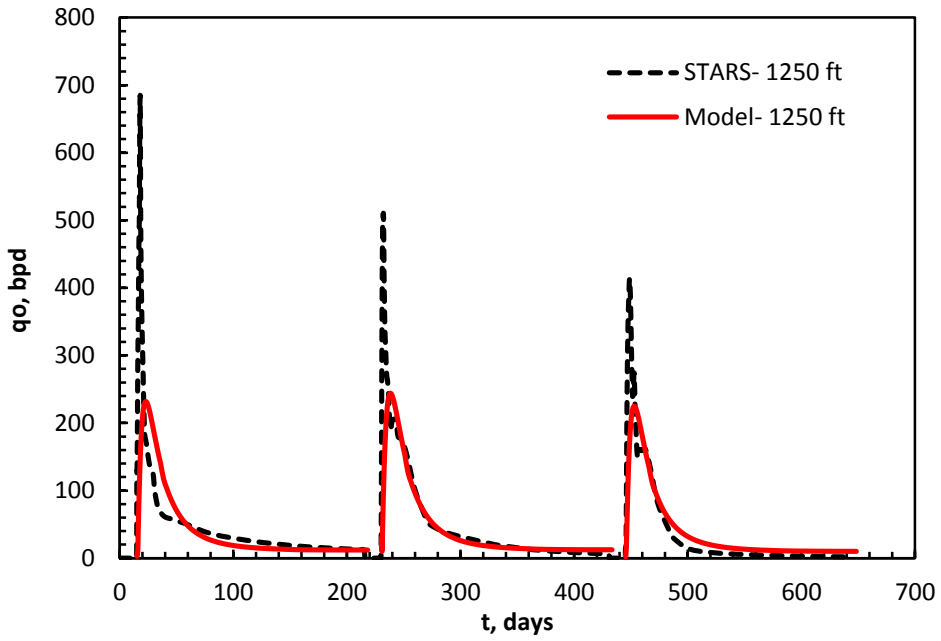

Figure 4.20: Comparison of oil production rates from STARS and model for a well length of 1250ft.

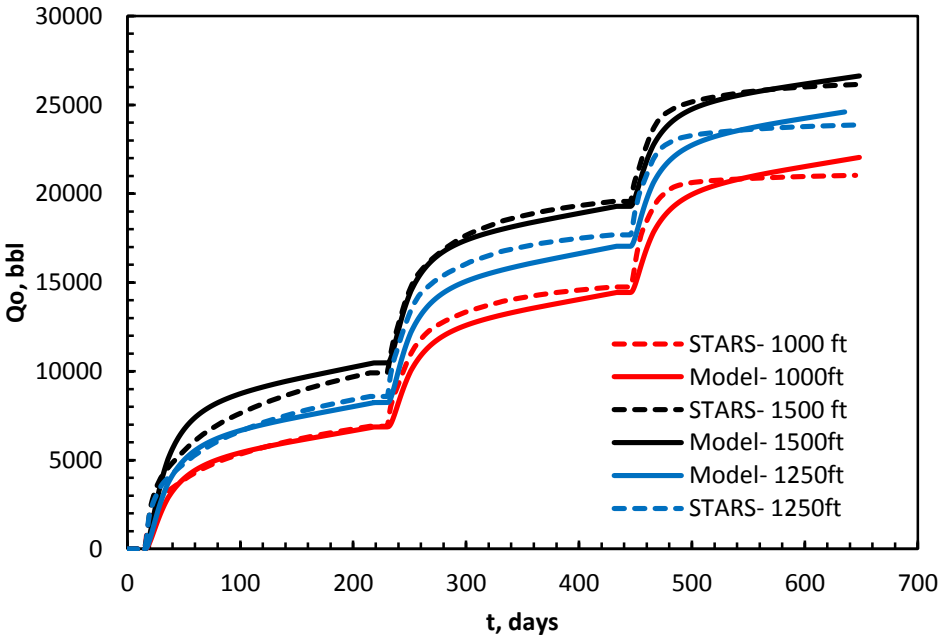

Figure 4.21: Cumulative oil production versus time for different lengths of the horizontal well.

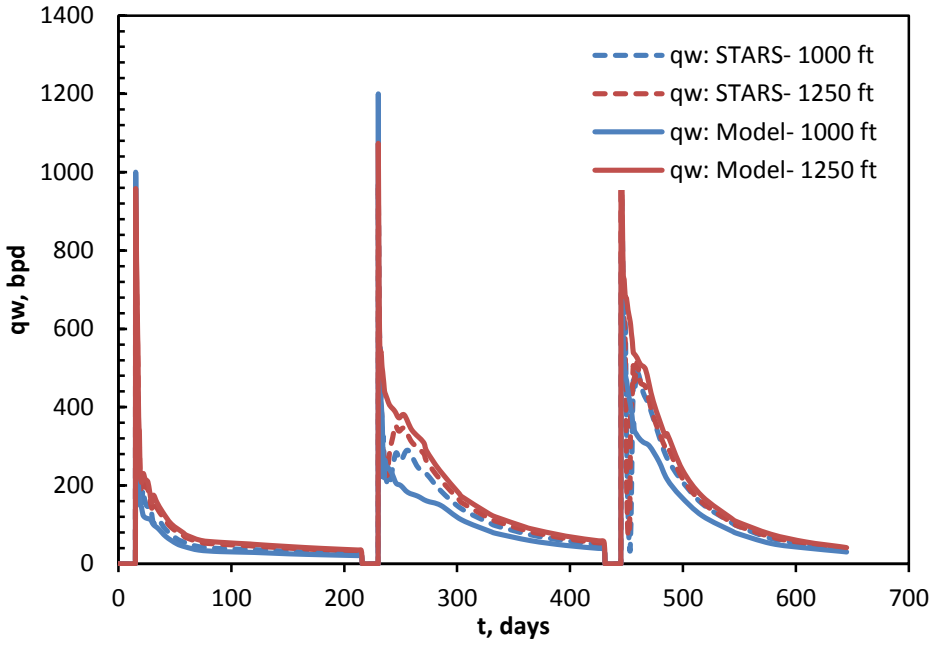

Figure 4.22: Comparison of water production rate from STARS and model for different horizontal well lengths.

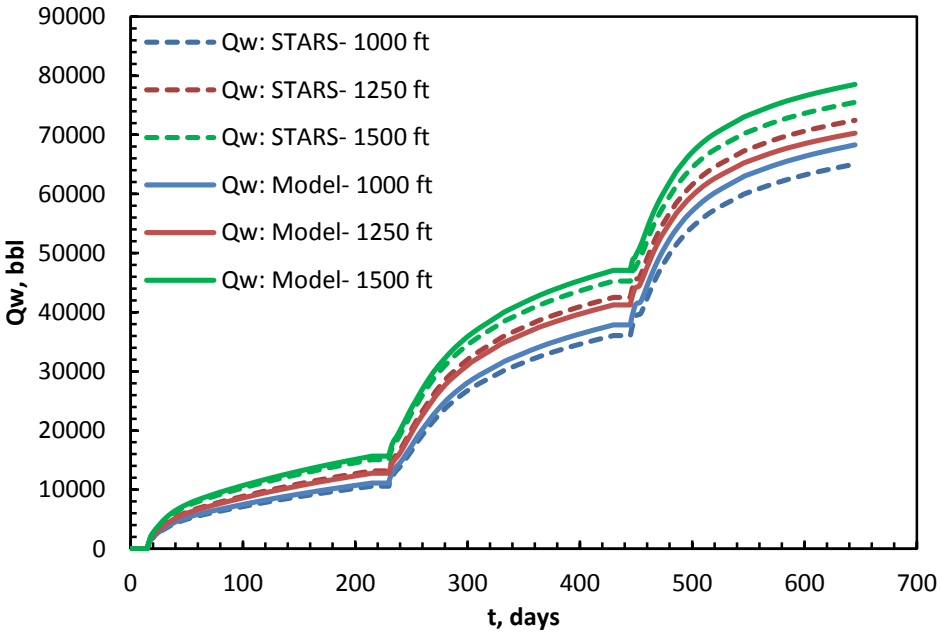

Figure 4.23: Comparison of cumulative water production from STARS and model for different lengths of horizontal well.

4.2.4 *Absolute permeability*

A case was run by changing the absolute permeability of reservoir. Three different scenarios were considered. One is the base case scenario where the permeability is 100 mD and the other two cases considered 150 mD and 200 mD. The other data used is same as the base case. Figure 4.24 and Figure 4.25 show the comparison of oil production rate obtained from the analytical model and the numerical simulator for absolute permeability values of 150 mD and 200 mD, respectively. Figure 4.26 shows a comparison of the cumulative oil production time for different absolute permeability values. It can be seen from the plot that as the permeability of the reservoir increases the cumulative oil production increases as well. Figure 4.27 shows a plot of the water production rate for different cases and it can be seen that the results obtained from the developed model and the simulator are fairly close to each other. Figure 4.28 depicts a plot of the cumulative water production versus time. Again, as expected, increase in the absolute permeability results in the increase in the cumulative water production.

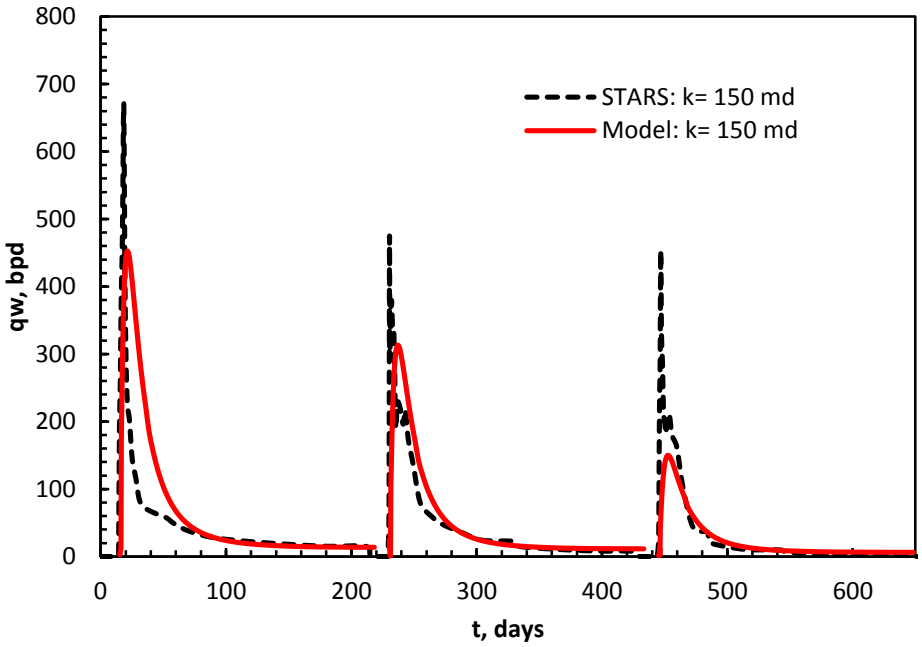

Figure 4.24: Comparison of oil rate from STARS and model for absolute permeability of 150 mD.

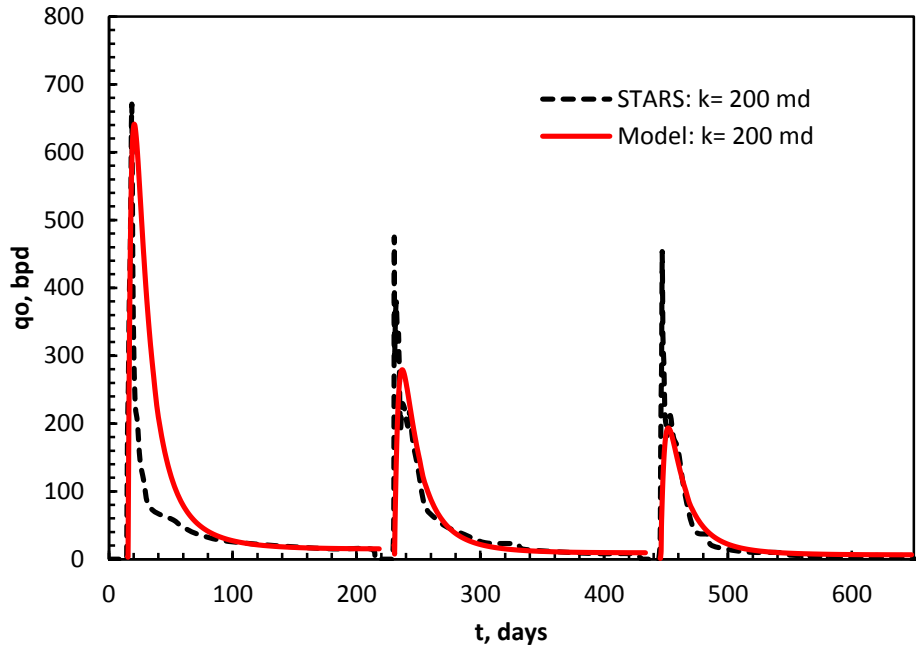

Figure 4.25: Comparison of oil rate from STARS and model for absolute permeability of 200 mD.

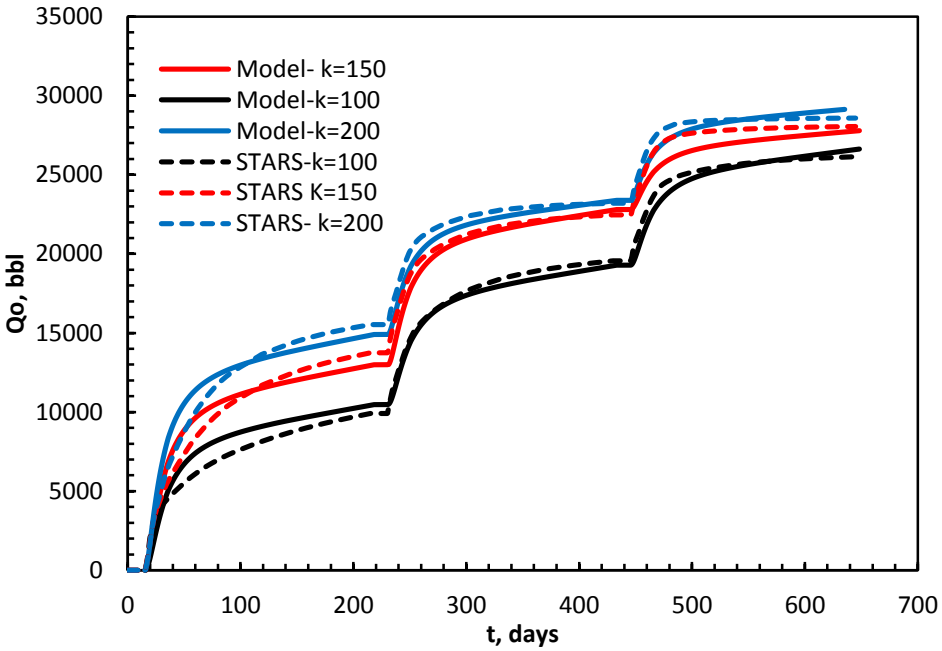

Figure 4.26: Comparison of cumulative oil production versus time from, STARS and developed model, for different absolute permeability values.

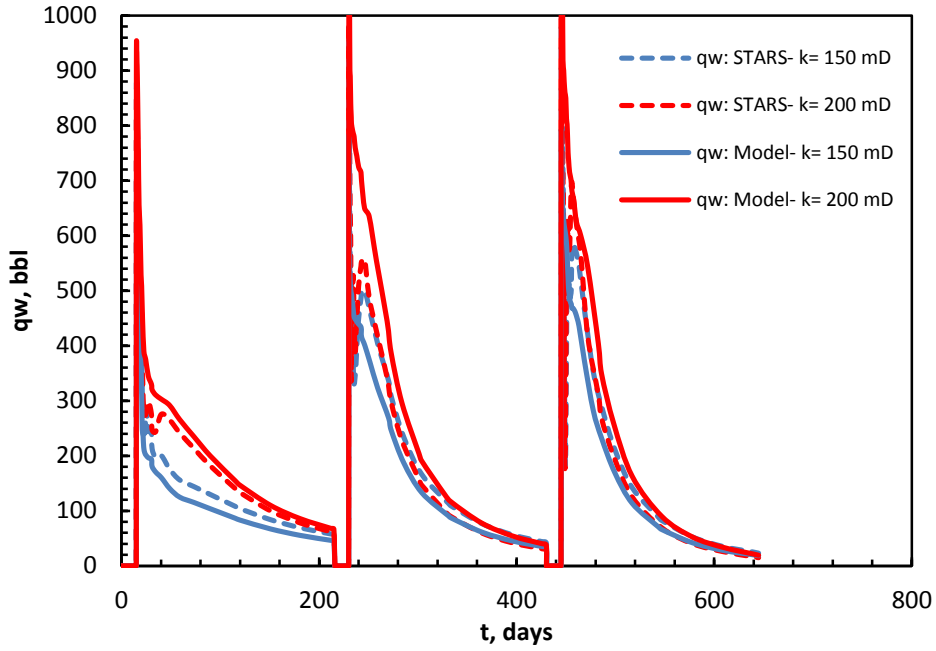

Figure 4.27: Comparison of water production rate versus time, form STARS and developed model, for different absolute permeability values.

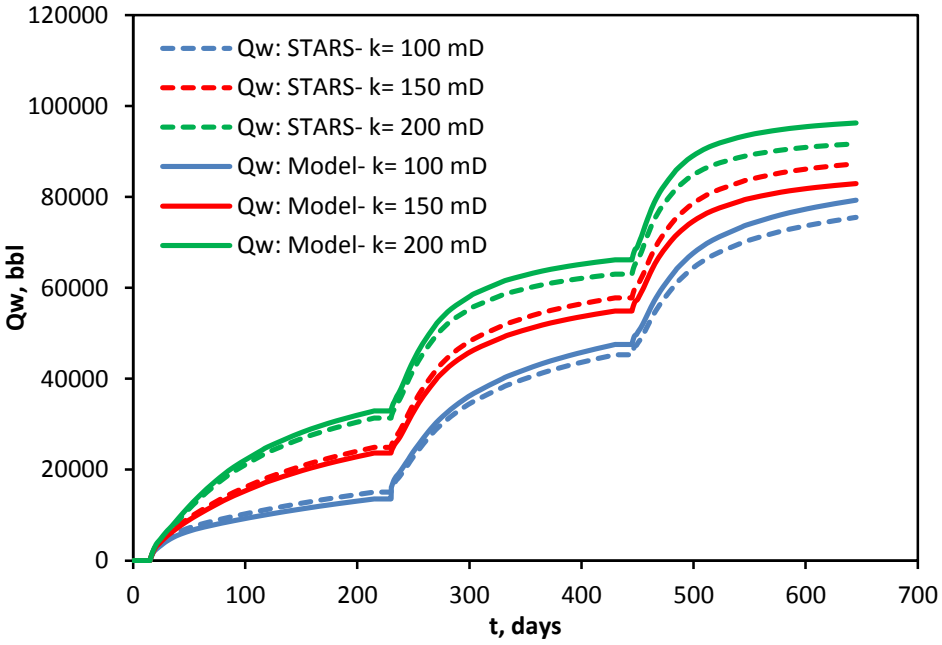

Figure 4.28: Comparison of cumulative water production versus time, from STARS and developed model, for different absolute permeability values.

The model is tested for a reservoir permeability of 1000 mD. A comparison of the oil production rate and cumulative oil production, obtained from the numerical simulator and

the analytical model, is shown in Figure 4.29 and Figure 4.30, respectively. Similarly, the water production rate and the cumulative water production are shown in Figure 4.31 and Figure 4.32, respectively. It can be seen from the plots that the results from the numerical simulator and the analytical model are very close to each other.

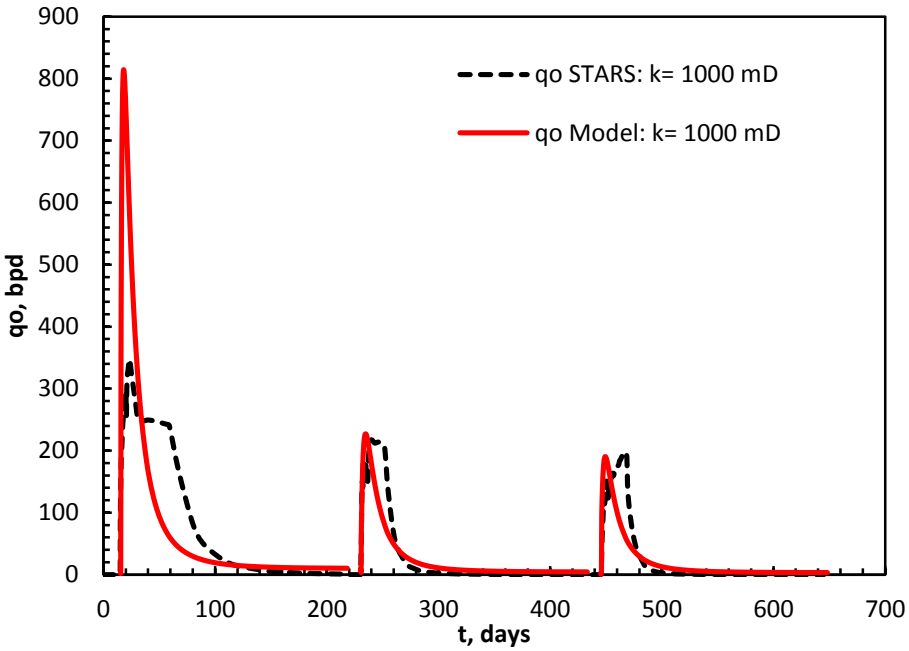

Figure 4.29: Plot of oil production rate, q_o, obtained from STARS and analytical model for a permeability of 1000 mD.

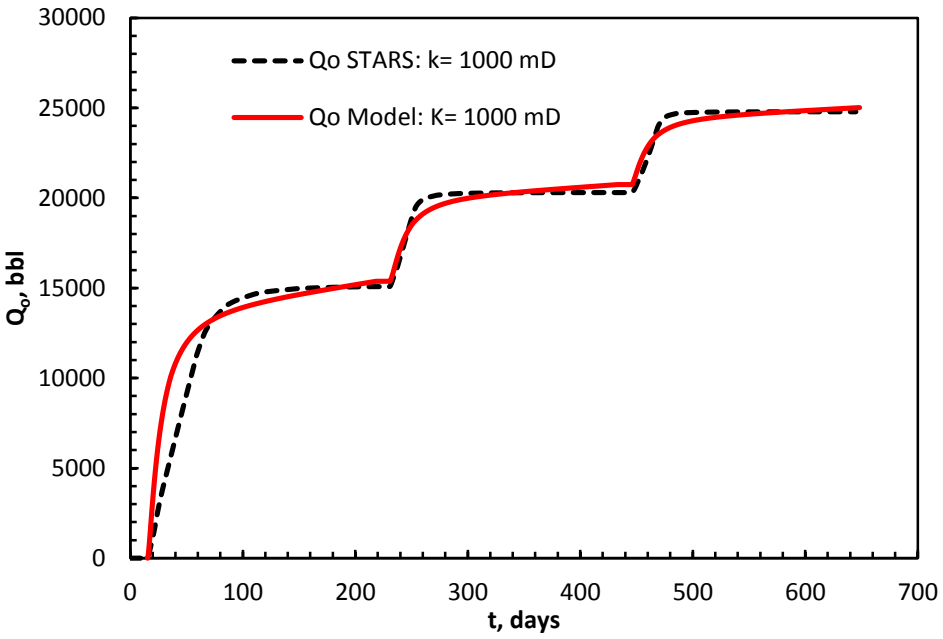

Figure 4.30: Plot of cumulative oil production, Q_o, obtained from STARS and analytical model for a permeability of 1000 mD.

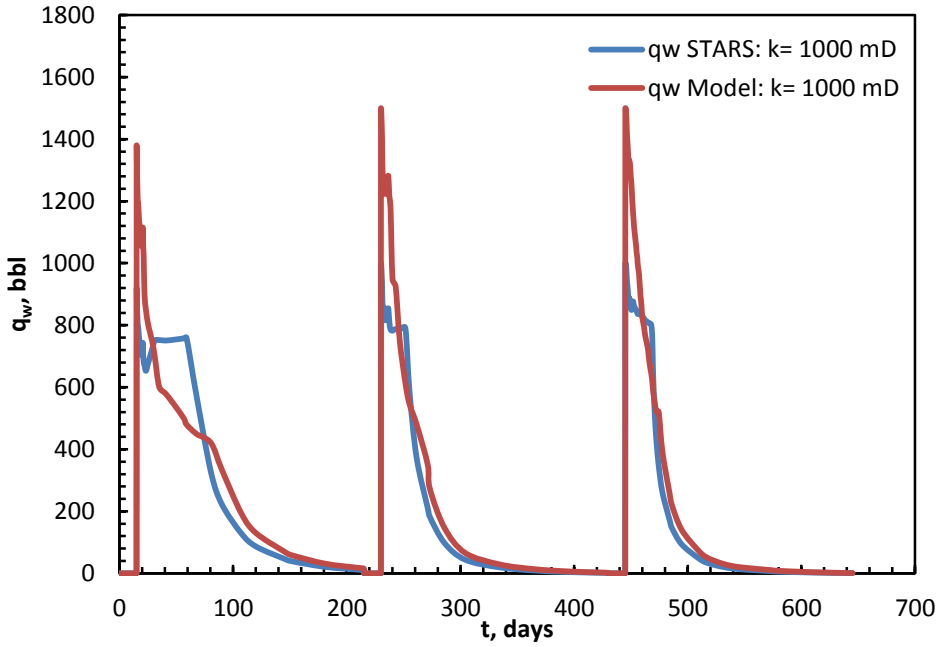

Figure 4.31: Plot of water production rate, Q_w, obtained from STARS and analytical model for a permeability of 1000 mD**.**

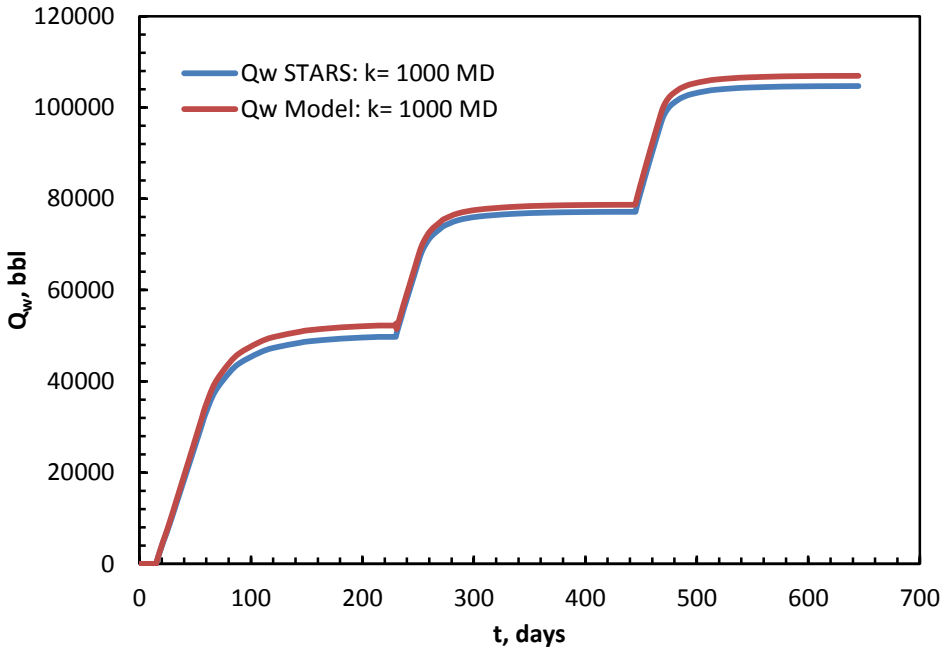

Figure 4.32: Plot of cumulative water production, Q_w, obtained from STARS and analytical model for a permeability of 1000 mD.

4.2.5 Relative permeability of oil and water

The model was tested for two different relative permeability models, as shown in the Figure 4.33. Figure 4.34 shows a plot comparing the oil production rate obtained from the numerical simulator and developed model for the new relative permeability model. Figure 4.35 shows the cumulative oil production versus time. Similarly, the plots for water production rate and cumulative water production are shown in Figure 4.36 and 4.37, respectively. Figure 4.35 shows that the cumulative oil production for the base case is higher than the cumulative oil production obtained from the new relative permeability curve. On the other hand, it can be seen from the Figure 4.37 that the cumulative water production from the base case is lower. An explanation for this could be that during the initial stages of a cycle, when the water saturation is high ($1-S_{orw}$), the relative permeability of water is lower in the base case than compared to the new case. For example, in base case when $S_w= 0.6$, the value of k_{rw} is about 0.18 and for the new case, when $S_w=0.75$ the value of k_{rw} is about 0.3. This implies that during the initial the initial

stages of the cycle (which accounts for major water production) the water production rate is higher in the new case than compared to the base case.

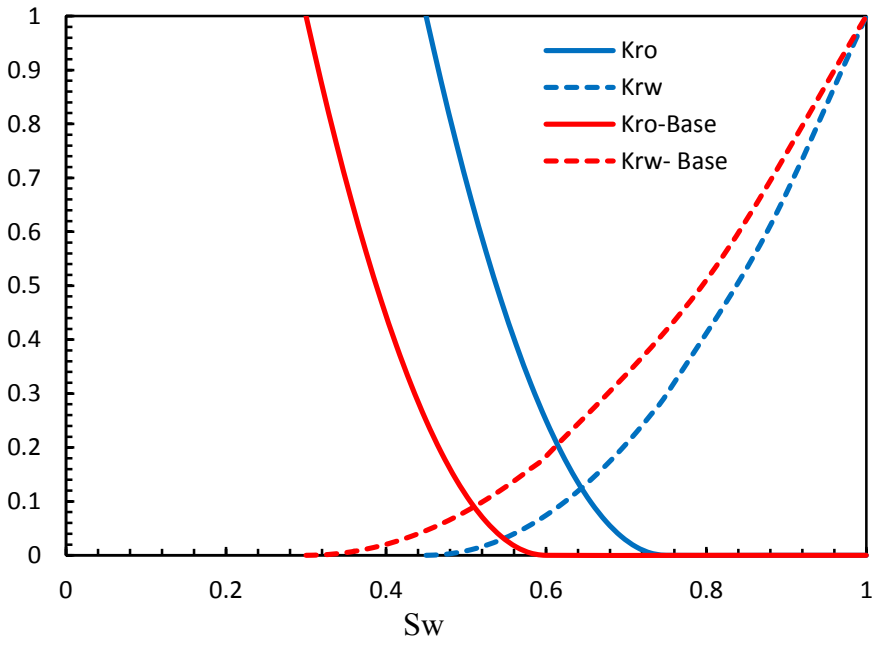

Figure 4.33: Different types of relative permeability curves versus water saturation.

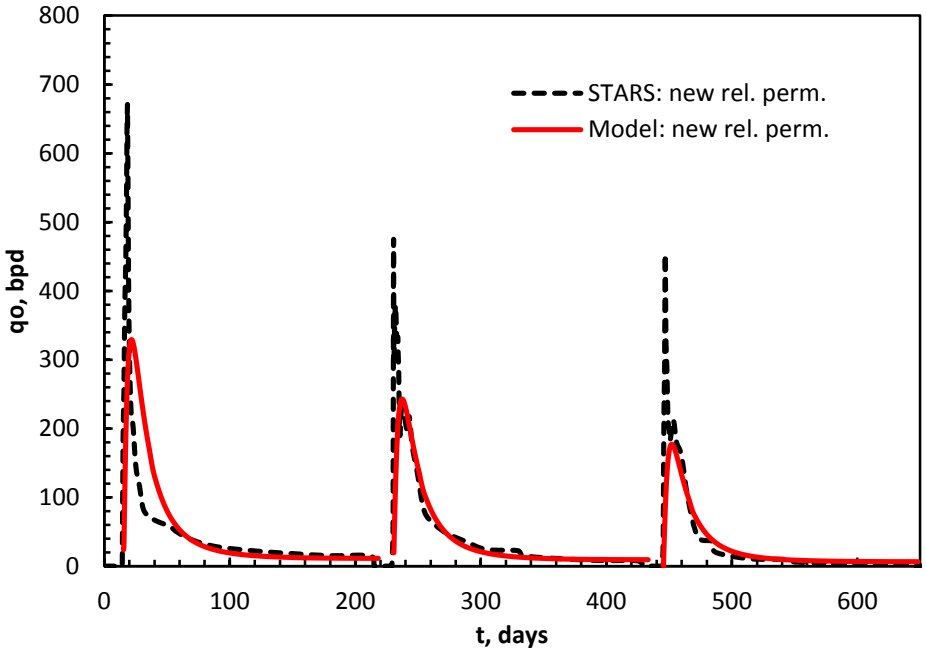

Figure 4.34: Comparison of oil production rate versus time, from STARS and developed model, for a different relative permeability model.

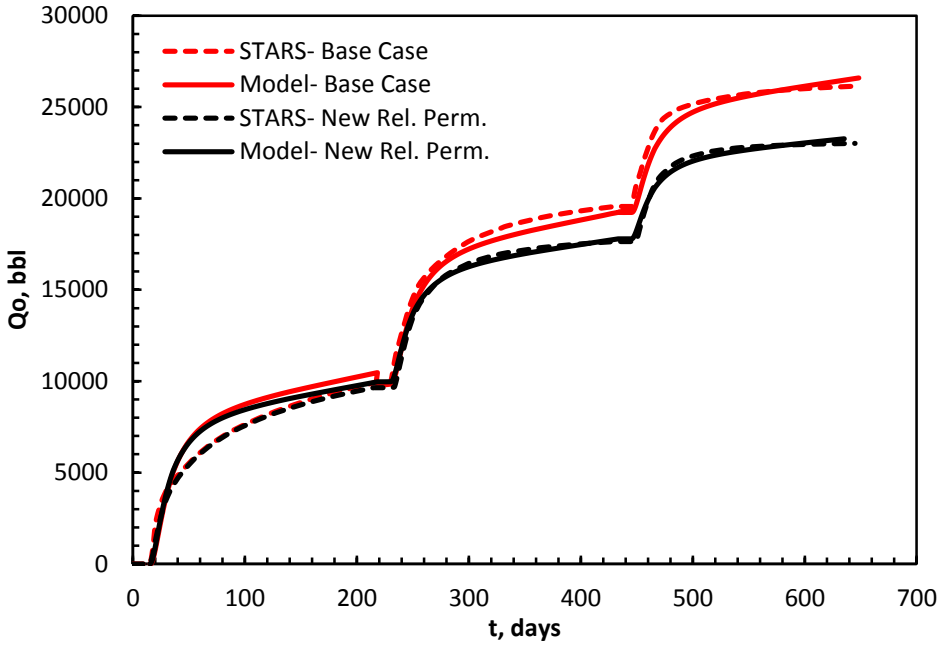

Figure 4.35: Comparison of cumulative oil production versus time, from STARS and developed model, for different relative permeability curves.

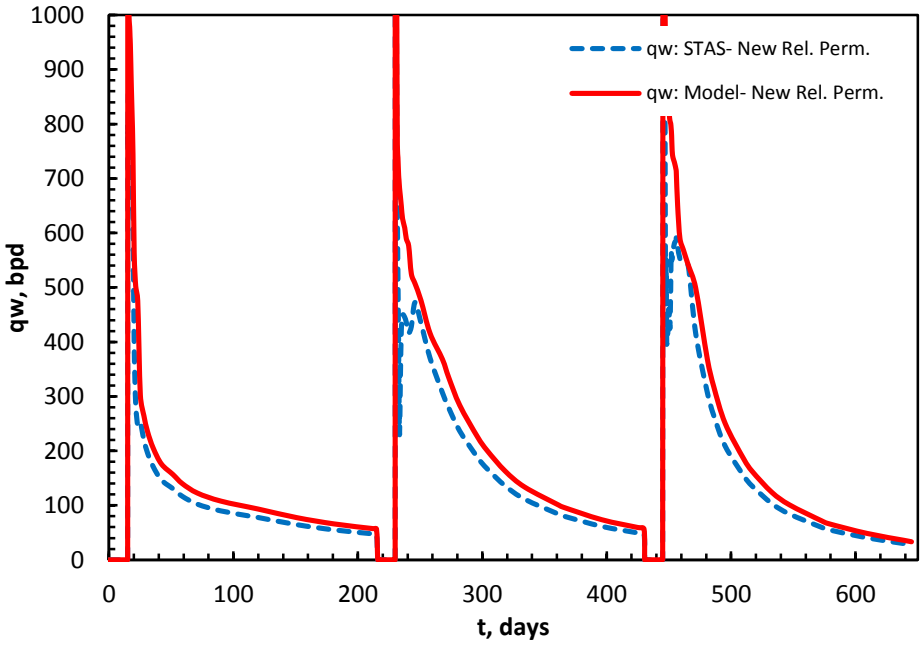

Figure 4.36: Comparison of water production rate versus time, from STARS and developed model, for a different relative permeability model.

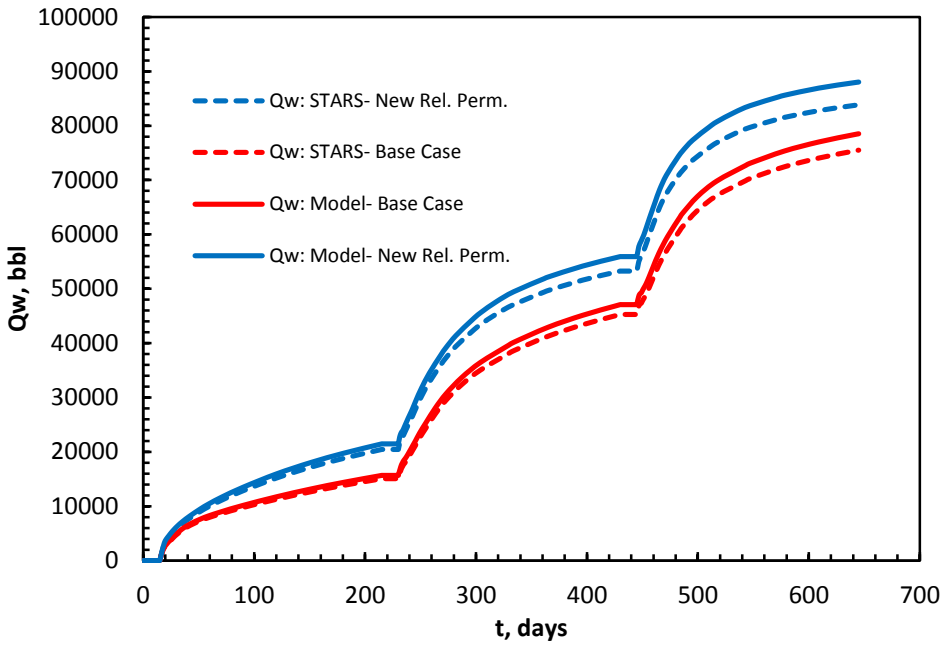

Figure 4.37: Comparison of cumulative water production versus time, from STARS and developed model, for a different relative permeability model.

4.2.6 Thermal diffusivity

The model was tested for two different thermal diffusivity values of the reservoir: 0.04ft^2/hr (base case) and 0.02ft^2/hr. Figure 4.38 shows a comparison of oil production rate obtained from the numerical simulator and developed model for the new thermal diffusivity value. Figure 4.39 shows a plot of the cumulative oil production obtained from the simulator and the model. Similarly, the water production rate and the cumulative water production are shown in Figure 4.40 and 4.41, respectively. For a rock with high thermal diffusivity, heat propagates faster because the rock conducts heat quickly relative to its volumetric heat capacity. Hence, the higher the thermal diffusivity, faster will be the heat loss to the surrounding during the soak and production period and lower the production rate. Figure 4.39 and 4.41 show that the cumulative oil and water production for the base case is lower than the latter case (base case has a higher thermal diffusivity value).

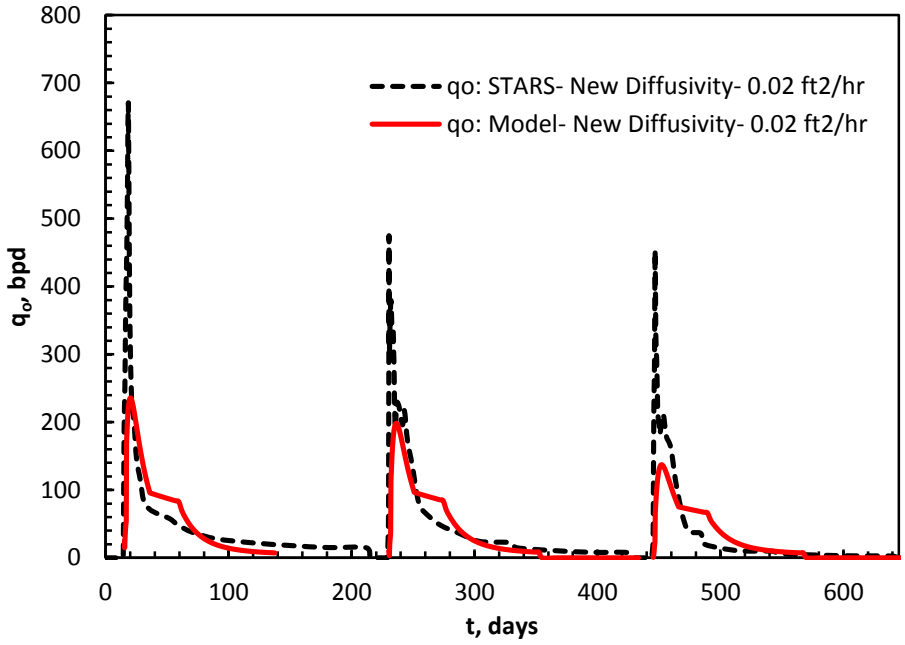

Figure 4.38: Comparison of oil rate versus time, from STARS and developed model, for a new diffusivity value.

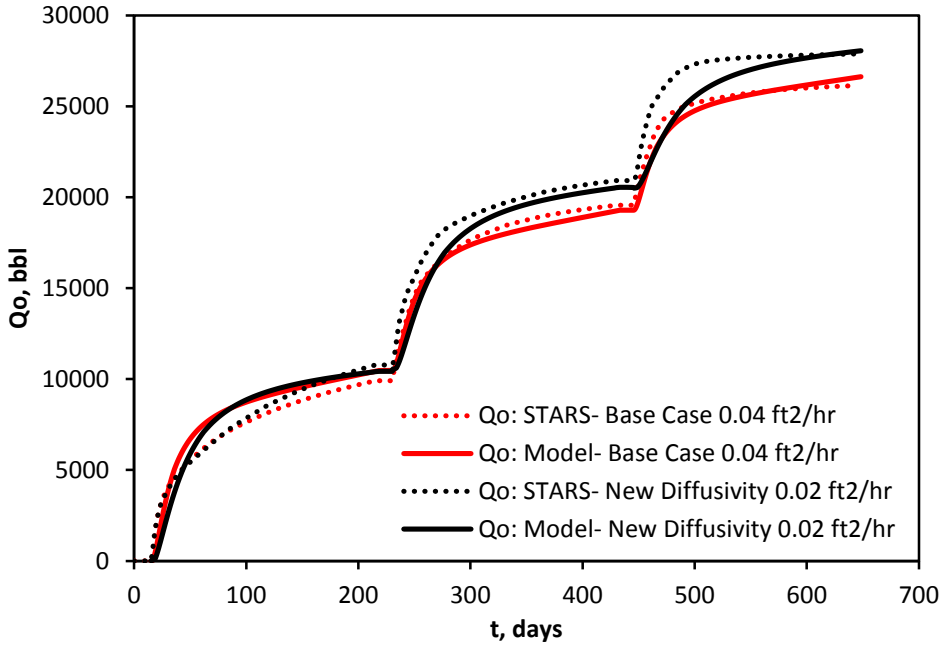

Figure 4.39: Comparison of cumulative oil production versus time, form STARS and developed model, for a different thermal diffusivity value.

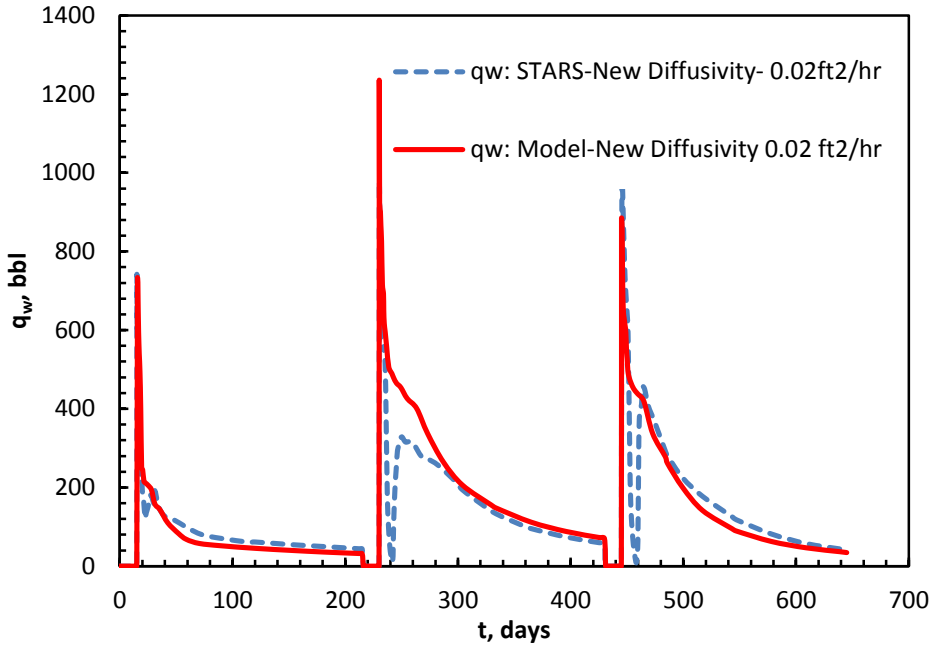

Figure 4.40: Comparison of water production rates versus time, form STARS and developed model, for a different thermal diffusivity value.

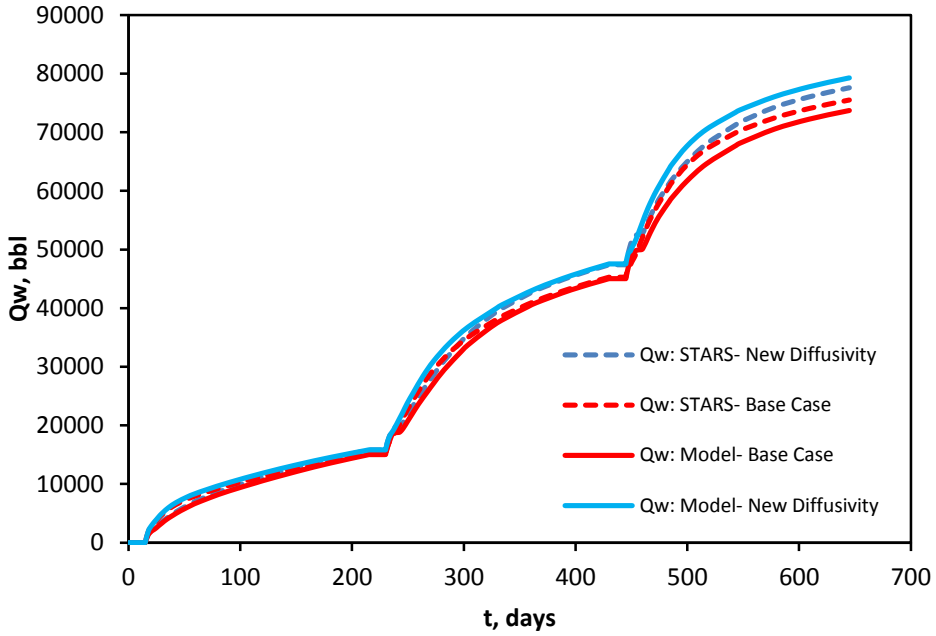

Figure 4.41: Comparison of cumulative water production versus time, from STARS and developed model, for different thermal diffusivities.

4.2.7 Types of oil viscosity

The model was tested for two different type of oil viscosity: base case; and viscosity data obtained from the research sponsor-PennWest Exploration. Figure 4.42 and Figure 4.44 show the oil and water production rates, respectively, obtained from the developed model and the simulator. Figure 4.43 shows the comparison of cumulative oil production obtained from the developed model and the numerical simulator for two different cases and the results are fairly close to each other. Similarly, the cumulative water production for both the cases shows an acceptable match, as depicted in Figure 4.45.

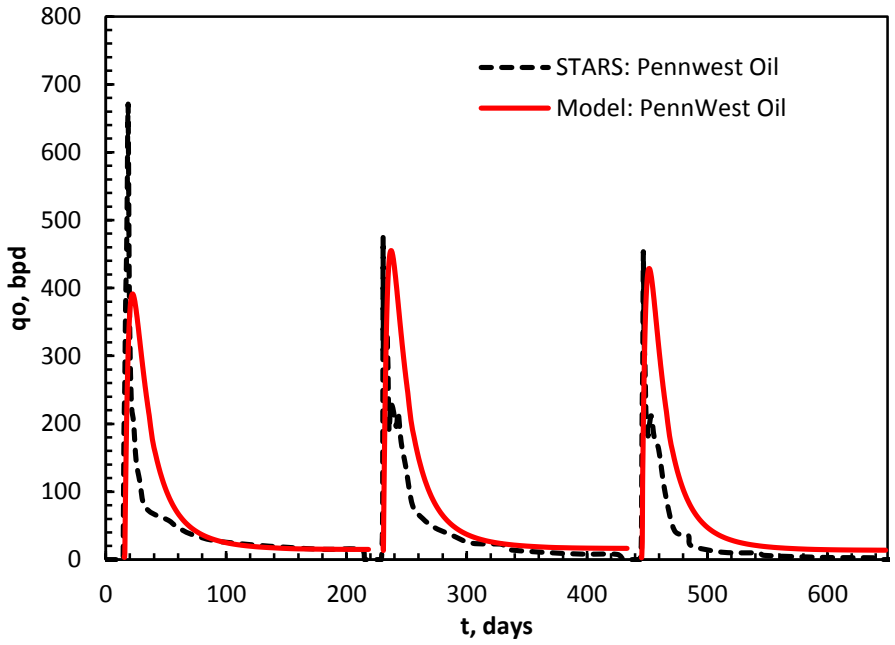

Figure 4.42: Comparison of oil rate versus time, from STARS and developed model, for PennWest oil viscosity.

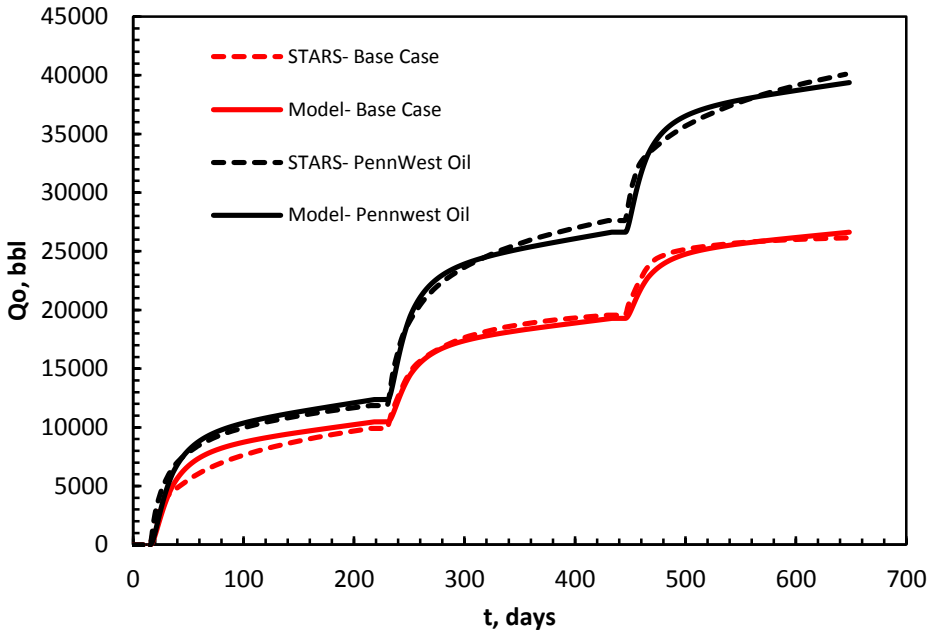

Figure 4.43: Comparison of cumulative oil production versus time, from STARS and developed model, for different types of oil- viscosity.

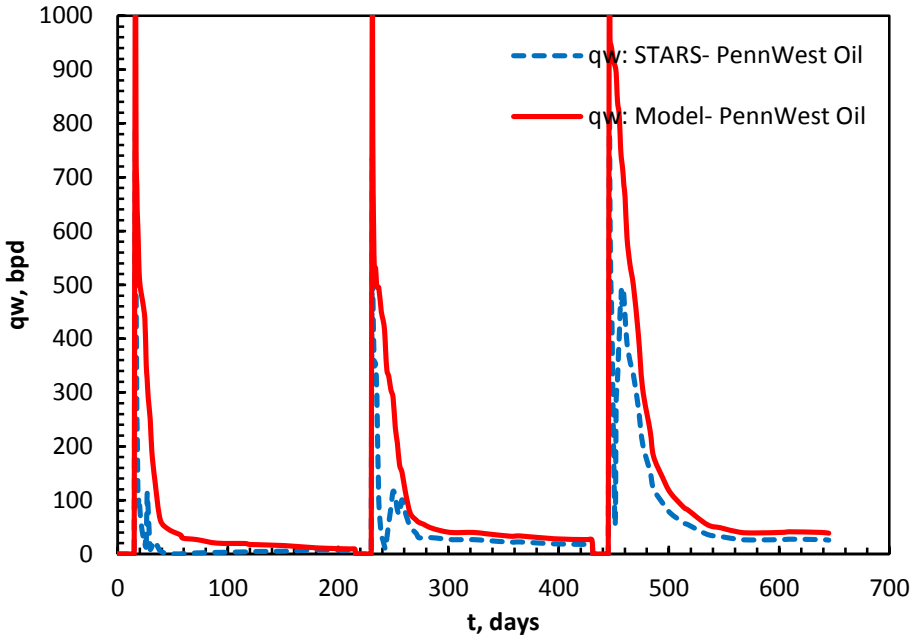

Figure 4.44: Comparison of water production rate versus time, from STARS and model, for PennWest oil viscosity.

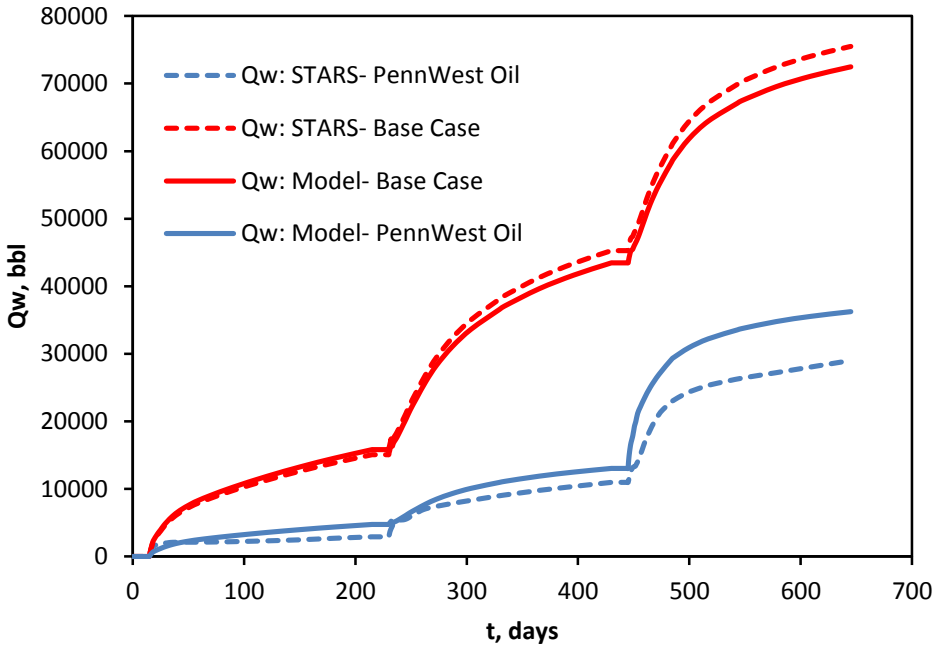

Figure 4.45: Comparison of cumulative water production versus time, from STARS and developed model, for PennWest oil viscosity.

4.2.8 Number of cycles

A cyclic steam stimulation process consists of many cycles, typically around 7-10 cycles or as long as it is economically viable. Hence, it is important to see if the developed model is able to accurately predict the performance of the process for more than just three cycles. The model was tested for ten cycles and the results are presented in this section. Figure 4.46 and Figure 4.47 show the oil production rate and cumulative oil production, respectively, for ten cycles. Similarly, the water rate and cumulative water production rate are plotted in Figure 4.48 and Figure 4.49. It can be verified from the plots that the model is robust to predict the performance for up to ten cycles.

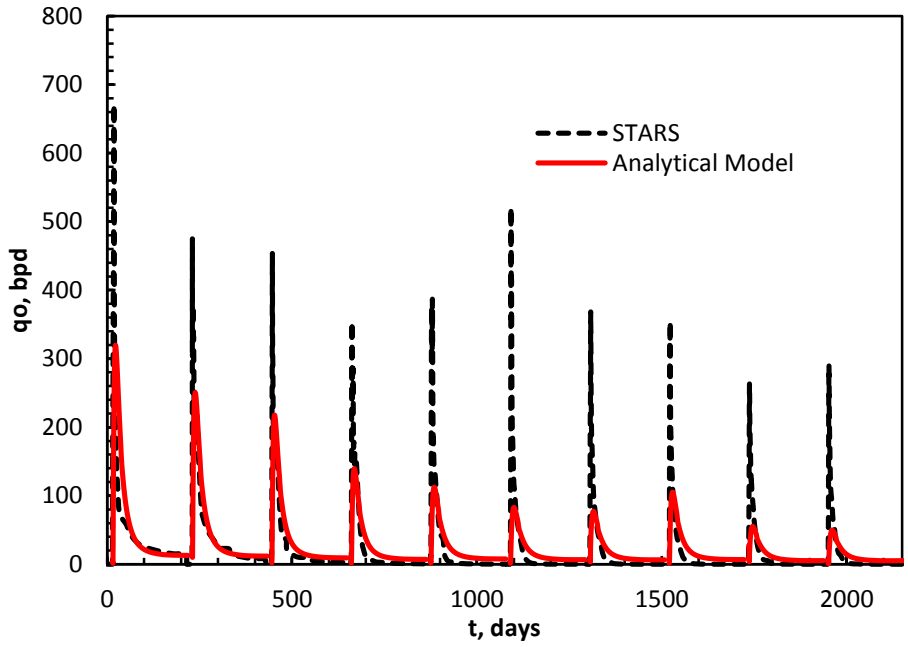

Figure 4.46: Comparison of oil production rate versus time, from STARS and developed model, for ten cycles.

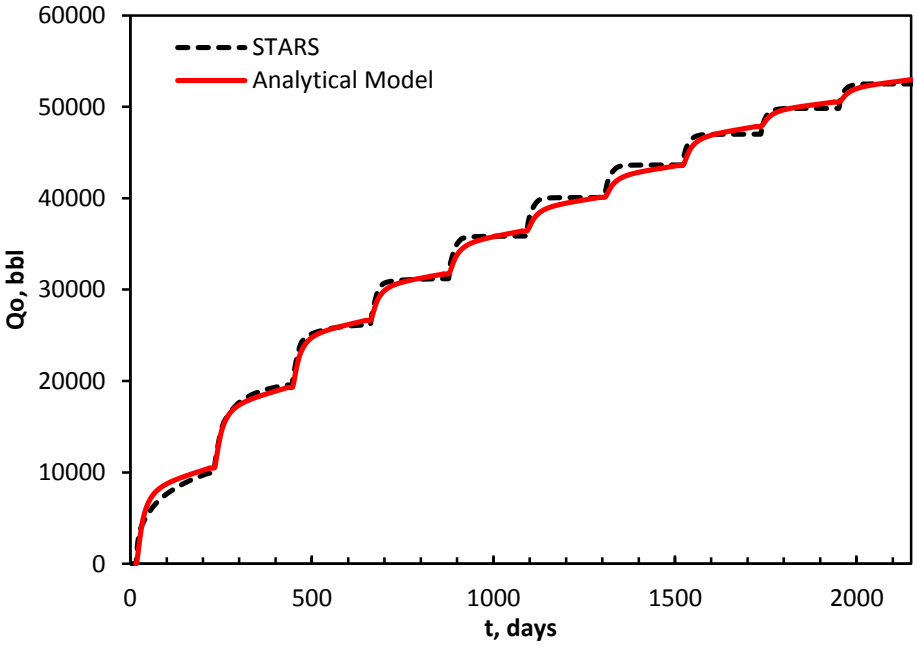

Figure 4.47: Comparison of cumulative oil production versus time, from STARS and developed model, for ten cycles.

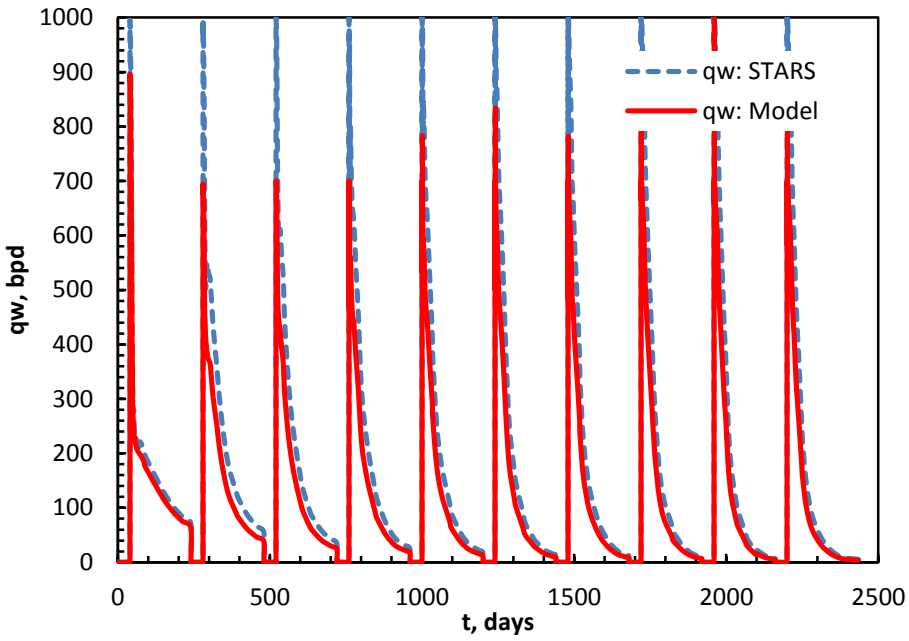

Figure 4.48: Comparison of water production rate versus time, from STARS and developed model, for ten cycles.

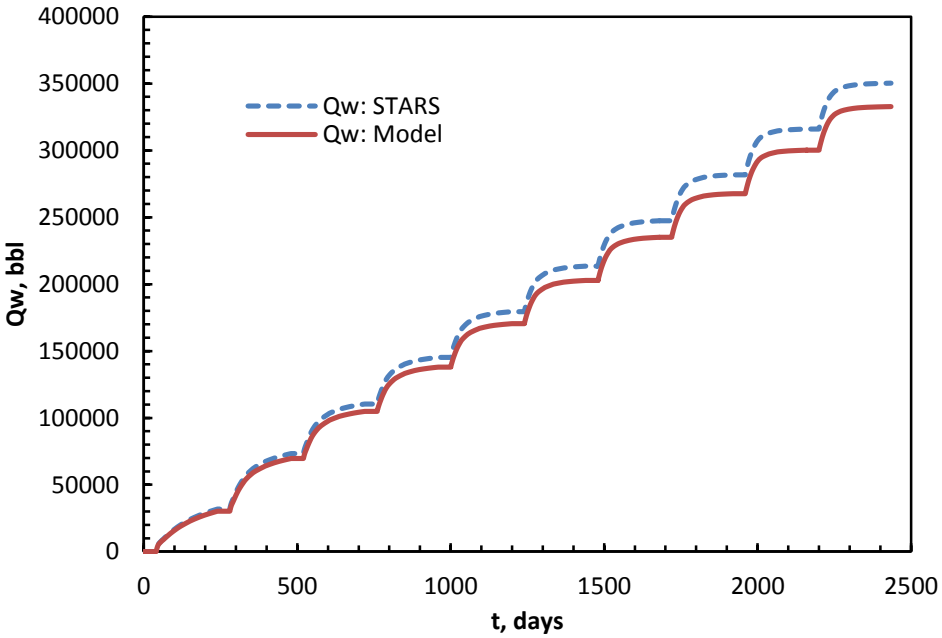

Figure 4.49: Comparison of cumulative water production versus time, obtained from STARS and developed model, for ten cycles.

4.2.8.1 Steam oil ratio

An important index used to evaluate the performance of a cyclic steam stimulation process is SOR (steam oil ratio). It is defined as the volume of steam required to produce one unit volume of oil. Hence, the lower the SOR value, the more efficient the process is. The cumulative steam oil ratio (CSOR) can be calculated as.

$$CSOR = \frac{Q_{s\,inj}}{Q_o}$$

where,

$Q_{s.inj}$ = the cumulative steam injected, bbl CWE

Q_o = the cumulative oil produced, bbl

Typical values of SOR for a cyclic steam stimulation process are in the range of three to eight. For a ten cycle process, the SOR is plotted and are shown in the Figure 4.50 and Figure 4.51. Figure 4.50 shows a plot of the cumulative steam oil ratio versus time. Initially, the SOR value is very high as the cumulative oil production is very low for the first time step. Figure 4.51 shows a plot of the average values of CSOR with respect to the number of cycles. It can be seen from the plots that the calculated values of SOR is in the range of three to six, which is typical of a cyclic steam stimulation process.

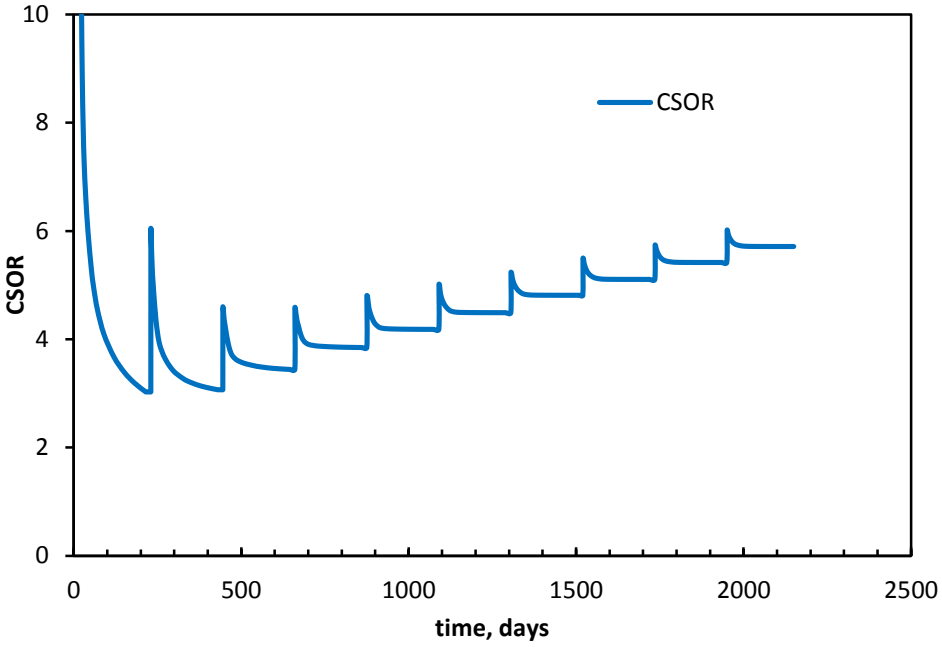

Figure 4.50: Plot of cumulative steam oil ratio versus time

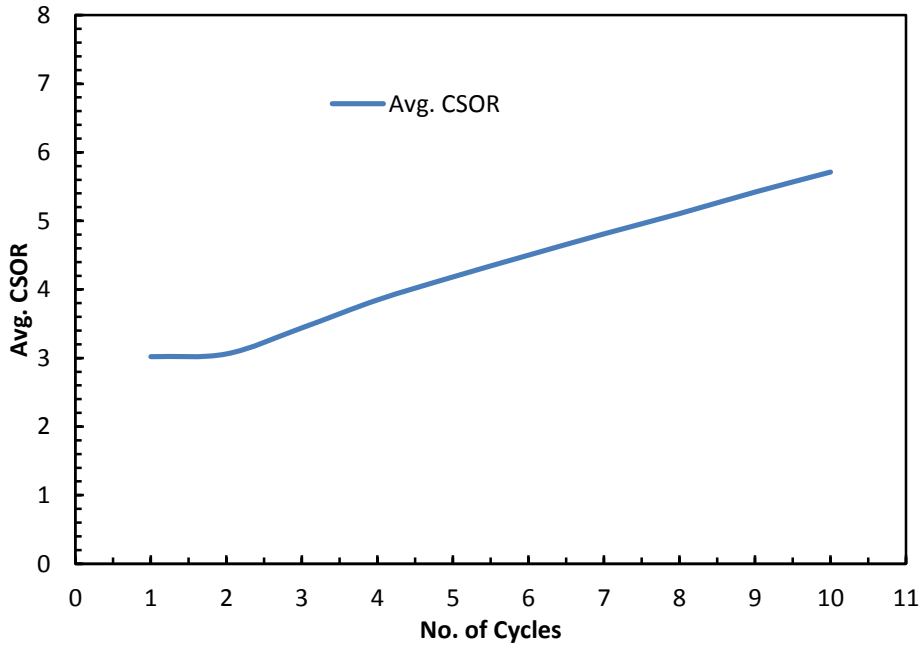

Figure 4.51: Plot of average steam oil ratio versus the number of cycles

4.3 Summary

The model is successfully validated and tested by comparing the fluid production (rate and cumulative production of both oil and water) obtained from the model with the fluid production obtained from STARS numerical simulator. The following parameters were considered: steam injection rates, length of the horizontal well, absolute permeability of the reservoir, relative permeability of oil and water, thermal diffusivity of the formation, oil with different viscosities, and finally the number of operational cycles.

All the calculations for the analytical model were done using MATLAB and an excel spreadsheet. The results obtained from the analytical model are compared with the results obtained from STARS numerical simulator. Step by step procedure to calculate the oil and water rates is presented in the *Section 4.1* and detailed sensitivity analyses are presented in *Section 4.2* of this chapter. It is concluded that the model is able to predict the performance of the CSS process and there is a good match with the results obtained from the numerical simulator. To obtain a good match for the water production, a corrected relative permeability of water was used.

CHAPTER FIVE:

5 Conclusions and Recommendations

5.1 Results

In this thesis, a radial one dimensional heat transfer model has been developed to predict the average temperature of the steam zone for a cyclic steam stimulation process with horizontal well configuration. The oil and water viscosities are calculated based on the average steam zone temperature. Correlations for fluids saturation and relative permeabilities of oil and water are described. This heat transfer model is coupled to a transient radial fluid inflow model that is used to calculate the fluid flow rates. A modified form of Joshi's in flow equation is used. Finally, detailed steps for calculations are shown and a flow chart is presented which outlines the important steps involved in the performance prediction for a CSS process for horizontal wells.

The developed model is validated using numerical simulation in CMG STARS. First, a base case is run to checked if the results from the simulator match with that of the developed analytical model. Next, sensitivity analyses were conducted to test the robustness of the model for parameters such as: steam injection rates, length of the horizontal well, absolute permeability of the reservoir, relative permeability of oil and water, thermal diffusivity of the formation, oil with different viscosities, and finally the number of operational cycles.

All the calculations for the analytical model were done using MATLAB and an Excel spreadsheet. The results obtained from the analytical model are compared with the results obtained from STARS numerical simulator. To obtain a good match for the water production, a corrected relative permeability of water is used. It is concluded that, with reasonable assumptions and using a correction factor for the water relative permeability, the model is able to predict the performance of the CSS process and there is a good match with the results obtained from the numerical simulator.

5.2 Future Work

5.2.1 Economic studies

Currently, the developed analytical model for cyclic steam stimulation process for a horizontal well configuration can be used to optimize production from a single well. The model has a potential to be coupled with an economic model to optimize steam injection rates, production rates based on the reservoir properties and conducting economic studies.

5.2.2 Pressure drop model and water relative permeability adjustment

The pressure drop model for predicting the pressure drawdown is based on a trial and error method. In order to obtain a good match for the oil production with STARS, the calculation of pressure drawdown requires an initial guess work, based upon the production data obtained from the numerical simulator and iteration. To match the water production, some adjustments were made to the water relative permeability curves. This area needs further investigation in order to minimize the need of matching parameters.

APPENDIX

A. Solution for Average Temperature of the Steam Zone (CSS)

Heat conduction in radial direction is given as:

$$\frac{1}{r}\frac{\partial}{\partial r}\left(r\frac{\partial T}{\partial r}\right)=\frac{1}{\alpha}\frac{\partial T}{\partial r} \tag{A.1}$$

We defined two zones-Zone 1, which is at the temperature, T_S, initially, and Zone 2, region beyond r_h, that is at an elevated temperature due to the heat transfer in the steam injection and soak period, $T_{2(0)}$. Let T_1 and T_2 be the temperatures of the Zone1 and Zone 2 at any time, t, respectively. The initial and boundary conditions are defined as below:

Initial Condition:

$T_1=T_s$ at t=0 (A.2)

The net heat flux at r=0 is zero because of the radial symmetry. The total heat from the boundary of zone 1 is equal to the amount of heat absorbed by the Zone 2. It is denoted by B.C. 2. These are represented mathematically below as:

Boundary Conditions:

$$\frac{\partial T_1}{\partial r}=0 \qquad \text{at} \quad r=0 \tag{A.3}$$

$$kA\frac{\partial T_1}{\partial r}\bigg|_{r=r_h}=-V.\rho c_p\frac{\partial T_2}{\partial t} \qquad \text{at} \quad r=r_h \tag{A.4}$$

For solving the PDE, the following dimensional parameters were defined and the above equation is converted into a dimensionless form.

Dimensionless Parameters

$$T_{D1} = \frac{T_S - T_1}{T_S - T_R} \tag{A.5}$$

$$T_{D2} = \frac{T_S - T_2}{T_S - T_R} \tag{A.6}$$

$$r_D = \frac{r}{r_w} \tag{A.7}$$

$$t_D = \frac{\alpha t}{r_w^{\,2}} \tag{A.8}$$

$$T_{D2(0)} = \frac{T_S - T_{2(0)}}{T_S - T_R} \tag{A.9}$$

Equation in dimensionless form:

$$\frac{\partial^2 T_{D1}}{\partial r_D^{\,2}} + \frac{1}{r_D}\frac{\partial T_{D1}}{\partial r_D} = \frac{\partial T_{D1}}{\partial t_D} \tag{A.10}$$

Initial Condition:

$$T_{D1} = 0 \qquad \text{at} \qquad t=0 \tag{A.11}$$

B.C. 1:

$$\frac{\partial T_{D1}}{\partial r_D} = 0 \qquad \textbf{at} \qquad r_D = 0 \tag{A.12}$$

B.C. 2:

$$kA\frac{\partial T_{D1}}{\partial r_D} = -\frac{\alpha}{r_w}(\rho c_p . V)\frac{\partial T_{D2}}{\partial t_D} \quad \text{at} \qquad r_d = r_{dh} \tag{A.13}$$

The PDE is solved by using Laplace transforms. The equation in Laplace domain is given as:

$$\frac{\partial^2 \widetilde{T}_{D1}}{\partial r_D{}^2} + \frac{1}{r_D}\frac{\partial \widetilde{T}_{D1}}{\partial r_D} = s\widetilde{T}_{D1} \tag{A.14}$$

Multiplying by $r_D{}^2$ on both sides:

$$r_D{}^2\frac{\partial^2 \widetilde{T}_{D1}}{\partial r_D{}^2} + r_D\frac{\partial \widetilde{T}_{D1}}{\partial r_D} - r_D{}^2 s\widetilde{T}_{D1} = 0 \tag{A.15}$$

The equation is a modified form of Bessel's equation and the solution is given as:

$$\widetilde{T}_{D1} = c_1 I_0(r_D\sqrt{s}) + c_2 K_0(r_D\sqrt{s}) \tag{A.16}$$

Applying B.C. 1, we get:

$$\left.\frac{\partial \widetilde{T}_{D1}}{\partial r_D}\right|_{r_D=0} = c_1\sqrt{s}I_1(\sqrt{s}r_D) + c_2\sqrt{s}K_1(r_D\sqrt{s})\Big|_{r_D=0} = 0 \tag{A.17}$$

i.e. $c_2 = 0$ (A.18)

Therefore,

$$\widetilde{T}_{D1} = c_1 I_0(rD\sqrt{s}) \tag{A.19}$$

Applying B.C. 2:

$$kA\left.\frac{\partial \widetilde{T}_{D1}}{\partial r_D}\right|_{r_D=r_{Da}} = -\frac{\alpha}{r_w}(\rho c_p.V)\left[s\widetilde{T}_{D2} - T_{D2(0)}\right] \tag{A.20}$$

At $r_D = r_{Da}$, $T_{D2} = T_{D1}$ (A.21)

Therefore,

$$kAc_1\sqrt{s}I_1(r_{Da}\sqrt{s}) = -\frac{\alpha}{r_w}(\rho c_p.V)\left[s.c_1 I_0(r_{Da}\sqrt{s}) - T_{D2(0)}\right] \tag{A.22}$$

Let,

$$Q = \frac{\alpha(\rho c_p).V}{r_w.kA} \tag{A.23}$$

The Equation A.22 can be written as:

$$c_1\sqrt{s}I_1(r_{Da}\sqrt{s}) = -Qsc_1.I_0(r_{Da}\sqrt{s}) + Q.T_{D2(0)} \tag{A.24}$$

$$c_1 = \frac{Q.T_{D2(0)}}{\sqrt{s}I_1(r_{Da}\sqrt{s}) + QsI_o(r_{Da}\sqrt{s})} \tag{A.25}$$

From Equations A.19 and A.25, we get:

$$\widetilde{T}_{D1} = \frac{Q.I_0(r_D\sqrt{s}).T_{D2(0)}}{\sqrt{s}I_1(r_{Da}\sqrt{s}) + QsI_0(r_{Da}\sqrt{s})} \tag{A.26}$$

The average temperature in Zone-1 can be calculated as:

$$\widetilde{T}_{D1\,Avg} = \frac{\int_{r_D=1}^{r_D=r_{Da}} 2\pi r_D \widetilde{T}_{D1} dr_D}{\pi({r_{Da}}^2 - 1)} \tag{A.27}$$

$$\widetilde{T}_{D1\cdot Avg} = \left(\frac{2}{{r_{Da}}^2 - 1}\right)\left(\frac{1}{\sqrt{s}}\right)\left[\frac{Q.\left(r_{Da}I_1(r_{Da}\sqrt{S}) - I_1(\sqrt{s})\right)}{\sqrt{S}I_1(r_{Da}\sqrt{S}) + QsI_0(r_{Da}\sqrt{S})}\right]T_{D2(0)} \tag{A.28}$$

Temperature of Zone-2 is given by:

$$\widetilde{T}_{D2} = \widetilde{T}_{D1}\Big|_{r_D=r_{Da}} = \frac{Q.I_0(r_{Da}\sqrt{s}).T_{D2(0)}}{\sqrt{s}I_1(r_{Da}\sqrt{s}) + QsI_0(r_{Da}\sqrt{s})} \tag{A.29}$$

References

[1] Farouq Ali, S.M.: "Practical Heavy Oil Recovery", ENCH 619 Notes, University of Calgary, 2010.

[2] Gutierrez, D., Moore, R.G., Mehta, S.A., and Skoreyko, F.: "The Challenge of Predicting Field Performance of Air Injection Process Based on Laboratory and Numerical Modeling", J.Can.Pet. Tech., March 2009.

[3] Boberg, T.C. "Thermal Methods of Oil Recovery", John Wiley & Sons, Inc., 1988

[4] Alvarez, J., and Coates, R., Heavy Oil Recovery; Cyclical Solvent Injection, CSI, Wednesday, 27 May 2009, Russian Oil and Gas Technologies. 2009.

[5] Butler R.M.: "Thermal Recovery of Oil and Bitumen", GravDrain Inc., July 2008.

[6] Schild, A. "A Theory for the Effect of Heating Oil Producing Wells", Trans. AIME, 210, 1 (1957)

[7] Fontanilla, J.P. and Aziz, K.: "Prediction of Bottom-Hole Conditions for Wet Steam Injection Wells", J.Can.Pet.Tech., March-April 1982.

[8] Marx J.W. and Langenheim R.H.: "Reservoir Heating by Hot Fluid Injection", Trans., Aw (19S9) 216, 312-314.

[9] Carter, R.D.: Appendix to "Optimum Fluid Characteristics for Fracture Extension", by G.C. Howard and G.R. Fast, Drill. And Prod. Prac., API (1957) 267.

[10] Boberg, T.C. and Lantz, R.B.: "Calculation of the Production Rate of a Thermally Stimulated Well", J.Pet.Tech., December 1966.

[11] Bensten R.G and Donohue, D.A.T.: "A Dynamic Programming Model of the Cyclic Steam Injection Process," JPT (Dec 1969) 2582- 96; Trans., AIME 246.

[12] Bidnr M.S. and Kostilia H.M.: "Analysis of Transient Production of a Thermally Stimulated Well," SPE 16997 (Sept. 1989).

[13] van Everdingen, A.F. and Hurst, W.: "The Applications of Laplace Transformations to Flow Problems in Reservoirs," Tran., AIME (1949) 186, 305-24.

[14] Towson, D.E. and Boberg, T.C.: "Gravity Drainage in Thermally Stimulated Wells", J. Can. Pet. Tech., (Oct- Dec. 1967) 130-135

[15] Matthews, C.S. and Leftkovics, H.C.: "Gravity Drainage Performance of Depletion-Type Reservoirs in the Stripper Stage", Trans., AIME (1956) 207, 265- 274.

[16] Seba, R.A. and Perry, G.E.: "A Mathematical Model of Repeated Steam Soaks of Thick Gravity Drainage Reservoirs", J. Pet. Tech. (Jan., 1969) 87-94.

[17] Kuo, C.H., Shain, S.A., and Phocas, D.M.: "A Gravity Drainage Model for the Steam Soak Process", paper SPE 2329 presented at the 39th Annual SPE California Fall Meeting, Bakersfield, California, Nov. 7-8, 1968.

[18] Jones, J.: "Cyclic Steam Reservoir Model for Viscous Oil, Pressure-depleted, Gravity-drainage Reservoirs", SPE 6544, 47th Annual California Regional Meeting of the SPE of AIME, Bakersfield (April 13-15, 1977).

[19] Butler, R.M., McNab, G.S., and Lo, H.Y.: "Theoretical Studies on the Gravity Drainage of Heavy Oil during in Situ Steam Heating", presented at the 29th Can. Chem. Eng. Conf., Sarnia, Ont., Oct. 1-3, 1979.

[20] Aziz, K. and Gontijo J.E.: "A Simple Analytical Model for Simulating Heavy oil Recovery by Cyclic Steam in Pressure-Depleted Reservoirs", paper SPE 13037 presented at the 59th Annual Technical Conference and Exhibition, Houston (September 16-19, 1984).

[21] Borisov, Ju.P.: "Oil Production Using Horizontal and Multiple Deviation Wells," Nedra Moscow, 1964. Translated by J. Strauss, S.D. Joshi (ed.). Phillips Petroleum Co., the R & D Library Translation, Bartlesville, Oklahoma, 1984.

[22] Giger, F.: "Reduction du nombre de puits par l'utilisation de forages horizontaux," Revue de l' Institut Francis du Petrole, vol. 38, No. 3, May- June 1983.

[23] Giger, F. M., Reiss, L. H., and Jourdan, A.P.: "The reservoir Engineering Aspects of Horizontal Drilling," paper SPE 13024 presented at the SPE59th Annual Technical Conference and Exhibition, Houston, Texas, Sept. 16-19, 1984.

[24] Renard, G. I. and Dupuy, J. M.: "Influence of Formation Damage on the Flow Efficiency of Horizontal Wells," paper SPE 19414 presented at the Formation Damage Control Symposium, Lafayette, Louisiana, Feb. 22- 23, 1990.

[25] Joshi, S.D.: "Augmentation of Well Productivity with Slant and Horizontal Wells", J Pet. Tech. 40 (6): 729- 739; Trans., AIME, 285. SPE- 15375- PA. doi: 10.2118/ 24941- PA, 1988.

[26] Dikken, B.J.: "Pressure Drop in Horizontal Wells and Its Effect on Production Performance", J. Pet. Tech. 1426- 1433, Nov. 1990

[27] Babu, D.K. and Odeh, A.S.: "Productivfity of a Horizontal Well" SPE Res. Eng 4 (4): 417- 421, SPE- 18298- PA

[28] Ozkan, E. Haciislamoglu,M. and Raghavan, R.: "The Influence of Pressure Drop Along the Wellbore on Horizontal Well Productivity, "SPE 25502, presented ar the Production Operations Sumposium, Oklahoma, March 21-23, 1993.

[29] Novy, R.A.: "Pressure Drops in Horizontal wells: When Can Theory Be Ignored?" Spe Res. Eng. 29-35, Feb 1995.

[30] Ozkan, E, Sarica and Haciislamoglu, M.: "Effect of Conductivity on Horizontal Well Pressure Behavior", SPE Adv. Tech. Series, Vol. 3. No. 1, pp. 85- 93, 1995.

[31] Archer, R.A., and Agbongiator, E.O.: "Correlation for Frictional Pressure Drop in Horizontal- Well Inflow- Performance Relationships," Feb 2005, SPE production & Facilities, 21-25.

[32] Lu, J.: "New Productivity Formulae of Horizontal Wells", J. of Can. Pet. Tech, Vol. 40, No. 10, Oct. 2001.

[33] Gunadi, B.: "Experimental and Analytical Studies of Cyclic Steam Injection using Horizontal Wells", Ph.D Thesis, December 1999, Texas A&M University.

[34] Diwan, U. and Kovscek, A.R.: "An Analytical Model for Simulating Heavy-Oil Recovery by Cyclic Steam Injection Using Horizontal Wells", July 1999.

[35] Butler, R.M. and Stephens, D.J.,: "The Gravity-drainage of Steam-Heated Heavy-Oil to Parallel Horizontal Wells", paper presented at the 31st Annual Technical Meeting of The Petroleum Society of CIM in Calgary (May 25-28,1980).

[36] Wu, Z., Vasantharajan, S., El-Mandouh, M., Suryanarayana, P.V.: "Inflow Performance of a Cyclic- Steam- Stimulated Horizontal Well Under the Influence of Gravity Drainage", SPE 127518, Sept, 2011.

[37] Aziz, K. and Gontijo J.E.: "A Simple Analytical Model for Simulating Heavy oil Recovery by Cyclic Steam in Pressure-Depleted Reservoirs", paper SPE 13037 presented at the 59th Annual Technical Conference and Exhibition, Houston (September 16-19, 1984).

[38] Prats, M.: "Thermal Recovery", Monograph – Volume 7, SPE of AIME, Henry L. Doherty Memorial Fund of AIME, 1982.

[39] Farouq Ali, S.M.: "Steam Injection Theories- A Unified Approach", paper SPE 10746 presented at the 57th Annual Fall Technical Conference and Exhibition, Denver, Oct. 9-12, 1977.

[40] Villinger, H., 1985, Solving cylindrical geothermal problems using Gaver-Stehfest inverse Laplace transform, Geophysics, vol. 50 no. 10 p.1581-1587

[41] Stehfest, H., 1970, Algorithm 368: Numerical inversion of Laplace transform, Communication of the ACM, vol. 13 no. 1 p. 47-49